CHEMICAL VAPOR DEPOSITION OF DIAMOND THIN FILMS ON TITANIUM SILICON CARBIDE

A Thesis Submitted to the College of

Graduate Studies and Research

In Partial Fulfillment of the Requirements

For the Degree of Doctor of Philosophy

In the Department of Mechanical Engineering

University of Saskatchewan

Saskatoon

By

SONGLAN YANG

PERMISSION TO USE

In presenting this thesis in partial fulfilment of the requirements for a Postgraduate degree from the University of Saskatchewan, I agree that the Libraries of this University may make it freely available for inspection. I further agree that permission for copying of this thesis in any manner, in whole or in part, for scholarly purposes may be granted by Professor Q. Yang, who supervised my thesis work or, in her absence, by the Head of the Department or the Dean of the College in which my thesis work was done. It is understood that any copying or publication or use of this thesis or parts thereof for financial gain shall not be allowed without my written permission. It is also understood that due recognition shall be given to me and to the University of Saskatchewan in any scholarly use which may be made of any material in my thesis.

Requests for permission to copy or to make other use of material in this thesis in whole or part should be addressed to:

Head of the Department of Mechanical Engineering

University of Saskatchewan

Saskatoon, Saskatchewan, Canada

S7N 5A9

ABSTRACT

Chemical vapor deposition (CVD) has been the main method for synthesizing diamond thin films on hetero substrate materials since 1980s. It has been well acknowledged that both nucleation and growth of diamond on non-diamond surfaces without pre-treatment are very difficult and slow. Furthermore, the weak adhesion between the diamond thin films and substrates has been a major problem for widespread application of diamond thin films. Up to now, Si has been the most frequently used substrate for the study of diamond thin films and various methods, including bias and diamond powder scratching, have been applied to enhance diamond nucleation density.

In the present study, nucleation and growth of diamond thin films on Ti_3SiC_2, a newly developed ceramic-metallic material, using Microwave Plasma Enhanced (MPE) and Hot-Filament (HF) CVD reactors were carried out. In addition, synchrotron-based Near Edge Extended X-Ray Absorption Fine Structure Spectroscopy (NEXAFS) was used to identify the electronic and chemical structures of various NCD films. The results from MPECVD showed that a much higher diamond nucleation density and a much higher film growth rate can be obtained on Ti_3SiC_2 compared with on Si. Consequently, nanocrystalline diamond (NCD) thin films were feasibly synthesized on Ti_3SiC_2 under the typical conditions for microcrystalline diamond film synthesis. Furthermore, the diamond films on Ti_3SiC_2 exhibited better adhesion than on Si. The early stage growth of diamond thin films on Ti_3SiC_2 by HFCVD indicated that a nanowhisker-like diamond-graphite composite layer, different from diamond nucleation on Si, initially formed on the surface of Ti_3SiC_2, which resulted in high diamond nucleation density. These results indicate that Ti_3SiC_2 has great potentials to be used both as substrates and

interlayers on metals for diamond thin film deposition and application. This research may greatly expand the tribological application of both Ti_3SiC_2 and diamond thin films.

The results demonstrated that NEXAFS is a reliable and powerful tool to identify NCD films.

ACKNOWLEDGMENTS

I would like to express deepest thanks and appreciation to my supervisor, Dr. Qiaoqin Yang, for her invaluable guidance and support throughout the duration of this research project. I wish to extend my appreciation to my supervisory committee members, Drs. Wenjun Zhang, Ikechukwuka N. Oguocha and Richard W. Evitts, for their criticisms, suggestions and useful feedback.

I would like to thank Dr. Akira Hirose, for his generous permission to use the MPECVD and HFCVD reactors in the Plasma Physics Laboratory of the University of Saskatchewan. Many thanks should also be given to Mr. Dave McColl and Mr. Rob Peace for their friendship and kind technical assistance whenever needed. I would also like to thank other colleagues for providing a great working environment.

I wish to express my appreciation to Mr. Ramaswami Sammynaiken, Mr. Jason Maley, Mr. Robert Blyth, Mr. Tom Regier, and Mr. Tom Bonli for their helps in diamond thin film characterization.

Finally, I would like to thank all my family members for their love throughout the tenure of my work on this thesis.

The financial support provided by the Canada Research Chair Program, the Natural Sciences and Engineering Research Council of Canada, Canada Foundation for Innovation, and the University of Saskatchewan is acknowledged with gratitude.

DEDICATION

My Parents

My wife Pu Sheng

And

My daughters

Annie Qi Yang

Iris Tong Yang

.

TABLE OF CONTENTS

LIST OF TABLES

LIST OF FIGURES

ACRONYMS

AFM	Atomic Force Microscope
AIST	National Laboratory for Advanced Industrial Science and Technology
APF	Atomic Packing Factor
BEN	Bias Enhanced Nucleation
BSE	Back Scattered Electron
CFI	Canada Fundation for Innovation
CVD	Chemical Vapor Deposition
DC	Direct Current
DLC	Diamond Like Carbon
ECR	Electron-Cyclotron Resonance
FA	Flame Assisted
FCC	Face Centered Cubic
FWHM	Full Width at Half Maximum
GB	Grain Boundary
HF	Hot Filament
HPHT	High Pressure High Temperature
IDLAS	Infrared Diode Laser Absorption Spectroscopy
MCD	Microcrystalline Diamond
MP	Microwave Plasma
NCD	Nanocrystalline Diamond

NEXAFS	Near Edge Extented X-Ray Absorption Fine Structure Spectroscopy
OES	Optical Emission Spectroscopy
PDS	Pulse Discharge Sintering
REMPI	Resonance Enhanced Multi-photon Ionization Spectroscopy
RF	Radio Frequency
SCCM	Standered Cubic Centimeter per Minute
SE	Secondary Electrons
SEI	Secondary Electron Imaging
SEM	Scanning Electron Microscopy
SSSC	Saskatchewan Structural Science Center
TE	Transmitted Electrons
UNCD	Ultrananocrystalline Diamond

CHAPTER 1
INTRODUCTION

1.1 Motivation

Diamond is the hardest known natural material and has many other unique properties: it has very low coefficient of thermal expansion, is chemically inert, offers the lowest friction and excellent wear resistant, has very high thermal conductivity, exhibits negative electron affinity and excellent biocompatibility, and is optically transparent from the ultraviolet to the far infrared. The combination of these extreme properties makes diamond an ideal thin film material for a wide range of applications in optics, semiconductors, microelectronics, biomedical, and manufacturing engineering.

Diamond thin films have been attracting increasing interests since the advent of diamond synthesis by chemical vapor deposition (CVD) at low pressures in the early 1980s. Hot-filament (HF) CVD and microwave plasma enhanced (MPE) CVD are the most widely used methods to synthesize diamond thin films. Both natural diamond and non-diamond materials have been used as substrates for CVD of diamond. However, diamond thin film formation on most hetero-substrate surfaces without pre-treatment is difficult due to the low diamond nucleation density. Intensive research indicated that the feasibility of diamond formation on hetero-substrate surfaces is dependent on the diffusivity and solubility of carbon in substrate: lowering the diffusivity and the solubility enhances diamond nucleation density, and thus diamond thin film formation rate. Si is the most frequently used substrate for CVD of diamond. Based on this, one can foresee that, carbides, such as TiC, SiC, WC, are good substrate materials for diamond deposition. Unfortunately, the rather high melting point of conventional carbides, generally around 3000 ^{O}C, renders them hard

to be sintered without binding additives. And these materials are too hard and brittle to be machined to complicated shapes. These disadvantages significantly limit the wide application of conventional carbides as substrates for diamond film depositions.

Recently, a new machinable carbide, Ti_3SiC_2, has been successfully developed by using various sintering techniques. It is lightweight (density of 4.52 g/cm^3), thermally (40 W/mK) and electrically ($4.5 \times 10^6\ \Omega^{-1}\ m^{-1}$) conductive, thermal shock resistant, highly damage tolerant and relatively soft (HV 4 GPa). Furthermore, its melting point is high (above 3000 $^{\circ}C$) and it is stable up to at least 1700 $^{\circ}C$ in inert atmospheres and vacuum. Due to its unique combination of both metallic and ceramic properties, it holds great potentials for many high-temperature applications, thus attracts growing interest in recent years. However, its low wear resistance due to the low hardness (compared with other wear resistant ceramics) may present problems for its future applications. Therefore, the successful deposition of a diamond thin film on its surface would be of great importance to improve its tribological properties for many applications, such as bearings, cutting tools.

Ti_3SiC_2, as a carbide, is promising to be a very good hetero-substrate material for diamond nucleation and growth. In addition, due to the metallic-ceramic properties of Ti_3SiC_2, Ti_3SiC_2 might be a good interlayer (having good thermal and mechanical compatibility with metal substrates) for diamond deposition on metallic materials. If an adhesive diamond thin film can be successfully coated on Ti_3SiC_2, the application of diamond thin films will be significantly expanded. Therefore, the study of diamond thin films deposition on Ti_3SiC_2 is theoretically interesting and practically important.

1.2 Objectives of the research

In this research, nucleation and growth of diamond on Ti_3SiC_2 slices were investigated by both MPECVD and HFCVD. The objectives included:

(1) Understanding of the nucleation and growth of diamond on Ti_3SiC_2.

(2) Deposition of well adhered diamond thin films on Ti_3SiC_2.

(3) Synthesis of nanocrystalline diamond (NCD) thin films on Ti_3SiC_2.

(4) Characterization of electronic structure of the NCD thin films by synchrotron-based near edge X-ray absorption fine structure spectroscopy (NEXAFS).

1.3 Organization of the Thesis

This thesis is composed of 9 chapters. The outline is summarized as follows:

Chapter 1 presents an overview of the research project, including motivation and main objectives.

Chapter 2 gives a comprehensive literature review, including carbon materials, advantages and disadvantages of various CVD techniques in diamond thin film growth, development and issues in nucleation of diamond thin films, and properties and synthesis of Ti_3SiC_2.

Chapter 3 introduces experiment methodologies adopted in this thesis. The components and parameters of the HFCVD and MPECVD reactors in the plasma physics laboratory used for growth of diamond thin films will be described. The techniques used to characterize the samples will also be explained.

Chapter 4 presents the results and discussion on nucleation and growth of diamond thin films on Ti_3SiC_2 by MPECVD. The results show that a much higher diamond nucleation rate and nucleation density can be achieved on Ti_3SiC_2 than on Si and thus adhesive diamond thin films with a high growth rate have been synthesized on Ti_3SiC_2.

In Chapter 5, the formation of NCD thin films on Ti_3SiC_2 will be introduced. Due to the high diamond nucleation rate, smooth NCD thin films can be feasibly

formed on the surface of Ti_3SiC_2 under the typical conditions for microcrystalline diamond thin film formation.

Chapter 6 presents the effects of power input on formation of diamond thin films on Ti_3SiC_2. Different microwave input powers, ranging from 500 to 800 W, were applied for the deposition. It has demonstrated that NCD thin film can be synthesized at low microwave power of 500 W and the increase of power inputs results in the formation of <001> highly oriented smooth diamond thin films.

Nucleation of diamond thin films on Ti_3SiC_2 by HFCVD is presented in Chapter 7. The results show that a dense and smooth NCD thin film can be synthesized on Ti_3SiC_2 within 1 h deposition. Observations at initial stage show that a nanowhisker-like diamond-graphite composite layer was firstly formed on the surface of Ti_3SiC_2, resulting in the high diamond nucleation density.

In Chapter 8, NEXAFS characterization of NCD thin films synthesized with high CH_4 concentrations by MPECVD will be presented. Those samples were prepared by Dr. Qiaoqin Yang. I was responsible for NEXAFS experiments and analysis. The results show that smooth fine NCD thin films with reasonably low sp^2 carbon concentration can be synthesized in pure CH_4 atmosphere with high growth rate (approximately 10 times faster compared with diamond growth under typical methane concentration of 1%).

Finally, the main results of the thesis work, the conclusions drawn from the results and some suggestions for future work are summarized in Chapter 9.

CHAPTER 2
LITERATURE REVIEW

2.1 Hybridization and Bonding in Carbon Materials

Carbon is a chemical element with an atomic number of six. It is the fourth most abundant element in the universe by mass after H, He and O. A neutral C atom has six electrons, which at the ground state (the lowest energy state) distribute themselves to fill the 1s and 2s subshells and the remaining two electrons occupy the 2p level, $1s^2 2s^2 2p_x^1 2p_y^1$. Bonding in any element will only take place with the valence shell electrons, found in the incomplete, outermost shell. By looking at the electron configuration, one is able to identify these valence electrons. Figure 2.1 shows the electron configuration of C. It has four valence electrons with two in the 2s subshell and two in the 2p subshell. The two 1s electrons are considered to be the core electrons and are not available for bonding. At the ground state (Figure 2.1 (a)), there are two unpaired electrons in the 2p subshell, hence, at most two bonds can be formed. Energy is released when bonds form, therefore, C tends to maximize the number of bonds to form solid carbon materials. For this reason, C usually forms excited states (Figure 2.1 (b)) by promoting one of its 2s electrons into its empty 2p orbital and hybridizes from the excited state. By forming this excited state, carbon will be able to form four bonds.

If the 2s orbital mixes with all the three 2p orbitals to form 4 sp orbitals, we call it sp^3 hybridization (Figure 2.2 (a)). The four sp^3 orbitals arrange themselves in the three dimensional space to get as far away from each other as possible to form a tetrahedral geometry with all the bond angles to be 109.5° (shown in Figure 2.3 (a)). Alternatively, the 2s orbital and two of the 2p orbitals may hybridize to form three sp^2 orbitals (Figure 2.2 (b)), which forms a trigonal geometry with 120° bond angles in a

plane, as shown in Figure 2.3 (b). In this case, the unhybridized 2p orbital lies perpendicular to the sp^2 orbitals plane. It is also possible that the 2s orbital hybridized with one of the 2p orbitals to form *sp* orbitals (Figure 2.2 (c)), resulting in linear geometry with a bond angle of 180°, as shown in Figure 2.3 (c). In this case, the two unhybridized pure p orbitals are perpendicular to *sp* orbitals. The hybridization in carbon induces carbon materials with different structures (allotropes), including sp^2 structured graphite, sp^3 structured diamond, and carbon nanostructures. The unhybridized 2p orbital(s) in sp^2 and sp^1 hybridization form π bond(s), while sp^3, sp^2 and sp^1 orbitals form σ bonds [1]. Therefore, in graphite, both π and σ exist whereas in pure diamond, only σ bonds present. Due to a less efficient overlap than in the case of a σ bond, the π bonds are somewhat weaker (lower bond energy). The difference in the bonding structure of those carbon allotropes induces significant difference in properties: for example, graphite is one of the softest known materials, while diamond is the hardness natural material; graphite is a solid lubricant, while diamond is a ultimate abrasive; graphite is an electrical conductor, while pure diamond is an excellent electrical insulator; graphite is opaque, while diamond is highly transparent.

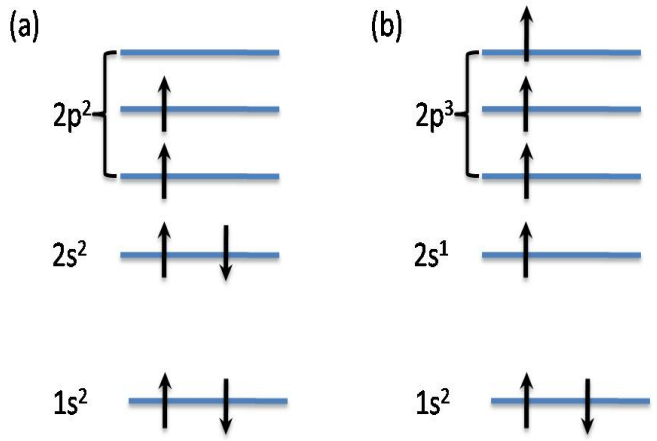

Figure 2.1 Electron configuration of C under (a) ground state in which only two bonds can be formed, and (b) excited state in which four bonds can be formed.

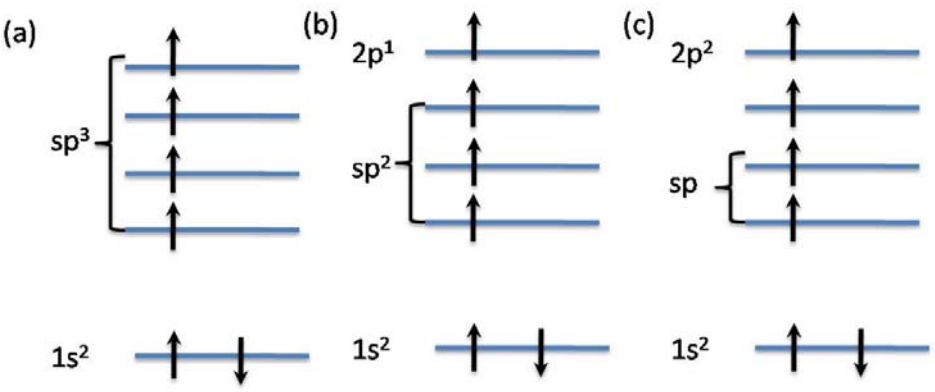

Figure 2.2 Atomic orbitals of excited state C with (a) sp^3, (b) sp^2, and (c) sp hybridization.

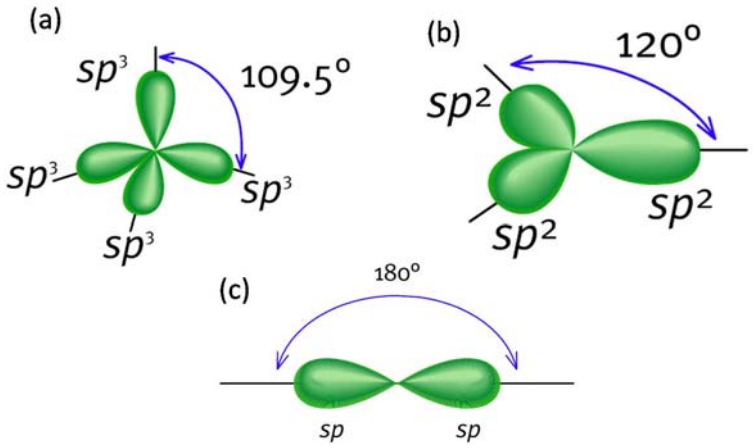

Figure 2.3 (a) sp^3, (b) sp^2 and (c) sp^1 hybridization in carbon materials [2].

2.2 Structure and Properties of Diamond

Diamond is the sp^3-bonded allotrope of carbon. Figure 2.4 shows a unit cell of diamond crystal, which is composed of eight corner atoms, six face-centered atoms and four internal atoms along the cube diagonals. A diamond unit cell contains eight C atoms. The crystal structure can be viewed as two interpenetrating FCC lattices, offsetting from one another along a body diagonal by one-quarter of its length. Each carbon atom bonds with four other carbon atoms to form a tetrahedral configuration.

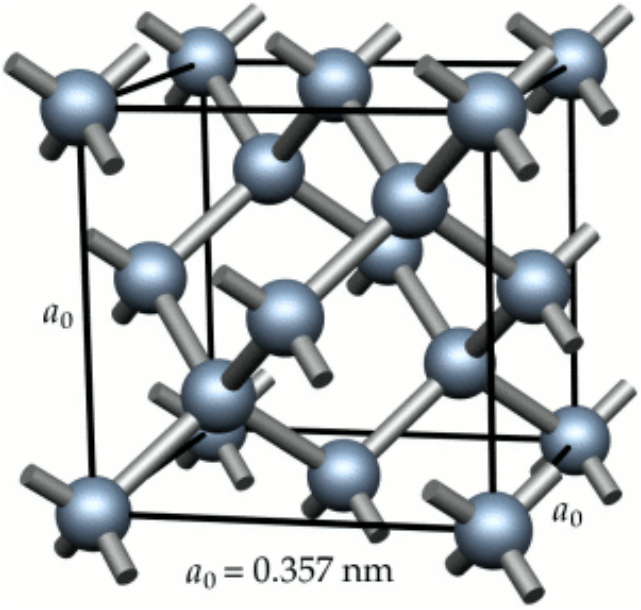

Figure 2.4 FCC structure of the diamond crystal [3].

At room temperature, the lattice constant a_0 for diamond is equal to 3.567 Å (0.3567 nm), from which a few other quantities can be derived. The C–C bond length d is equal to a quarter of the cube diagonals, that is $d = \sqrt{3}a_0/4 \approx 1.54$ Å. The corresponding C atomic radius, R, is given by:

$$R = d/2 = 0.077 \text{ nm} \tag{1}$$

And its Atomic Packing Factor (APF) can be calculated as:

$$APF = \frac{volume\ of\ atoms\ in\ a\ unit\ cell}{total\ unit\ cell\ volume} = \frac{V_s}{V_c} \tag{2}$$

The volume for a sphere is $\frac{4}{3}\pi R^3$, since there are 8 atoms in a diamond unit cell, therefore,

$$V_s = (8)\frac{4}{3}\pi R^3 = \frac{32}{3}\pi R^3 \tag{3}$$

And the total unit cell volume for diamond is

$$V_c = a_0^{\ 3} \tag{4}$$

From Equation 1, we have

$$R = d/2 = \frac{\sqrt{3}}{4} a_0 / 2 = \frac{\sqrt{3}}{8} a_0 \tag{5}$$

Therefore,

$$APF = \frac{V_s}{V_c} = \frac{\frac{32}{3}\pi(\frac{\sqrt{3}}{8}a_0)^3}{a_0^3} = 0.34 \tag{6}$$

The density, can be calculated by

$$\rho = \frac{nA}{V_c N_A} \tag{7}$$

Where

n is the atomic number in each diamond unit cell;

A is the atomic weight, for carbon, it is 12.011 g/mol;

N_A is the Avogadro's number, being $6.023 \times 10^{23}\ atoms/mol$

Hence,

$$\rho = \frac{(8\ atoms/unit\ cell)(12.011\ g/mol)}{(0.357\ nm)^3 (6.023 \times 10^{23}\ atoms/mol)} \tag{8}$$

$$= 3.515\ g/cm^3$$

Which is much higher than that of graphite (approximately 2.3 g/cm^3).

The structure of diamond accounts for its unique properties. As listed in Table 2-1 [4], diamond is the hardest, stiffest and least compressible natural material. It is chemically inert, offers very low friction and very high wear resistance, has the lowest coefficient of thermal expansion and the highest thermal conductivity at room temperature. It is electrically insulating and optically transparent from ultraviolet to the far infrared.

The combination of these extreme properties makes diamond an ideal material for a wide range of applications in optics, semiconductors, microelectronics, biomedical, and manufacturing engineering. It is not surprising that diamond has been

holding a special position in the hearts and minds of both scientists and the public for a long time [5] and has sometimes been referred to as "the ultimate engineering material".

Table 2.1 Some properties of diamond at room temperature [4].

Density, g/cm^3	3.52
Microhardness, GPa	≈90
Young's modulus, GPa	910-1250
Poisson's ratio	0.10-0.16
Compression strength, GPa	8.68-16.53
Coefficient of friction	
In air	0.05-0.1
In Vacuum	Near 1
Thermal conductivity, W•m^{-1}•K^{-1}	2×10^3
Thermal expansion coefficient, K^{-1}	0.8×10^{-6}
Electrical resistivity, Ω•cm	$\approx10^{16}$
Chemical resistance	High

2.3 Synthesis of Diamond

2.3.1 Phase Diagram of Carbon

Figure 2.5 shows the phase diagram of carbon, describing the equilibrium phase structure of carbon at different temperatures and pressures [6]. It can be seen from the figure, under relative low pressures (the bottom region of the figure), graphite, the most common form of carbon, is stable from room temperature up to its melting temperature at approximately 4000 $^{\circ}$C, whereas diamond is meta-stable at low-pressure low-temperature conditions and stable only at very high pressures.

Diamond exists in nature. However, natural diamond is scarce and costly, far below demand. This has motivated scientists around the world for more than one century to explore the artificial synthesis of diamond using various techniques with different C sources. High temperature high pressure (HPHT) and Chemical Vapor Deposition (CVD) are the most two commonly used techniques for diamond synthesis.

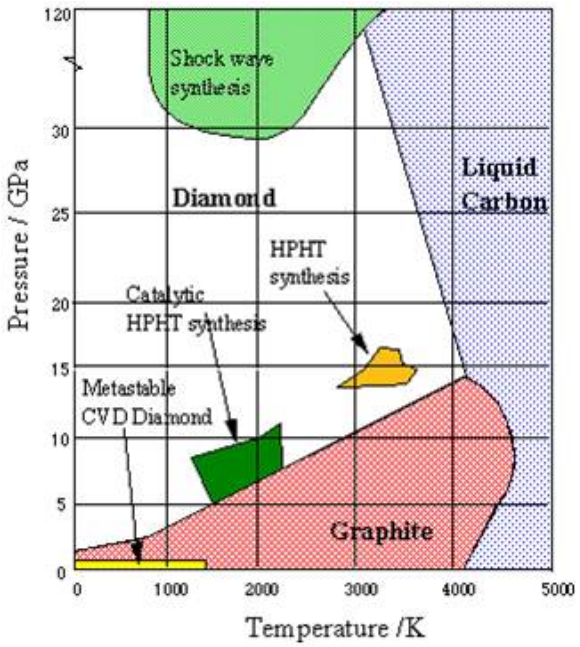

Figure 2.5 Pressure-temperature phase diagram for carbon [6].

2.3.2 HPHT Diamond Synthesis

Since both diamond and graphite are pure carbon allotropes, and graphite is rich in earth, the synthesis of diamond using graphite is reasonable. Although the difference in standard enthalpies for diamond and graphite is only 2.9 $kJ \cdot mol^{-1}$ [6], a large activation barrier separates these two carbon phases and prevents the mutual conversion between them at room temperature under atmospheric pressure. The phase diagram of carbon, shown in Figure 2.5, indicates the appropriate directions towards the conversion of graphite to diamond. Although graphite is stable at room temperature and low pressures, diamond, whose density is much higher than graphite (3.52 g/cm^3 for diamond and 2.25 g/cm^3 for graphite), becomes more stable with high pressure. However, the thermal energy at room temperature is not enough to break the C-C bonds in graphite and the diffusion of carbon is very difficult, thus, high temperature is also a requirement in order to convert graphite into diamond. The fact that natural diamond is produced at high pressure and high temperature in volcanic shafts also suggests the possibility of diamond synthesis through heating graphite

under extreme high pressures. The HPHT diamond synthesis essentially duplicates the natural diamond formation process and the synthesized diamond exhibits similar properties [7] as the natural one. The first successful synthesis of diamond using HPHT method was reported by the General Electric in 1960s [8, 9]. Since then, the HPHT technique has been the main method to produce "industrial diamond" for several decades. During the HPHT process, the transformed diamond must be cooled under high pressure in order to avoid its transformation back into graphite.

In order to perform the direct transformation from graphite to diamond at a noticeable rate, very high pressure and high temperature are required based on transformation kinetics. In the first successful synthesis of diamond by General Electric, pressure as high as 12.5 GPa and temperature as high as 3000 ºC were reported [8, 9]. These conditions are very harsh and costly to achieve. Fortunately, it is possible to overcome these limitations via solvent-catalyst reaction [7]. The solvent-catalyst process was invented and developed by General Electric [10]. It established a reaction route with activation energy lower than that of the direct transformation, and thus a faster transformation under more benign conditions is feasible. As a result, the solvent-catalyst HPHT diamond synthesis is readily performed and has been widely used in industry to produce diamond.

The solvent-catalysts used during the HPHT process are transition metals and their alloys, including Fe, Co, Cr, Ni, Pt and their alloys. These metal-solvents can break the bonds between carbon atoms, dissolve carbon and improve the diffusion of carbon to the growing diamond surface. The most common catalysts currently applied include Fe-Ni and Co-Fe alloys, where pure metals are rarely used [7].

HPHT synthesized diamond, due to its high purity and uniformity, has taken an increasing share of the industrial diamond market and has replaced natural diamond in many areas [7]. Micron-sized diamond crystals can be produced in a few

minutes by HPHT. However, large diamond crystals are difficult and expensive to be synthesized by HPHT, although HPHT process can produce commercial diamonds up to 6 mm in size with a mass of 2 carats (0.4g) in hydraulic presses and larger crystals up to 17 mm have been announced by de Beers in South Africa and others [7]. Small HPHT synthesized diamond crystals (< 1 mm) are used as powders and grits (in six different sizes) for fine grinding, lapping and polishing compounds, matrix-set drill bits and tools, saw blades. Larger crystals (> 1 mm) are polished, shaped and handled as individual stones for drill bits, glass cutters, abrasive wheel truers, single-point turning, shaping and cutting tools, heavy-duty truing and large plunge cutting tools, and wire-drawing dies. The main advantages of the HPHT synthesized diamond over the natural one are the ability to control the uniformity, size, crystal habit, crystal friability, the higher general quality and consistency [11]. Research in HPHT diamond synthesis is continuing in the direction to lower the production costs and to increase the crystal size.

2.3.3 CVD of Diamond Thin Films

Besides the high processing cost, the diamond synthesized by HPHT is usually in the form of powders/particles or small bulk materials with the size ranging from nanometers to a few millimeters. These drawbacks limit its more widely technological applications [12]. The world's attention to diamond has been further increased by the discovery in 1980s that it is possible to produce polycrystalline diamond thin films by CVD techniques [13, 14], typically using hydrogen (H_2) and methane (CH_4) gas mixtures at low pressures (vacuum). CVD diamond shows mechanical, tribological, and even electronic properties comparable to those of natural diamond, as shown in table 2-2 [15-19].

Table 2.2 Properties of CVD diamond [15-19].

	CVD diamond	Natural diamond
Density (g/cm^3)	3.51	3.515
Thermal conductivity at 25 °C (W/m·K)	2100	2200
Thermal expansion coefficient at 25-200 °C (10^{-6}/°C)	2.0	0.8-1.2
Band gap (eV)	5.45	5.45
Coefficient of friction in air	0.035-0.3	0.05-0.15
Compression strength (GPa)		8.68-16.53
Poisson's ratio		0.10-0.16
Vickers hardness range (GPa) (Varies with crystal orientation)	50-100	57-104
Young's Modulus (GPa)	820-900 (0-800 °C)	910-1250

CVD process involves the dissociation and/or chemical reaction of gaseous reactants in an activated (heat, light, plasma) environment, followed by formation of a stable solid product [20]. The CVD techniques used to synthesize diamond thin films have the following characteristics:

1) The gas phases contain a carbon-containing species, such as hydrocarbon, alcohol, carbon monoxide, or carbon dioxide. Practically, CH_4 is the most frequently used carbon-containing gas for diamond CVD.
2) The gas phases are activated. The activation can be achieved by high temperature (e.g. hot filament (HF)), or electric discharge (e.g. microwave plasma (MP)), or a combustion flame (e. g. oxyacetylene torch).
3) As graphite or other carbon structures may be formed simultaneously with diamond during the deposition, they must be effectively etched during the diamond deposition. Atomic hydrogen, H, has been proven to be effective to etch graphite and/or other carbon structures and stabilize diamond structure. Therefore, high concentration of H_2 is generally present in the gas mixtures for CVD of diamond (typically, 99 vol.% H_2 mixed with 1 vol.% CH_4). In

addition, other "anti-graphite" species including OH, O_2, atomic O and F_2 have been also used [21].

4) The substrates used for diamond deposition are limited. They should support nucleation and growth of diamond and withstand the deposition temperature. Firstly, the surface of the substrate should not include any catalysts which enhance the formation of graphite and/or other carbon structures. It is better that the substrate surface should be at or near the solubility limit for carbon at the deposition temperature in order to favor the stabilization of diamond on the substrate surface instead of the inward diffusion of carbon to the substrate [22]. From this point of view, transition metals, such as Fe, Co, Ni, which are widely used as the solvent-catalysts in the HPHT diamond synthesis, are not good substrate materials for CVD of diamond, due to their high carbon solubility.

HFCVD, MPECVD and arc discharge CVD are the most widely used methods for synthesizing diamond thin films. Figure 2.6 illustrates the configurations of these methods [12].

In HFCVD process, the deposition gas pressure is typically kept at 20-30 Torr (2.7-4.0 kPa), the filament, made from W or Ta, is electrically heated to temperatures above 2200 $^{\circ}$C, the substrate to be coated is typically a few millimeters beneath the filament, and a gas mixture containing H_2 and CH_4 is typically used, thus CH_3 radicals and atomic H are produced around the hot filament, leading to growth of diamond on a substrate surface at temperatures typically between 700 and 1100 $^{\circ}$C. During the diamond deposition, these metal wires unavoidably react with the carbon-containing gases and are carbonized to form metallic carbide, which changes their electrical resistivity, makes them rather brittle, and thus shortens the filament lifetime [12]. Low equipment cost, feasible configuration variation, and convenient operation are the

main advantages of HFCVD method. It can produce polycrystalline diamond thin films of reasonable quality at a rate of about 1-10 $\mu m \cdot h^{-1}$, depending on the actual deposition conditions [12]. However, this technology also suffers from a number of major disadvantages [12]. The filament is particularly sensitive to oxidizing or corrosive atmospheres, and this limits the variety of gas mixtures which can be employed. Diamond thin films are usually contaminated with the filament material due to the high temperature of filament. In the case of diamond thin films for mechanical applications, metallic impurities at the level up to dozens of ppm would not cause any problem. However, the filament contamination becomes unacceptable for many functional applications including optical and semiconductor applications, where high purity is required. Furthermore, the thermal nature of the process indicates that there are very few ions to be created, thus weakens the effectiveness of biasing the substrate on the improvement of diamond nucleation density, film growth rate, and the control thin film orientation.

MPECVD (Figure 2.6 (b) and (c)) utilizes similar conditions as HFCVD to grow diamond thin films. In an MP reactor [12], microwave power is coupled into the chamber through a dielectric window (usually quartz) in order to create a discharge. The microwaves provide energy to generate and accelerate electrons, which in turn transfer their energy to the gas molecules through collisions. This leads to the heating and dissociation of the gas molecules, and formation of the active species, which are the precursors for diamond deposition. There are two common types of MPECVD reactor, NIRIM-type (Figure 2.6 (b)) [23] and the ASTEX-type reactor (Figure 2.6 (c)) [24]. In MPECVD, microwave power up to 5 kW can be used and diamond growth rates higher than 10 $\mu m \cdot h^{-1}$ is possible. Another advantage [12] of MPECVD over other types of methods is that they can use a wide variety of gas mixtures, including

those with high O_2 content or containing chlorinated or fluorinated gases. Since no filament is involved in MPECVD systems, they are inherently cleaner than HFCVD systems, which guarantees the high purity of the deposited thin films. Furthermore, the presence of a significant number of ions within the discharge allows the possibility of adjusting the deposition conditions by biasing the substrate. The most widely recognized application in this aspect has been the so-called bias enhanced nucleation (BEN), in which a negative potential (typically 200-300 V) is applied to the substrate at the beginning of the deposition. It is believed that the applied bias voltage accelerates the movement of carbon-containing ions onto the substrate, causing them to be implanted beneath the surface and create a carbon-rich layer in the topmost of the substrate. It has been found that BEN can significantly increase the initial nucleation density/rate and result in diamond thin films with a preferred orientation (will be introduced in later section). Even though MPECVD system is more expensive than HFCVD system, MPECVD is currently the most widely used techniques for diamond growth.

Plasma jet, arc jet or plasma torch methods are promising alternatives to the more conventional HF and MP methods. They were introduced in the mid- to late-1980s. In a plasma jet, gas at relatively high flow rates (liters per minute compared with cm^3 per minute used for HFCVD and MPECVD) passes through a high-powered electrical discharge and forms a jet of ionized particles, atoms and radicals, which then expands into a secondary chamber to strike the substrate surface at a high velocity. Plasma jets are usually distinguished by the methods in which the electrical discharge is sustained. The most commonly used plasma jet is the DC arc jet (see Figure 2.6 (d)), which uses a direct current to drive high, relatively stable currents through the ionized flowing gases. Other technologies which are emerging include electrodeless discharges, including RF inductively coupled and microwave plasma jet

sources. The main advantage of all these plasma jet techniques is the high diamond thin film growth rate that can be achieved, typically greater than 100 $\mu m \cdot h^{-1}$. The reported highest diamond growth rate by arc jet is approximately 900 $\mu m \cdot h^{-1}$ [25], three orders of magnitude greater than that for typical HF or MPECVD methods. However, these techniques have a main drawback: the deposition area is limited to small area struck by the jet (typically less than 1 cm^2). In addition, it is difficult to maintain uniform substrate temperature due to the high energy input. The temperature difference between the deposition surface and the backside of the substrate is very large. Even with the excellent cooling, the thermal shock experienced by the substrate from the jet ignition and extinguishing prevents many substrate materials to be used. The rapid contraction of the substrate occurred when the jet is turned off, and often induces the delamination of the diamond coating from the substrate, forming a free-standing diamond plates. This is a problem for deposition of adherent coatings on substrates but an advantage to make free-standing diamond plates.

Another method, oxyacetylene welding torch or the combustion flame [26, 27], was also widely used to grow diamond thin films in the 1980s. The system is very cheap, and can be operated in air at atmospheric pressure without the need for complex vacuum equipment. The torch is operated in a regime where the acetylene flow is slightly higher than the oxygen flow, and this creates a region with high carbon containing radical species. If a substrate is placed within this region, a diamond film will grow at a rate up to 200 $\mu m \cdot h^{-1}$. However, this method has similar drawbacks as for the plasma jet. The radial non-uniformity of the deposited material limits the area which can be coated, and cooling the substrate in a reliable and uniform manner is also problematic, leading to the presence of a significant amount of non-diamond carbon in the deposited thin films.

Other methods for diamond thin films deposition include laser-assisted CVD, pulsed laser deposition, and hydrothermal growth [28]. However, highly pure diamond thin films are difficult to be achieved by using these methods.

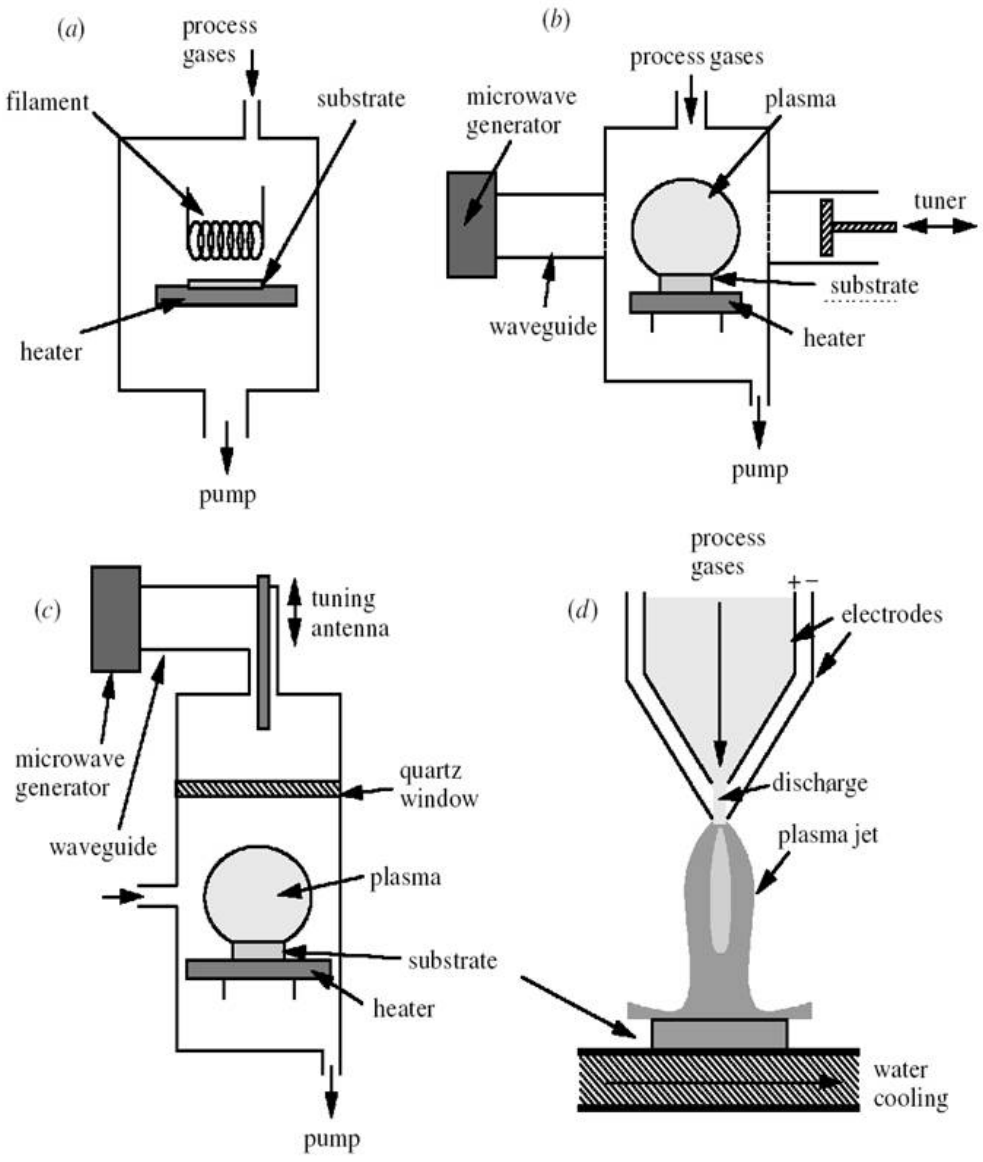

Figure 2.6 Schematics of low pressure CVD methods for diamond thin film synthesis (*a*) HF, (*b*) 'NIRIM-type' MP reactor, (*c*) 'ASTEX-type' MP reactor, and (*d*) DC arc jet (plasma torch) [12].

2.4 Physical and Chemical Aspects of CVD Diamond

At the first glance, the reaction in CVD of diamond seems to be very simple and only involves the decomposition of the carbon containing species, e.g. CH_4 as following [7]:

$$CH_4\ (g) \xrightarrow{activation} C\ (diamond) + 2H_2\ (g)$$

As a matter of fact, the mechanism of diamond synthesis by CVD is a complex integration of many factors and has not been fully understood until now. Nevertheless, it has been found that there are two essential conditions which are crucial for the process [24]: (a) the activation of the carbon containing species and (b) the presence of the atomic H.

In the case of diamond synthesis using hydrogen (H_2) and methane (CH_4) gas mixtures as the reactants, Figure 2.7 demonstrates the possible physical and chemical processes involved [12, 5]. Firstly, reactive gases of CH_4 and H_2 are mixed in the reactor. Then they pass through a high temperature or energetic region where the molecules in the gas phases are broken and activated to form reactive radicals and/or atoms by plasma or hot filament or combustion flame front. Generally, it is believed that CH_4 decomposes into two primary stable species: the methyl radical (CH_3) and acetylene (C_2H_2) [29]. Beyond the activation region, these reactive species continue to be transported and mixed by forced flow, diffusion as well as convection throughout the reactor, and undergo a complex set of chemical reactions until they strike the colder solid substrate surface or being exhausted from the reactor. On the substrate surface, various processes may occur, the species can either be adsorbed by the surface or be desorbed again back into the gas phase. They can diffuse along and into the substrate surface or react with the substrate to form various structures depending on the processing conditions and exposed substrate surface states.

In order to identify and understand the fundamental aspects involved in the diamond synthesis by CVD, various diagnostic techniques have been developed and applied in the in-situ analysis of gas compositions during the processing. Optical Emission Spectroscopy (OES) provides a sensitive detection of a few excited species which fluoresce, including C, C_2, H, CH, CH_2, and H_2 [4]. OES in-situ analysis of diamond growth has been performed in microwave [30-33] and DC [32] plasma reactors containing H_2, CH_4, and rare gases. However, due to the selective sensitive of OES, the use of OES data alone may provide a misleading picture about the primary chemical reactants in the CVD process. In-situ detection of diamond growth species was also reported using Infrared Diode Laser Absorption Spectroscopy (IDLAS) [35]: in addition to CH_4, species including CH_3 radical, C_2H_2, and C_2H_4 has been detected. In 1989, Celili et al. reported on the detection of both the atomic H [36] and CH_3 [37] radicals in flame assisted (FA) CVD reactor by using Resonance Enhanced Multi-photon Ionization Spectroscopy (REMPI). It has been found that CH_3 is the predominant species and the crucial radical for diamond growth [38, 39].

Atomic H also plays an essential role in the deposition of diamond thin films by CVD. In a HFCVD system, atomic H comes from the thermal decomposition of H_2 on the surface of the hot filament. In a plasma system, it is created by dissociation of H_2 due to the impact of electrons. The main functions of atomic H in the diamond deposition including:

(1) Keeping diamond lattice stable by terminating the “dangling bonds” on the surface of diamond films.

(2) Creation of dangling bonds for carbon-containing radicals, e.g. CH_3, to be attached to the growing diamond surface by reacting with the H on the diamond surface to form H_2.

(3) Creation of CH_3 radicals by reacting with CH_4. Even though CH_3 radicals are predominantly created through the decomposition of CH_4 by thermal or discharge methods, the reaction between H atoms and CH_4, will also create CH_3 radicals, which can then be attached to suitable surface sites to grow diamond.

(4) Etching non-diamond carbon structures like graphite. During the diamond CVD, other carbon allotropes, such as graphite and graphitic amorphous carbon, are unavoidably formed in the thin film. It is well known that the etching of non-diamond carbon by atomic H is many times faster than the etching of diamond. Through this way, the non-diamond carbon structure can be removed during the processing and diamond is preferably nucleated and grown.

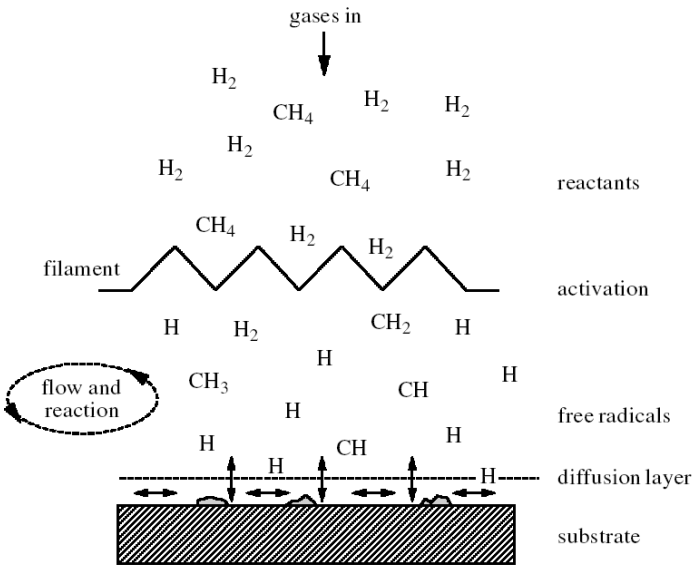

Figure 2.7 Schematic of the physical and chemical processes occurring during the CVD of diamond [12, 5].

Figure 2.8 shows the surface structure of diamond thin films [29]. The carbon sp^3 dangling bonds on the surface are terminated and stabilized by H atoms.

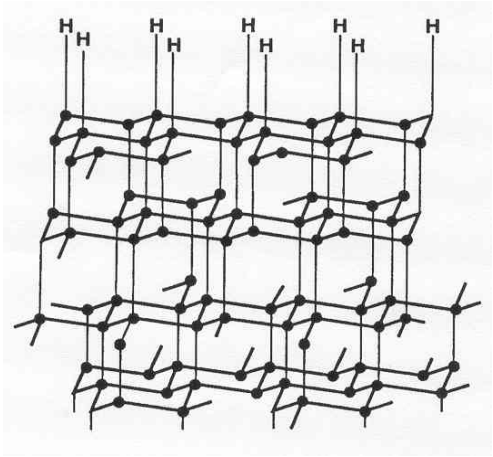

Figure 2.8 Structure of CVD diamond surface [27].

Figure 2.9 schematically illustrates the reaction process at the diamond film surface during the CVD process [5]. Diamond growth can be considered as a stepwise addition of carbon atoms to the existing diamond lattice, catalyzed by the presence of excessive atomic H. At first, the reaction between the atomic H in the gas phase and the H atom bonded to the sp^3 carbon dangling bond induces formation of H_2 gas, leaving behind a reactive surface site. CH_3 radicals (gas phase) then collide and react with the reactive surface site, adding a carbon atom to the lattice. The same process of H atom abstraction and CH_3 addition may happen on the adjacent site. The further H abstraction on one of the chemisorbed groups creates a radical, which attracts the other nearby carbon group to form the ring structure, locking the two carbon atoms into the diamond lattice.

2.5 Nucleation of Diamond

Growth of polycrystalline diamond thin films on hetero-substrate by CVD techniques typically includes several distinguishable stages [40]:

(a) Incubation period;

(b) 3-D surface nucleation;

(c) 3-D growth of nuclei to grains;

(d) Coalescence of grains and formation of continuous film;

(e) Growth of continuous film.

Nucleation is the most crucial step in diamond growth by CVD. The control of nucleation is essential for optimizing the diamond properties such as grain size, orientation, transparency, adhesion, and surface roughness, which are required for targeted applications [41]. Two criteria must be satisfied for "spontaneous" (non-epitaxial) diamond nucleation [42]:

(a) The saturation of carbon at the substrate surface;

(b) The presence of high-energy sites (dangling bonds).

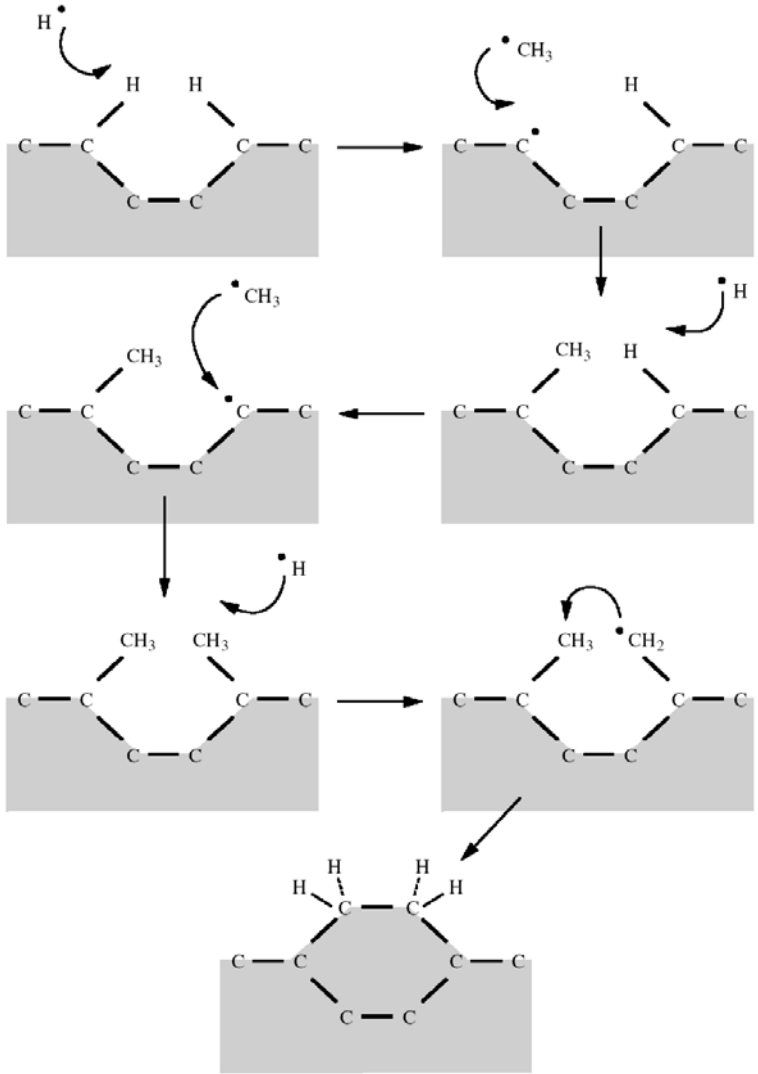

Figure 2.9 A schematic of the reaction process occurring at the diamond surface leading to stepwise addition of CH_3 species and diamond growth [51].

Various hetero-substrate materials, as listed in Table 1.3, have been used for diamond thin film growth [43]. However, diamond nucleation density and rate on non-diamond surfaces without pretreatment are usually very low [43].

Table 2-3. Physical parameters of currently used or potential materials for diamond epitaxy [43].

Substrate material	Lattice constant (Å)	C diffusivity ($cm^2 \cdot s^{-1}$)	Thermal expansion coefficient ($10^{-6}K^{-1}$)	Surface energy ($J \cdot m^{-2}$)
Diamond (Cubic)	3.567 [7]	-	0.8 [7]	5.3 (111) [7]
Si(diamond-cubic)	5.42[44]	7×10^{-15} [45]	7.6 [44]	1.46 (111) [7]
Cu (f.c.c.)	3.61 [44]	-	17.0 [44]	2.08 (100) [46]
Ti(α)<900 °C (h.c.p.)	2.95, 4.68 [44]	7×10^{-9} [44]	8.9 [44]	
(β)>900 °C (b.c.c.)	3.29 [44]	2×10^{-6} [45]	9.9 [44]	2.570/1.723 [47]
Al (f.c.c.)	4.04 [44]	-	23.5 [44]	1.085/0.939 [47]
Au (f.c.c.)	4.07 [44]	-	14.1 [44]	1.626/1.345 [47]
Pt (f.c.c.)	3.92 [44]	-	9.0 [44]	2.691/2.055 [47]
Ta	3.30 [44]	10^{-14}[48]	6.5 [44]	3.018/2.270 [47]
Nb (b. c. c.)	3.294 [47]	3×10^{-12} [45]	7.2 [44]	2.983/2.022 [47]
Cr<1840 °C (b.c.c)	2.89 [44]	4×10^{-8} [45]	6.5 [44]	2.056/1.913 [47]
Mo	3.14 [44]	10^{-11} [45]	5.1 [44]	2.877/2.116 [47]
W(α) (b.c.c.)	3.16 [44]	10^{-13} [45]	4.5 [44]	3.468/2.487 [47]
Fe(γ) 912-1400 °C (f.c.c.)	3.56 [44]	2×10^{-7}[45]	>14.6 [44]	
Fe(α)<912 °C (b.c.c.)	2.86 [44]	8×10^{-7}[45]	12.1 [44]	2.939/1.923 [47]
Ni (f.c.c.)	3.52 [44]	2×10^{-8}[45]	13.3 [45]	2.364/1.773 [47]
Co(α) (h.c.p.)	2.51, 4.07[44]	-	12.5 [44]	
Co(β)>390 °C (f.c.c.)	3.54 [44]	1×10^{-8}[44]	-	2.709/2.003 [47]
cBN (cubic)	3.615 [45]	-	0.59 [45]	-
TiC (f.c.c.)	4.32 [45]	-	6.53 [45]	
TiN (cubic)	4.24 [45]	-	9.35 [45]	
NbC (b.c.c.)	4.24-4.57 [44]	-	6.52 [49]	
WC (h.c.p.)	2.90, 2.83 [44]	-	3.58 [49]	
Mo_2C (h.c.p.)	3.01, 4.74 [45]	-	7.8-9.3 [50]	
ZrC (f.c.c.)	4.67 [44]	-	6.1 [45]	
B_4C (rhombohedral)	5.60, 12.12 [44]	-	4.5 [45]	
Al_2O_3 (hexagonal)	4.785, 12.991 [44]	-	7.5 [45]	
Si_3N_4(β) (hexagonal)	7.603,2.909 [44]	-	2.11 [45]	

Diamond nucleation on non-diamond substrates is proposed to occur mostly on intermediate layers, such as diamond-like amorphous carbon [51-54], metal

carbides [55-72] or graphite [73-79]. Those interlayers are formed at the substrate surface through the chemical reactions between the activated gas species and the substrate surface during the incubation period.

2.5.1 Diamond Nucleation on Diamond-like Amorphous Carbon

Figure 2.10 illustrates the diamond nucleation mechanism on the interlayer of diamond-like amorphous carbon based on high resolution TEM study of diamond on copper grids by HFCVD [51].

In step I, carbon clusters are formed on the substrate surface, and a change in the bonding structure from sp^1 to sp^2 takes place.

In step II, sp^2-bonded carbon atoms are converted into a relatively stable network of sp^3-bonded carbon. The continuous molecular rain of activated hydrocarbon and atomic hydrogen on the substrate surface provides sufficient energy for the conversion from sp^1 to sp^2 to sp^3. At the same time, as mentioned above, the etching of sp^1 and sp^2 carbon phases by atomic H is obviously faster than the etching of the sp^3 carbon phase. This promotes and stabilizes the sp^3 phase.

In step III, a transition of the bonding state in the carbon network occurs from a disordered domain with sp^3-bonded carbon to sp^3-bonded diamond. Crystallization in the amorphous layer also includes chemical reactions, such as hydrogen abstraction, dehydrogenation of absorbed complexes, recombination of hydrogen atoms, and so on. The crystallized regions then act as nuclei for following diamond growth.

In steps IV to VI, diamond growth takes place. Carbon atoms added to the surface (step IV) diffuse inwards by a solid-state diffusion process. The initial diamond shape is hemispherical (step IV), as confirmed by examining a planar view of diamond growth on iron silicide. Once a diamond crystal reaches a critical size (step V), it will acquire a faceted crystallographic shape characterized by defects such as points, stacking faults and twins (step VI).

In step VII, secondary nucleation takes place as a result of the concentration fluctuation on the surface of the diamond crystal. This fluctuation leads to an uneven surface of the disordered domain; its thickness varies from 8 to 14 nm, depending on deposition conditions. Once the thickness of the disordered domain exceeds a critical thickness (above15 nm), there will not be enough localized thermal energy and time available for carbon atoms to diffuse into the diamond crystal, leading to the secondary nucleation on the surface.

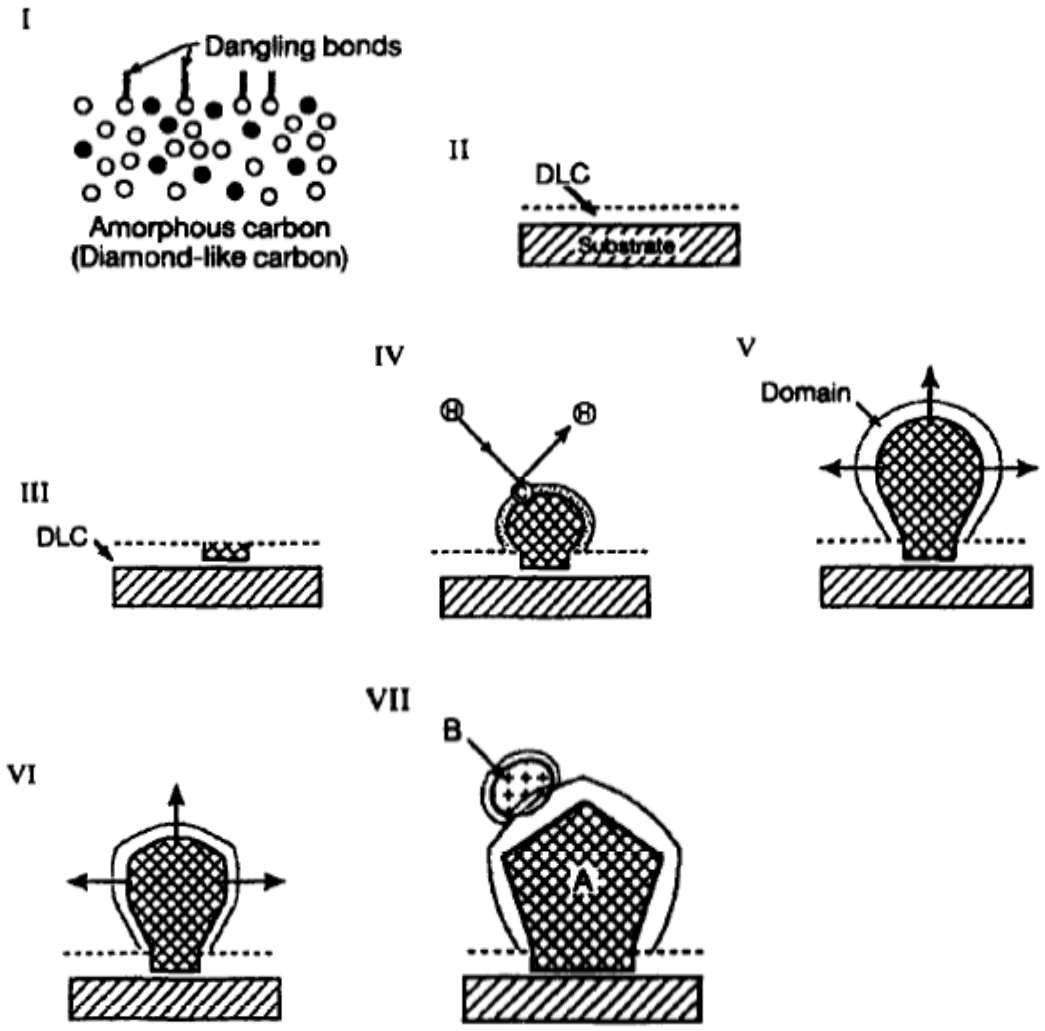

Figure 2.10 Diamond nucleation mechanism on DLC interlayer [51].

2.5.2 Diamond Nucleation on Carbide Layer

Diamond nucleation on carbide buffer layer was first reported by Badzian et al. [66] in 1988. They found that diamond nucleation on Si is preceded by formation of

SiC interlayer, and diamond nucleation occurs on the surface of carbide. This is supported by many diamond growth experiments on Si using MPECVD [55, 56, 59, 61-64, 67-69]. The systematic studies of diamond growth on carbide-forming refractory metals by Joffreau et al. [70] also illustrated that diamond nucleation occurred only after formation of a thin carbide layer. Haubner et al. [80] subsequently proposed a model to elucidate the mechanism governing the nucleation process on a carbide-forming substrate. It was suggested that carbon dissolves into the substrate initially, resulting in formation of a stable carbide. Diamond nucleation occurs on the carbide layer when the carbon concentration on the surface reaches its saturation value. Haubner and co-workers [80] also compared diamond nucleation densities on Ti, Hf, Nb, Ta, Mo and W, and found that the nucleation density is related to the diffusivity of carbon in the respective substrates. The incubation period for nucleation is the shortest on the metal that can most rapidly achieve a supersaturation of carbon on the surface.

2.6 Methods of Nucleation Enhancement

Different methods including mechanical abrasion and biasing have been applied to enhance the nucleation of diamond on foreign substrate materials.

2.6.1 Mechanical Abrasion of Substrate

In 1987, Mitsuda and co-workers reported on the enhancement of diamond nucleation density through scratching the substrate surface with diamond powders [81]. Thereafter, scratching of substrate with diamond powders has become the most common and powerful method for growth of continuous diamond thin films with fine uniform grain size on hetero-substrate. Similar effect has also been achieved by scratching with SiC [82] and cubic-BN [83]. In the case of polished single crystal Si substrates, which have been intensively studied, the nucleation density can be roughly enhanced by three orders of magnitude through the diamond scratching, 10^7-10^8 cm^{-2}

with diamond scratching compared with 10^4 cm^{-2} without diamond scratching. Why would scratching enhance diamond nucleation? One possible reason is that the residual powders or fragments are unavoidably left in the scratched groove and act as seeds for diamond growth [84]. Although BN and SiC are not diamond, their structures are similar to that of diamond. Thus, diamond nucleates easily on them. Another possibility is that scratching with the hard powders induces surface defects including edges, steps, and dislocations. Those defects are chemical active sites with high energy and prefer to adsorb diamond precursors for diamond to nucleate [85, 86].

2.6.2 Bias-Enhanced Nucleation in MPECVD and HFCVD

In 1991, Yugo et al. [87] achieved a diamond nucleation density of 10^9-10^{10} cm^{-2} on a mirror-polished Si substrate by applying a negative substrate bias voltage to the substrate in a MPECVD system. Since then, the nucleation mechanism has been extensively studied and different models have been proposed.

Yugo et al. [88] and Gerber et al. [89] suggested a shallow ion implantation model in which the sp^3 bonded carbon clusters, formed by low energy ion implantation, function as the nucleation precursors. The negative bias causes the positively charged ions in the growth chamber to accelerate towards and bombard the substrate surface, removing the contamination and facilitating cluster formation on the surface, which favor diamond nucleation. Stoner et al. [90], on the other hand, suggested that the critical process should be the change in plasma chemistry, such as the increase in the concentration of atomic H caused by substrate biasing and formation of a carbide surface layer. Jiang et al. [91, 92] found that the overall temporal evolution of the nucleation density corresponds well with a surface kinetic model involving immobile active nucleation sites, germs, and nuclei. They suggested that the enhanced surface diffusion and sticking probability of carbon on silicon due to the ion bombardment played the decisive roles in the nucleation enhancement.

2.6.3 Diamond Nucleation at Low Gas Pressure

In 1997, Lee and co-workers [93] reported a high diamond nucleation density of 10^{10}-10^{11} cm^{-2}) on mirror-polished Si substrates under very low pressures (0.1-1 Torr) of H_2/CH_3 in a HFCVD without applying surface scratching or a substrate bias.

The mechanism for the enhanced nucleation at very low pressure was explained by the combinative effect of larger mean free path and increased concentration of active or nucleating species at the substrate. They estimated that the concentration of the active species at the substrate went through a maximum at a pressure of 0.02 Torr. As the mean free path increases with decreasing pressure, the active species undergo fewer collisions and thus suffer less loss of the active species energy during their transport to the substrate. Because of higher kinetic energy, these species are more effective in inducing surface aggregation and reconstruction as well as in removing surface oxide, which also promotes diamond nucleation.

2.6.4 Ion Implantation-Enhanced Nucleation

Yang et al. [94] used ion implantation to modify the surface structure of the substrate to enhance the diamond nucleation density. In their research, Si^+ ions with energy of 25 keV and an implantation dose of 2×10^{17} cm^{-2} were implanted into a mirror-polished Si wafer. After the treatment, enhanced diamond nucleation has observed and continuous diamond films have been synthesized. Since the implantation of Si+ ions changes the surface structure but not the composition, it indicates that surface structure also plays an important role in diamond nucleation.

2.7 CVD of NCD Thin Films

Under typical diamond growth conditions, the grain size of diamond formed is in micro-scale and the diamond grains are randomly oriented. Those microcrystalline diamond thin films usually have rough surface, too rough for many applications In addition, the polishing of diamond surface through mechanical and chemical methods

is rather difficult and costly due to diamond's high hardness and good chemical stability. Therefore, it is desirable to directly deposit highly smooth diamond thin films. It has been found that the surface smoothness of diamond thin films can be increased significant by decreasing diamond grain size from micro-scale to nano-scale, thus the synthesis of NCD thin films has been attracting growing interests in recent years.

A high nucleation density is necessary to synthesize smooth NCD thin films. Some researcher [95-97] focused their attentions on the improvement of diamond nucleation density through different pre-treatments on substrate surface. A number of different deposition techniques, including remote microwave plasma [98], DC arc [95, 99-100], HFCVD [101], RF plasma [102], MPECVD [95-97, 103-104], carbon sputtering [105] and ECR [106] have been employed for NCD thin films deposition. It has been found that increasing CH_4 content [107-110] and addition of N_2 [110-114] or O_2 [98, 114, 115] to CH_4-H_2 gas mixture is favorable for NCD thin film deposition. Inert gas Ar and CH_4 mixtures with or without hydrogen have been also developed by Gruen et al. in the Argonne National Laboratory to produce NCD thin films and UNCD (grains are 3-5 nm in size) thin films [115-121] in which carbon dimer, C_2, is suggested to play a crucial role in nucleation and growth of NCD or UNCD thin films [117].

2.8 Adhesion of Diamond Thin Films

2.8.1 Fundamental Information on Adhesion of Thin Films

According to ASTM D907, adhesion is defined as "the state in which two surfaces are held together by interfacial forces which may consist of valences forces or interlocking forces or both". It indicates that adhesion strength depends on the chemical and mechanical aspects of the interfacial region. For practical applications,

coatings or thin films must have sufficient adhesion to prevent from being peeled off or failing under service conditions [122].

2.8.2 Factors Influencing the Adhesion of Diamond Thin Films

2.8.2.1 Interface Structures

When the diamond nucleation density/rate on the substrate surface is too low, voids may form at the interface between diamond thin films and substrate. These voids are the main sites for interfacical crack initiation. In addition, the existence of interfacial voids accelerates the crack propagation and induces the failure of brittle CVD diamond thin films. Therefore, the formation of a dense voids-free interface with intimate contacting between diamond thin film and substrate surface is very important for achieving high adhesion of diamond thin film to substrate.

2.8.2.2 Interface Chemical Aspects

It has been reported that the existence of Co as a binder in WC-Co hard alloys induces poor adhesion of diamond coatings on the alloys [123-125]. The reason is that transition metals such as Co, Ni, and Fe catalyze the formation of graphitic carbon, thus a layer of graphitic carbon is formed on the alloy surface prior to the nucleation of diamond. This graphitic layer is weak and thus results in poor diamond thin film adhesion [125-128] to substrates. Hence, it is important to avoid weak interfacial layer formation in order to achieve high adhesion of diamond thin films. In order to achieve high adhesion of diamond thin films, direct chemical bonding between the C atoms in diamond and the atoms in the substrate is desirable.

2.8.2.3 Mechanical Locking

In addition to chemical bonding, mechanical locking can also significantly increase the adhesion of diamond thin films. Figure 2.11 schematically shows the formation of mechanical interlocking on the substrate surface [129]. The interlocking action can occur with two contact modes as shown in Figure 2.11, depending on the

relationship between the diamond inter-growth grains and the adjacent substrate grains. For the first mode, the resistance to spallation/peeling is generated by the substrate grains, thus the substrate strength decides the magnitude of the detachment force. For the second mode, the resistance to peeling is dependent on the friction force between the diamond grains and the contacting substrate grains. It is desirable to implement conditions in which the first mode would be dominant in order to increase adhesion. The first mode of interlocking can be enhanced through proper seeding substrate with diamond powders prior to diamond deposition and optimizing the substrate roughness [129]. Roughing substrate surface creates surface cavities that trap seeding diamond particles and barriers for crack propagation at interface.

2.8.3 Measurement of Adhesion of Diamond Thin Films

Quantitative measurement of the adhesion strength of thin films is of practical importance and desirable. In order to measure the adhesion, a controlled load is usually applied to produce a critical stress at the interface to initiate interfacial failure. Depending on the way to apply load, different test methods have been developed to access diamond coating adhesion. These methods include pull-off, scratching and indentation testing [130].

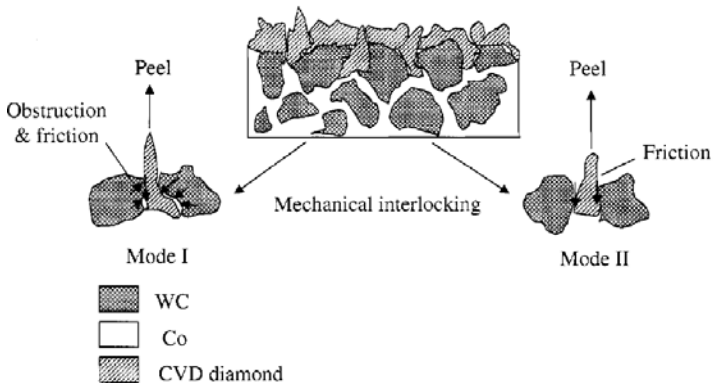

Figure 2.11 The two modes of mechanical interlocking on the surface of WC-Co. Mode (I): resistance to peeling is offered by combined friction and obstruction forces. Mode (II): resistance to peeling is offered by friction forces [129].

The pull-off testing is quantitative and accurate if the pulling force can be calibrated well to the surface normal of the testing samples. The main difficulty encountered with this method is that the applied stress is limited by the strength of the adhesives, which is normally lower than 90 MPa. Thus, the method can only be used to test low adhesion coatings. For most diamond coatings, adhesive usually fails prior to the failure of interface [130].

In scratching tests, a loaded diamond (or WC in some cases) tip is drawn across the surface of the testing film with different loads and monitored by acoustic emission and/or electrical resistance and/or friction force measurement. Obvious acoustic emission, and sudden resistance and/or friction coefficient changes are used to characterize the interfacial failure and the critical load, at which the interfacial failure occurs, is used to evaluate the film adhesion. The resulting groove can also be examined using microscopies. At loads below the critical load, a smooth groove is usually observed whereas at or above a critical load, ragged edges appear on the groove, indicating the detachment of thin film. However, the high hardness of the diamond film may lead the cleavage of the scratching tip, resulting in loss of repeatability and even breaking of tips.

In indentation tests, a loaded micro/nano diamond (or WC in some cases) tip is impressed into the thin films without transverse movement. The impressions are observed by microscopes. Interfacial failure is characterized by film delamination. A critical load is the load at which film delamination initiates. Indentation tests reduce considerably the possible damage to the indenter tip and therefore are more suitable to analyze the adhesion of diamond coatings. The indentation method has been applied by several researchers [131-142] to qualitatively evaluate the adhesion of diamond thin films. Both Rockwell and microhardness indentation tests have been employed. The numerous applications of these two indentation methods are due to the ease of the

process. A few seconds are enough to finish a single test and the sample can be readily examined under a scanning electron microscope.

2.9 Are Carbides Good Substrate Materials for Diamond Nucleation?

As aforementioned, nucleation is very important for both the synthesis and application of diamond thin films. Up to now, Si has been the most widely used substrate material for diamond deposition due to its acceptable diamond nucleation density and relatively high adhesion of diamond thin film on it. It has been found that the chemical interactions between the substrate surface and the deposition species from the gas phase determine the incubation time for diamond nucleation [80]. Based on carbon/substrate interactions, substrate materials for diamond growth can be classified into following three groups:

1) Group 1 e.g. diamond and cubic BN. The materials have little or no reaction with carbon and the solubility limit of carbon in them is very low. It has been found that nucleation and growth of diamond on them are easy and fast.
2) Group 2 e.g. Fe, Ni, and Co, which are widely used as catalyst for diamond formation under HPHT conditions. The materials dissolve carbon with noticeable concentration and the diffusivity of C in them is very high. It has been found that these materials catalyze the formation of graphitic carbon under CVD conditions which results in poor adhesion of diamond thin films on them.
3) Group 3 e.g. Ti, Zr, Hf, Nb, Ta, Cr, MO, W, Si. The materials react with carbon to form stable carbide layers during the initial CVD processing and diamond nucleates and grows on the carbide interlayers.

It indicates that low diffusivity and low solubility of carbon are required for substrate materials in order to synthesize diamond thin films with high adhesion.

Based on this, carbides might be good substrates for diamond deposition. Unfortunately, the melting point of conventional carbides, such as SiC and TiC, is very high, around 3000 °C, thus are difficult to be sintered without metallic binding additives, which may catalyze the formation of graphite structure. Besides, the conventional carbides are very hard and brittle, thus are difficult to be machined to complicated shapes. These disadvantages significantly limit the carbides to be used as substrates for diamond thin film deposition. It is interesting that a ceramic-metallic material, Ti_3SiC_2, with good sinterability and machinalibity, has been recently synthesized.

2.9.1 What is Ti_3SiC_2?

According to its molecular formula, Ti_3SiC_2 is a carbide and belongs to ceramics. It is the representative of a novel "$M_{n+1}AX_n$" phase, where M is an early transition metal, A is an A-group element (mostly IIIA and IVA) and X is either C and/or N. Figure 2.12 shows the unit cell of Ti_3SiC_2 as determined by Jeitschko and Nowotny [143]. The structure of Ti_3SiC_2 is hexagonal with a of 3.07 Å and c of 17.67 Å, composed of Ti-C layers interleaved with layers of Si. One unit cell has 6 Ti atoms, 2 Si atoms and 4 C atoms, and the theoretical density of Ti_3SiC_2 is 4.525 g/cm^3.

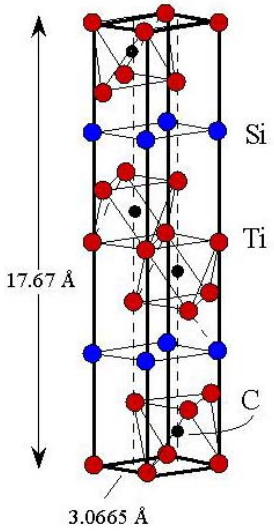

Figure 2.12 Ti_3SiC_2 unit cell [143].

Table 2.4 lists some typical properties of Ti_3SiC_2. Like ceramics, its density is low, and its melting point is high. Like metals, it is thermally and electrically conductive. Most importantly, the hardness of Ti_3SiC_2 is much lower compared with other traditional ceramics such as TiC and WC. Therefore, it can be readily machined into different complex shapes, as shown in Figure 2.13. Besides, it has high thermal stability (stable up to at least 1700 $^{\circ}C$ in vacuum and inert gas atmosphere) and good corrosion resistance. The reported combination of high-temperature strength and oxidation resistance of Ti_3SiC_2 with silicidation is even better than the widely used Ni-based superalloys (Figure 2.14), therefore, it holds great potentials for many high-temperature applications, including in jet engines, automobile engines, and petrochemical industry.

Table 2.4 Typical properties of Ti_3SiC_2.

	Ti_3SiC_2	TiC	WC	Ti	Ni
Density (g/cm^3)	4.53	4.94	15.7	4.5	8.88
Melting Point ($^{\circ}C$)	>3000	3065	2800-2870	1650-1670	1455
Hardness, Viker's	400-600	3200	2200	40	75
Young's Modulus (GPa)	283-320	448-451	669-696	116	207
Thermal Conductivity at Room Temperature ($W \bullet m^{-1} \bullet K^{-1}$)	30-45			17	60
Coefficient of Thermal Expansion ($10^{-6}K^{-1}$)	8-12	7.7	5.2	8.9	13.1
Electrical Resistivity (10-6 Ω•cm)	22-50	180-250	53-80	55.4	6.4

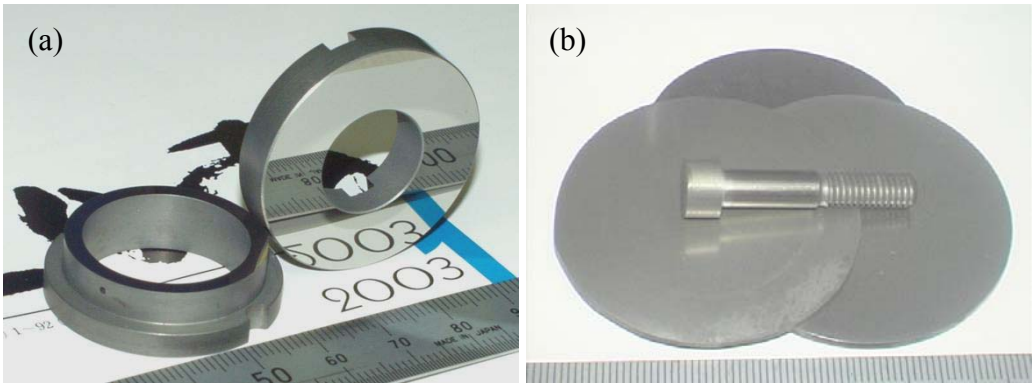

Figure 2.13 Good machinability of Ti_3SiC_2. (a) mirror-polished Ti_3SiC_2 parts, (b) plates and bolt made from Ti_3SiC_2. (Photograph courtesy of Dr. Z.M. Sun, AIST, Japan.).

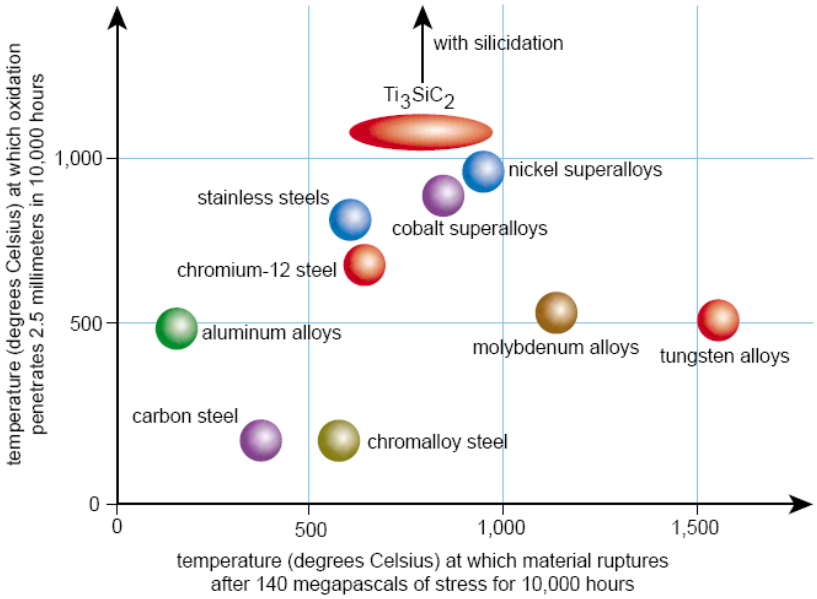

Figure 2.14 High-temperature strength and oxidation resistance of some materials. Materials toward the right resist breakage under stress at high-temperatures; materials toward the top can reach high-temperatures before oxidation attacks the material surface. Ti_3SiC_2 exceeds all current materials for oxidation resistance and approaches the Ni-based superalloys in strength [144].

Scanning electronic microscopy (SEM) analysis indicates that Ti_3SiC_2 has nanolayered microstructure as shown in Figure 2.15 [145], therefore it has been refereed as a nanolaminate material. Due to its nanolaminate microstructure, the

mechanical properties of Ti_3SiC_2 are different with those of traditional ceramics. For example, the fracture morphology of Ti_3SiC_2, like that of deformed wooden materials, is observed with bundles of ligaments forming in the spreading crack, as shown in Figure 2.16 (a) [144]. These ligaments are crucial to endow the material with rather high fracture toughness. And at high temperature, it can be deformed plastically (Figure 2.16 (b)) [146].

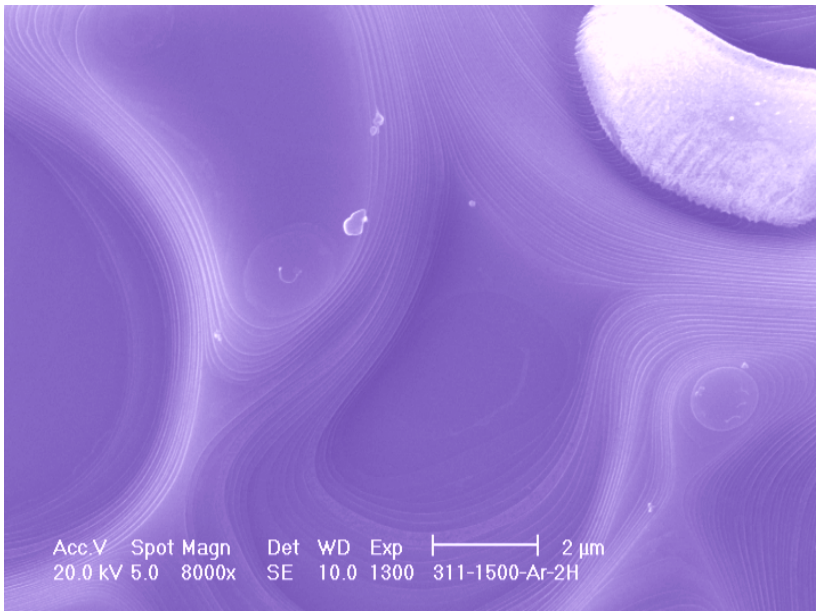

Figure 2.15 Nanolaminate microstructure of Ti_3SiC_2 (The image was got from the surface of an as-sintered sample through a pressureless sintering process by using a field emission SEM).

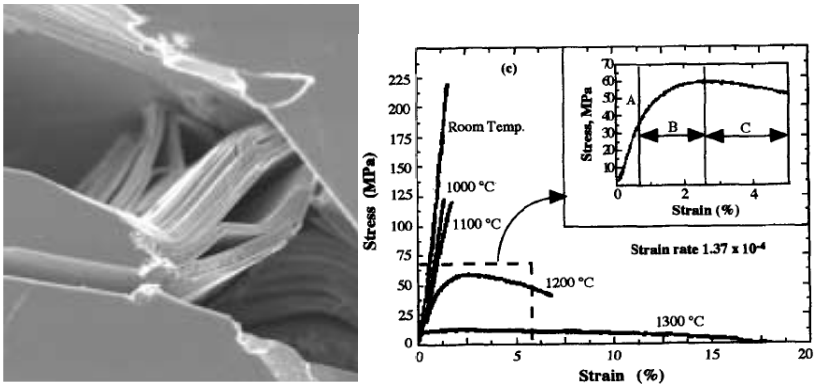

Figure 2.16 (a) Fracture of Ti_3SiC_2 [145]; (b) The stress-strain curves for Ti_3SiC_2 at different temperatures [146].

2.9.2 The Synthesis of Ti_3SiC_2

Ti_3SiC_2 was firstly synthesized via chemical reaction in 1967 [143], and then by CVD in 1987 [147]. After that the research progress on Ti_3SiC_2 seemed to be very slow until 1996. In 1996, the first successful synthesis and characterization of high purity Ti_3SiC_2 bulk material was reported by Barsoum et al, through reactive hot-pressing Ti, graphite and SiC powders at 40 MPa and 1600 $^{\circ}$C for 4 h [148], and thereafter, various methods, such as, HIP or SHS-HIP [149-150], reactive sintering [152-158], have been employed for the synthesis of bulk Ti_3SiC_2 using Ti/Si/C [149, 150, 152-157], Ti/SiC/C [151] or Ti/Si/TiC [158] powders. The purity of Ti_3SiC_2 is different depending on the processing conditions and TiC has been frequently reported as the impurity phase in the final product.

Dr. Sun's group at the AIST, Japan reported that high purity Ti_3SiC_2 (about 99 vol.%) can be synthesized from Ti, Si, and TiC powders with the molar ratios of 2:2:3 using pulse discharge sintering (PDS) technique at relative lower temperature in short time (1300 $^{\circ}$C for about 15min) [159]. Later they found that the addition of Al in the starting powder mixture may enhance the formation of Ti_3SiC_2 by decreasing the optimal reaction temperature and increasing the formation rate [160, 161].

2.9.3 Disadvantages of Ti_3SiC_2 for Application

As aforementioned, the hardness of Ti_3SiC_2 is much lower compared with that of the conventional ceramics, such as TiC and WC, which allows much better machinability. However, its low hardness also results in relatively high friction coefficient (about 0.82 against stainless steel) and low wear resistance [162], which may present problems for some applications. Therefore, the successful deposition of hard thin films on its surface would be desirable and of great importance in order to improve its tribological properties.

CHAPTER 3
EXPERIMENTAL EQUIPMENTS AND SUBSTRATE MATERIALS

A MPECVD reactor and a HFCVD reactor in the Plasma Physics Laboratory of the University of Saskatchewan, purchased with Prof. Akira Hirose's CFI grant, were employed for the CVD of diamond-related materials in this thesis. In this chapter, a description of these two CVD reactors is given. After deposition, thin films were characterized by Scanning Electronic Microscopy (SEM), Atomic Force Microscopy (AFM), Microhardness indentation, Raman spectroscopy, as well as synchrotron-based Near Edge X-ray Absorption Fine Structure spectroscopy (NEXAFS). In this chapter, principles and descriptions of these main analytical techniques are also given.

3.1 CVD Reactors

3.1.1 MPECVD Reactor

Figure 3.1 shows a picture of the MPECVD reactor (Plasmionique, MW-PECVD 1250UOS) used in this thesis. It is an ASTEX-type 2.45 GHz single mode cavity reactor, consisting of a microwave source, a vacuum system, a gas injection control box, a manual control cabinet, and a computer control system. The upper output power limit of the microwave source is 1.2 kW. The inner diameter of the vertically oriented stainless steel vacuum chamber is 140 mm. There are three windows on the wall of the vacuum chamber, which are used to check samples during deposition. Inside the vacuum chamber, there is a stainless steel substrate holder with a diameter of 122 mm, being concentric in the vacuum chamber. The substrate holder is electrically floating, so a biasing voltage can be applied on it. Beneath the sample holder, there is a thermal couple to measure the temperature during deposition. To

minimize the reflected microwave power, the distance between the substrate and the plasma ball can be adjusted through the vertical movement of the sample stage. Three gas lines were arranged to introduce H_2, CH_4 and N_2 into the vacuum chamber for deposition. The process parameters, including gas composition/flow rate and the microwave output power can be preset through the manual control cabinet. Normally a gas mixture of H_2 with a flow rate of 99 sccm and CH_4 with a flow rate of 1 sccm is used for diamond deposition at a pressure of 30 Torr (4 kPa) and microwave output power below 1.1 kW.

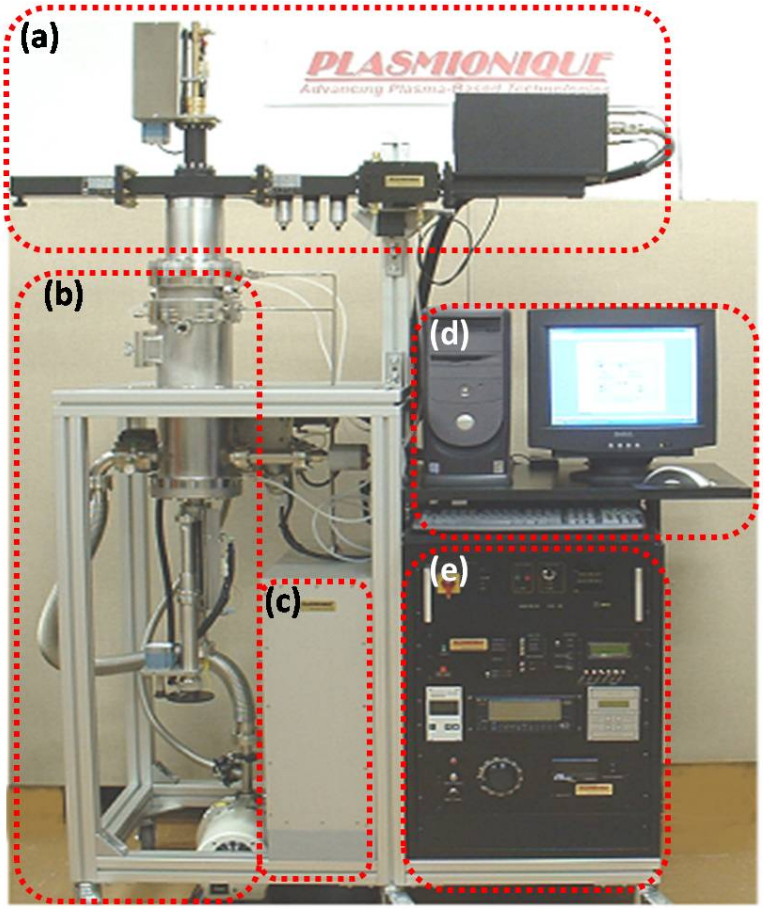

Figure 3.1 A picture for the MPECVD reactor: (a) microwave system, (b) vacuum system, (c) gas injection control box, (d) computer control system, and (e) manual control cabinet.

3.1.2 HFCVD reactor

Figure 3.2 shows a picture of the HFCVD system used in the present study. The main components of this HFCVD system include a vacuum chamber, a pumping system, a gas supply system and an electrical system. The vacuum chamber is made from a cross-shaped glass tube with a diameter of 150 mm. The pumping system includes a rotary pump and a diffusion pump. The pressure in the chamber can be adjusted by a needle valve in the pumping line. A two-channel gas flow controller is used to control the flow rate of the input gases, normally H_2 and CH_4. Then the gas mixture is guided through a stainless tube directly to the top of the vacuum chamber. The hot filament in the reactor is a tungsten coil with a diameter of 4 mm and a length of around 40 mm. The diameter of the tungsten wire used is 0.3 mm. The tungsten wire is connected to a power source and is ohmically heated to provide the thermal energy for dissociation of the processing gases. The substrate temperature during deposition is measured by using a thermal couple mounted right behind the sample holder. The distance between the sample holder and hot filament can be changed manually to meet the deposition requirement.

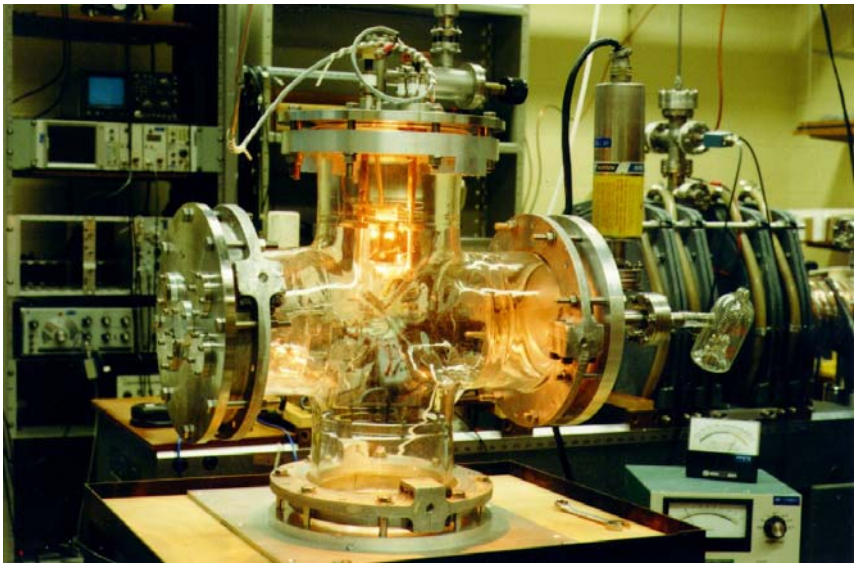

Figure 3.2 HFCVD reactor in the Plasma Physics Laboratory for the present thesis.

3.2 Main Analytical Facilities

3.2.1 SEM

SEM is one of the most widely used surface characterization techniques. It images the sample surface by scanning it with a high-energy electron beam. Figure 3.3 is a simple schematic drawing of an SEM. Electrons are thermionically emitted from an electron gun fitted with a filament cathode. Tungsten is normally used as the filament in thermionic electron guns, its high melting point and low vapor pressure allowing it to be heated for the easy electron emission. Other types of electron emitters include lanthanum hexaboride cathodes, which can be used in a standard tungsten filament SEM if the vacuum system is upgraded, and field emission guns, which is of the cold-cathode type using single crystal tungsten emitters or the thermally-assisted Schottky type using zirconium oxide emitters. When electrons pass through the condensing lens, made by a coil of current-carrying wire, they are collimated into a small beam by a force from a magnetic field. After the condensing lens, there is another coil which scans the beam of electrons over the sample. The electron beam is finally focused to a small spot on the sample surface by a final objective lens. All the SEM components are contained inside a vacuum chamber to minimize electron-gas interactions.

When the high-energy electrons interact with the atoms at or near the sample surface, signals that contain information about the sample's surface topography and composition can be produced. The signals produced by an SEM include, for example, Secondary Electrons (SE), Back Scattered Electrons (BSE), characteristic x-rays, and Transmitted Electrons (TE). Different specialized detectors are used to detect and collect these different types of signals. In the most common or standard detection mode, Secondary Electron Imaging (SEI), SEM can produce very high resolution, up to 1 nm, images of a sample surface. Due to the way these images are created, SEM

micrographs have a very large depth of field yielding a characteristic three-dimensional appearance useful for understanding the surface structure of a sample. A wide range of magnifications is possible, generally from 25 times (equivalent to that of a powerful hand-lens) to 250,000 times, approximately 250 times the magnification limit of the best optical microscopes. BSE are electrons that are reflected from the sample by elastic scattering. The intensity of the BSE signal is strongly related to the atomic number (Z) of the chemical elements in specimen, hence, BSE images can provide elemental distribution information in a sample. Characteristic X-rays are emitted when the electron beam removes an inner shell electron from the sample, causing a higher energy electron to fill the shell and release energy. These characteristic x-rays are used to identify the composition and measure the abundance of elements in the sample.

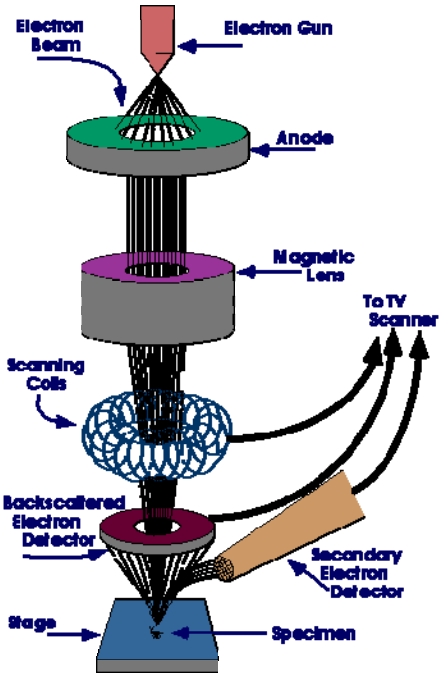

Figure 3.3 A schematic drawing of an SEM [163].

Since the SEM utilizes vacuum conditions and uses electrons to form an image, special sample preparations must be took into account. All water must be removed from the samples because the vaporization of water would damage the vacuum. And

all the samples must be electrical conductive to prevent the discharging. Therefore, all samples of non-metals with high resistivity need to be made conductive by covering the sample surface with a thin layer of conductive materials. Normally the sputtered carbon or golden thin films can be used to improve the sample conductivity.

In this thesis, a JEOL 840A SEM in the Department of Geological Science, University of Saskatchewan, was used to characterize the surface morphology of the resulted samples. Figure 3.4 shows the picture of this SEM. The maximum theoretical resolution of this SEM is 10 nm. Its accelerating voltage can be variable from 200 V to 40 kV. The probe current can be adjusted in the range of 1×10^{-8} to 1×10^{-12} Amps. The working distance can be from 8 to 48 mm. Theoretically, its magnification can be from 10 to 300,000 times. In the present study, an accelerating voltage of 20 kV and a working distance of 8 mm are normally applied.

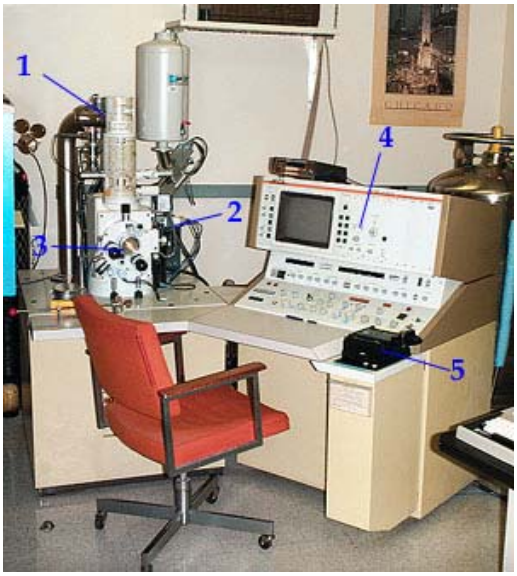

Figure 3.4 The JEOL 840A SEM used in the present study: (a) acceleration potentials; (b) secondary electron and backscattered electron detectors; (c) sample chamber; (d) control panel.

3.2.2 AFM

AFM, invented in 1986, is a high-resolution scanning probe microscope. Instead of using an electrical signal, AFM relies on forces between the atoms in the

tip and in the sample. Its resolution can down to several angstroms, much better than that of SEM and optical microscope. It is one of the most widely used tools for imaging, measuring and manipulating matters at the nano-scale. The information is collected by "feeling" the sample surface with a mechanical probe. Figure 3.5 shows the schematic of a typical AFM equipment. It is composed of a micro-scale cantilever with a sharp tip (probe) at its end which is used for scanning the specimen surface. The cantilever is typically made from silicon or silicon nitride with a tip radius of curvature on the order of nanometers. When the tip is brought into proximity of a sample surface, forces between the tip and the sample lead to a deflection of the cantilever according to Hooke's law. The deflection can be measured using a laser spot reflected from the top surface of the cantilever into an array of photodiodes.

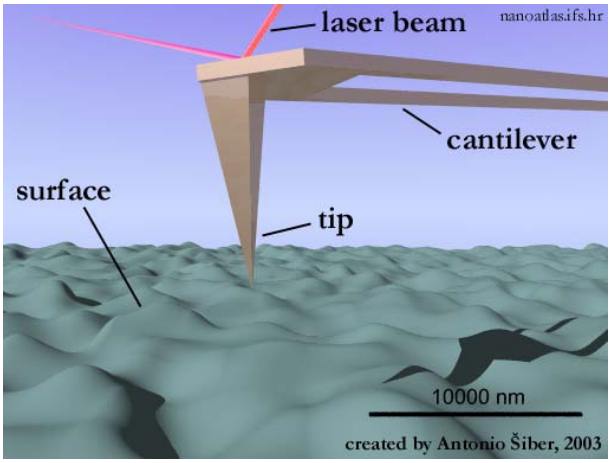

Figure 3.5 A schematic for AFM setup [164].

AFM can operate in three modes: contact mode, where the tip is in constant contact with the sample; non-contact mode, where the tip is slightly above the sample; “tapping” mode, where the tip is intermittently tapping gently on the sample. The latter approach works well with soft samples that might be harmed if the tip stayed in contact. In addition to imaging the topography of a sample, AFM can measure the friction between the tip and the sample and the elasticity of a sample.

AFM has several advantages over SEM. In addition to its higher resolution as mentioned, unlike the SEM, which provides a two-dimensional image of a sample, AFM provides a true three-dimensional surface profile. Additionally, samples viewed by AFM do not require any special treatments (such as metal/carbon coatings) that would irreversibly change or damage the sample. Moreover, AFM can work well in ambient air or even a liquid environment, which makes it possible to study biological macromolecules and even living organisms, whereas SEM needs an expensive vacuum environment for proper operation.

A disadvantage of AFM compared with the SEM is that the image size of AFM is much smaller. The SEM can image an area on the order of millimetres by millimetres with a depth of field on the order of millimetres. The AFM can only image a maximum height on the order of micrometres and a maximum scanning area of around 150 by 150 micrometres. Another inconvenience of AFM is that an incorrect choice of tip for the required resolution can lead to image artifacts. In addition, AFM could not scan images as fast as an SEM, requiring several minutes for a typical scan, while a SEM is capable of scanning at near real-time (although at relatively low quality) after the chamber is evacuated.

In this thesis, AFM measurements were carried out on a PicoSPM instrument (Molecular Imaging, Tempe, AZ) at the Saskatchewan Structural Science Center (SSSC), University of Saskatchewan, operated in contact modes.

3.2.3 Raman Spectroscopy

Raman spectroscopy is a spectroscopic technique used in condensed matter physics and chemistry to study vibrational, rotational, and other low-frequency modes in a system [165]. It is a popular non-destructive, ambient probing tool to characterize the structure of materials. Figure 3.6 shows the energy level diagram indicating the states involved in the Raman signal. When a light quantum $h\nu_0$ hits a surface, an

elastic scattering process, Rayleigh scattering, in which a photon keeps its energy $h\nu_0$ and an inelastic process, in which a photon alters its energy by a vibrational energy of $h\nu_s$, occur simultaneously although Rayleigh scattering occurs with much higher probability. The inelastic process is called Raman scattering and the energy of a Raman scattered photon is equal to $h\nu_0 \pm h\nu_s$. Because the atoms in the excited state is much less than that in the ground state at ambient temperature according to Boltzmann's law, the probability to excite ground-state atoms to a vibrationally excited state is much higher than to receive the decay energy from the vibrating atoms. Hence, the emitted photons having energy of $h\nu_0 - h\nu_s$ are more prevalent than that with an energy of $h\nu_0 + h\nu_s$. The Raman lines corresponding to the photons with an energy of $h\nu_0 - h\nu_s$ are referred to as the Stokes lines whereas the higher energy lines ($h\nu_0 + h\nu_s$) are called the anti-Stokes lines. As the intensities of the anti-Stokes lines are much lower, only the Stokes lines are usually recorded in the Raman spectrum [166, 167].

Typically, a sample is illuminated with a laser beam. Light scattered from the illuminated spot is collected with lens and sent through a monochromator. Wavelengths close to the laser line, due to elastic Rayleigh scattering, are filtered out while the rest is dispersed onto a detector.

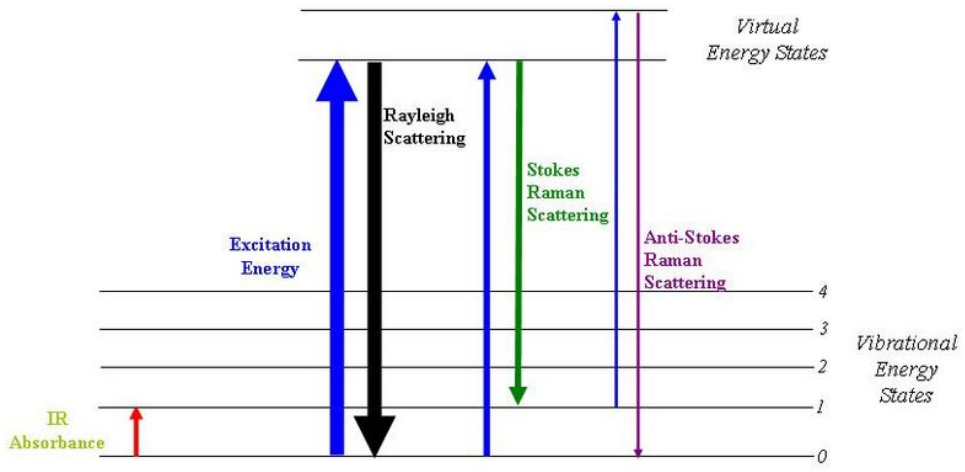

Figure 3.6 Energy level diagram showing the states involved in Raman signal [165].

Raman spectroscopy is an effective technique to investigate the detailed bonding structure of carbon materials, e.g. diamond and graphite. Figure 3.7 presents the typical Raman spectra for various carbon-based materials [168] in the range of 1000 to 1800 cm^{-1}. The sharp peak at around 1332 cm^{-1} with Full Width at Half Maximum (FWHM) less than 2 cm^{-1} is the signature for high purity microcrystalline diamond crystallites. With the decrease in the diamond grain size, the FWHM of the 1332 cm^{-1} peak may be widened. The characteristic peak for single crystal graphite locates at around 1580 cm^{-1} (G-band), while for polycrystal graphite, another peak centered at 1350 cm^{-1} (D-band) is also observable.

Under the typical CVD conditions, both diamond and graphite may appear in the synthesized thin films, and Raman has been the primary tool to distinguish between the sp^2 graphite structure and sp^3 diamond structure. In the present thesis, The Raman spectra were obtained using a Renishaw micro-Raman system 2000 spectrometers at the SSSC, University of Saskatchewan, operated at a laser wavelength of 514.5 nm generated by an argon laser. The spot size was approximately 1 μm. The scanning range was typically from 1100 to 1700 cm^{-1}, where the characteristic peaks for both graphite and diamond structures locate.

However, Raman spectroscopy also suffers from several drawbacks, especially for the quantitative characterization of nanostructured carbon materials. One main drawback is that the difference in the Raman cross sections for sp^2 graphitic features and sp^3 diamond hybridized carbon is large. The Raman cross section for sp^2 carbon can be up to 233 times higher than that for sp^3 diamond when a 514.5 nm wavelength argon ion laser is employed [21], the spectra observed is thus completely dominated by the scattering from the sp^2 carbon when the amount of sp^2 carbon is over 5% [169]. A second shortcoming of the Raman measurement is its dependence on the long range order parameter of the materials. The Raman incident photon wavelength is on the

order of microns, which leads to strong crystal size dependence and a critical crystallite size.

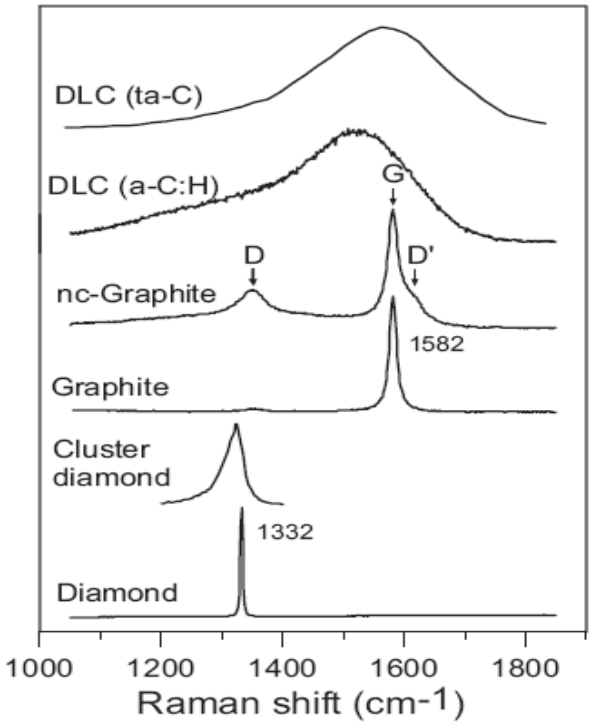

Figure 3.7 Characteristic Raman Spectra for some carbon-based materials: diamond (sp^3 bonded), single crystal graphite (sp^2 bonded); polycrystalline graphite (disordered sp^2 bonded); a-C:H (DLC, disordered sp^3*and* sp^2 bonded); and ta-C (DLC, disordered sp^3*and* sp^2 bonded). The spectra were excited by the λ=514.5 argon ion laser [168].

3.2.4 Synchrotron-Based NEXAFS

A synchrotron is a source of brilliant light that can be used to collect information about the structural and chemical properties of materials at the molecular level [170]. In the synchrotron, electrons are accelerated by using powerful electro-magnets and radio frequency waves to relativistic speeds. The high speed electrons are confined by bending magnets to travel within a storage ring. While travelling in the circular path in the storage ring, they emit a very brilliant, low divergence light. Different spectra of light such as Infrared, Ultraviolet or X-rays can be directed to samples to study their various structures.

NEXAFS is a technique used to probe the local partial unoccupied electron density of states in an atom and thus their chemical bonding states. Figure 3.8 shows the schematic of the photo-absorption and relaxation processes occurring in a NEXAFS experiment [171]. There are several distinctive processes that can occur during the generation of the NEXAFS spectrum [171]. The incident photon beam excites an electron from a core state into an unoccupied electronic state and the subsequent relaxation of the excited molecule results in the ejection of either an Auger electron or an energetic photon with the cross-section of each process being atomic number dependent [172]. As illustrated in Figure 3.9 [171], it is possible to monitor each of these processes. And thus there are several ways of obtaining a NEXAFS spectrum. By preparing thin samples, it is possible to monitor the transmitted photons in order to deduce the number absorbed. Other methods quantify the NEXAFS photo-absorption by detecting the processes that occur following photo-absorption. Total electron yield (TEY), partial electron yield (PEY) and Auger electron yield (AEY) techniques measure the quantity of emitted electrons with different electron energy discrimination regimes, whereas fluorescence yield (FY) techniques measure the ejected energetic photons. Electron yield is surface sensitive and thus gives information ranging from 2 to 10 nm in the surface. The detection depth increases as atomic number decreases, so it is more useful for light elements. Compared with electron yields, FY is more bulk sensitive. However, "self-absorption" will distort the data for thick samples.

NEXAFS is sensitive to short range order and local chemical bonding. In addition, it has similar cross section for different carbon allotropes, and thus more suitable to elucidate chemical bonding and to estimate sp^2 carbon concentration in carbon materials, especially in NCD films [117, 169]. In the present thesis, the NEXAFS experiments were performed at the High Resolution Spherical Grating

Monochromator (SGM) beamline at the Canadian Light Source Inc. (CLS), University of Sasktchewan. NEXAFS were recorded in both total electron yield (TEY) and fluorescence yield (FY). TEY was recorded by monitoring the sample current, and FY was measured with a MCP (multi-channel plate) detector.

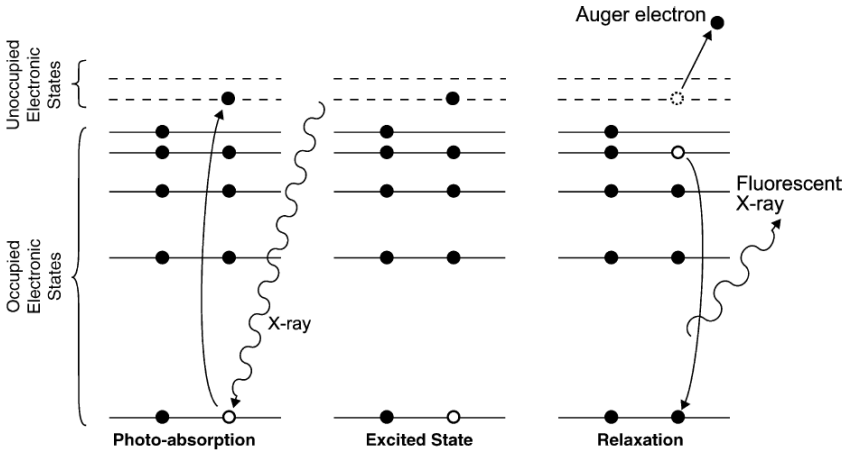

Figure 3.8 The schematic of the photo-absorption and relaxation processes occurring in a NEXAFS experiment [171].

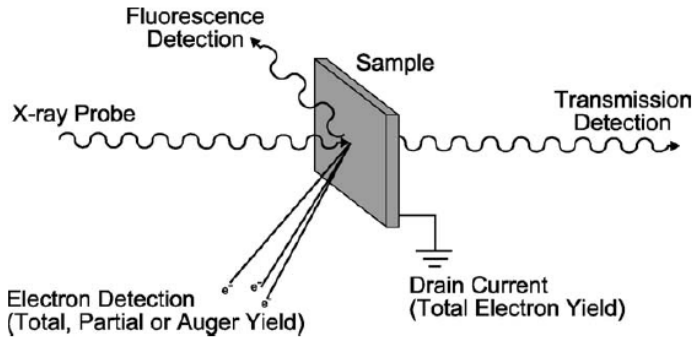

Figure 3.9 Schematic of the possible measurement techniques for NEXAFS spectroscopy. The absorption process depicted in Figure 3.8 cannot be detected directly and so the NEXAFS signal must be detected through either the absence of the absorbed photons in the transmitted X-rays (transmission detection) or through the particles ejected during the relaxation process that follows (fluorescence detection or electron detection). Energy discrimination allows the electron detection technique to be broken down into total (TEY), partial (PEY) and Auger (AEY) electron yield detection schemes [171].

3.3 Substrates for Diamond Deposition

Ti_3SiC_2 slices of 5×10×2 mm were cut by electric-discharge machining from bulk Ti_3SiC_2 prepared by pulse discharge sintering (PDS) [161] and ground with SiC papers down to grits of 600 followed by the ultrasonic cleaning in acetone. The Ti_3SiC_2 samples are single phase, as indicated by the X-ray diffraction (XRD) (Figure 3.10). P-type (100)-oriented mirror polished Si, the most commonly used material for diamond deposition, was also used as substrate in the present study for comparison.

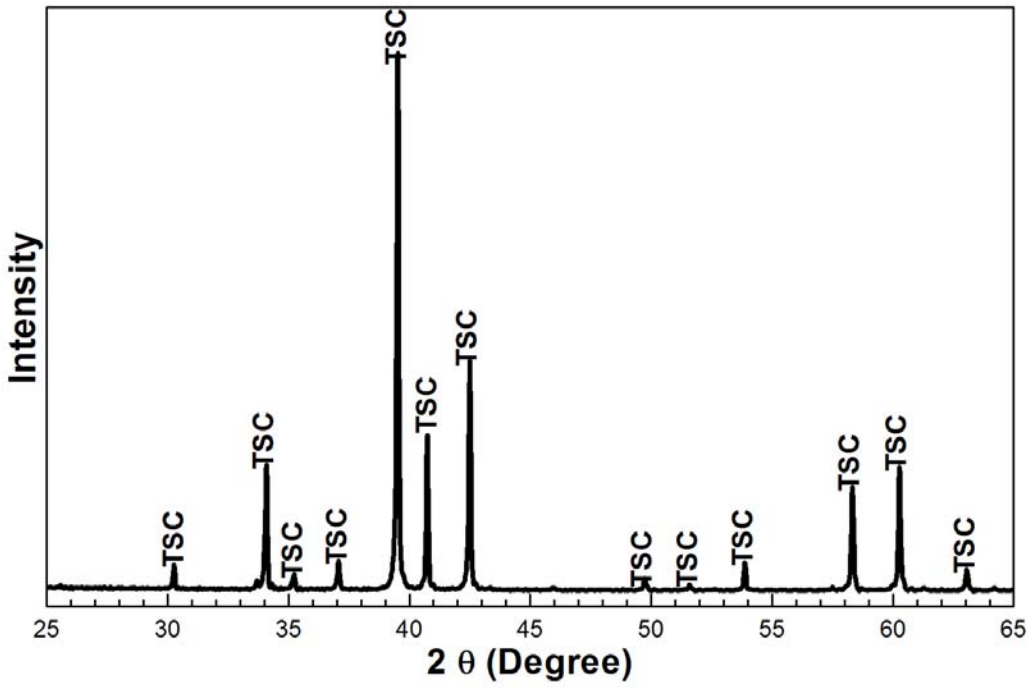

Figure 3.10 XRD profiles for Ti_3SiC_2 substrate used in the present thesis.

Prior to deposition, some substrates were ultrasonically scratched in a solution containing diamond powders. Figure 3.11 shows the morphology of Ti_3SiC_2 substrate after diamond scratching. The small particles attached on the substrate surface are diamond, which can serve as the seeds for the subsequent diamond nucleation and growth.

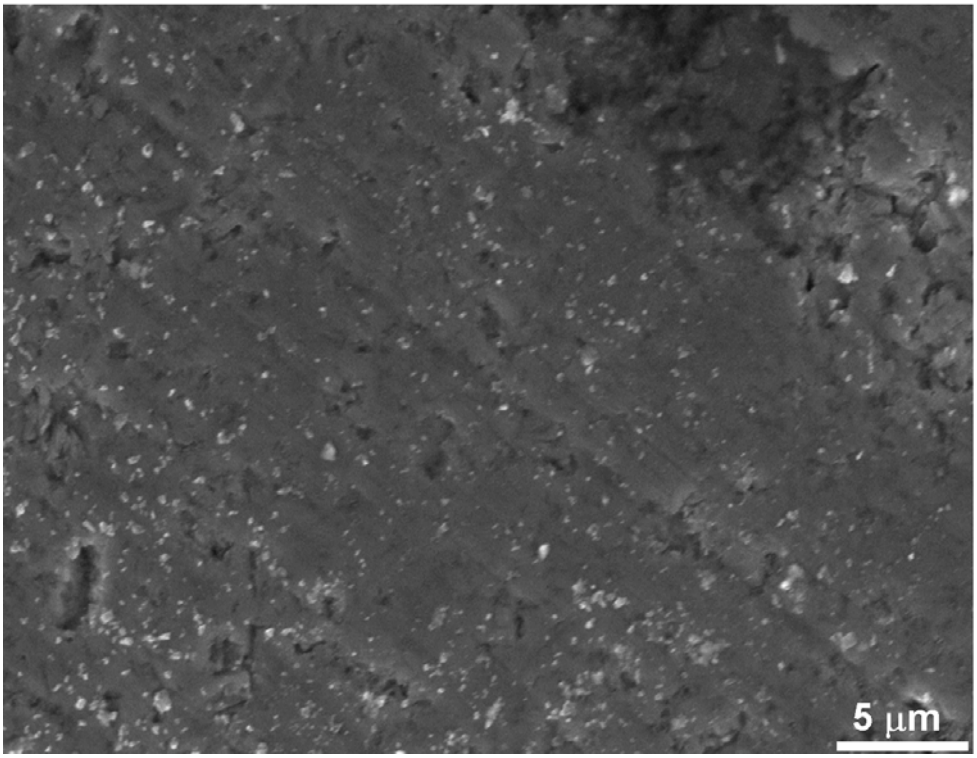

Figure 3.11 Morphology of Ti_3SiC_2 substrate after diamond scratching.

CHAPTER 4
NUCLEATION AND GROWTH OF DIAMOND ON TI_3SIC_2 BY MPECVD *

4.1 **Introduction**

Few studies have been reported relating diamond with Ti_3SiC_2. Recently, Ti_3SiC_2 was found to be a good bonding material for synthesis of polycrystalline diamond composite by HPHT process [173]. Diamond coated Ti_3SiC_2 samples showed very low friction coefficient (0.01) against stainless steel [174]. These results suggest that it is promising to obtain strong bonding between diamond and Ti_3SiC_2. However, as well as we know, no detailed information about diamond nucleation and growth on Ti_3SiC_2 has been reported up to now. Here, for the first time, we report the nucleation and growth of diamond on Ti_3SiC_2 slices by MPECVD.

To perform the experiment, some of Ti_3SiC_2 (with thickness around 2 mm) and P-type (100)-oriented mirror polished Si (with thickness of 0.66 mm) substrates were ultrasonically scratched in a solution containing micrometer-sized diamond powders, the vacuum chamber of the MPECVD was pumped down to a pressure of 6.65×10^{-4} Pa using a turbo-molecular pump and then filled with a gas mixture of H_2 and CH_4. The flow rate of H_2 and CH_4 were 99 sccm and 1 sccm, respectively. The working gas pressure was maintained at 4 KPa. Microwave powers from 600 to 800 W were applied for the deposition. During the deposition, samples were heated only by plasma. The substrate temperature during the deposition was typically around 480 $^{\circ}$C at 800 W.

4.2 Results and Discussions

4.2.1 Nucleation of Diamond

Figure 4.1 shows the typical SEM surface morphologies of Ti_3SiC_2 and Si substrates with and without diamond scratching after 20 min deposition at 800W

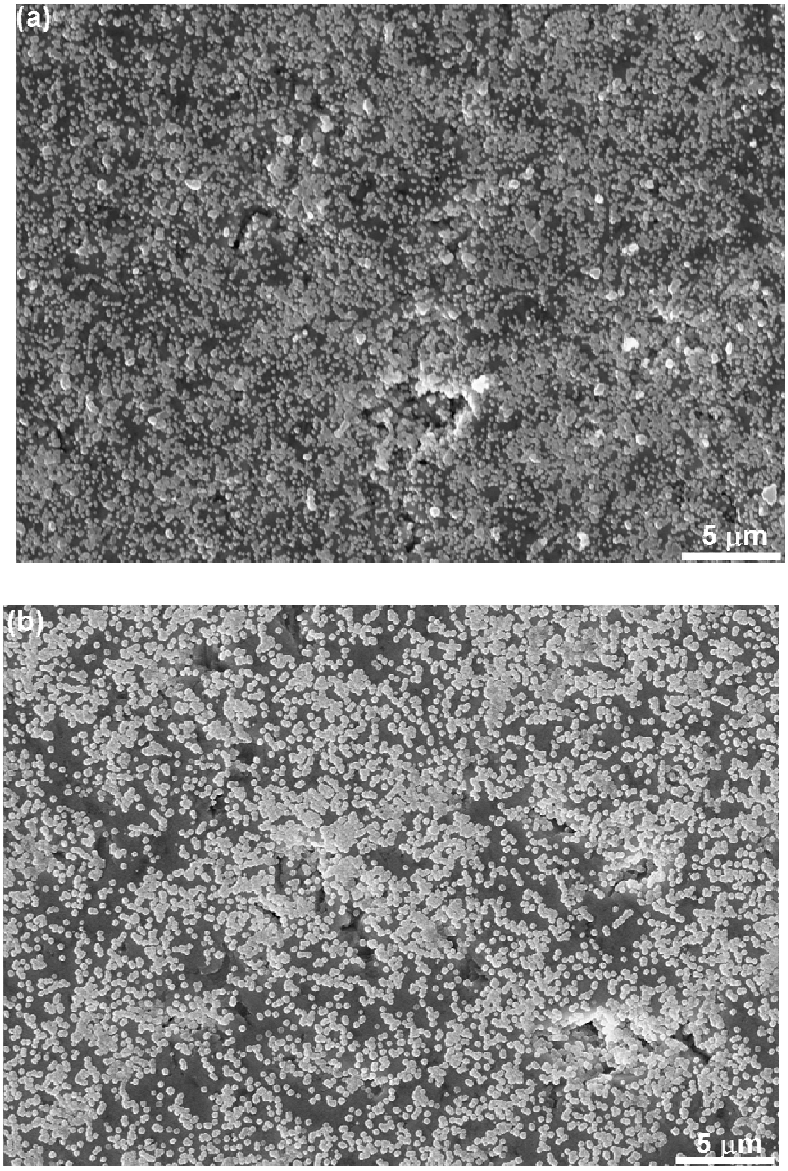

Figure 4.1 Typical SEM surface morphologies of Ti_3SiC_2 (a) with and (b) without diamond scratching, and Si (c) with and (d) without diamond scratching after 20 min deposition at 800 W [175].

[175]. Fine particles with different density have been formed on all the surfaces. The particle distribution is more uniform on Ti_3SiC_2 than on Si. The particle size is about 300 nm on Ti_3SiC_2, and ranges from several dozens of nanometers to 1 μm on Si. The particle density on Si increases significantly (from $10^4/cm^2$ to $10^8/cm^2$) through diamond scratching, while it is very close ($10^9/cm^2$) on Ti_3SiC_2 with and without diamond scratching.

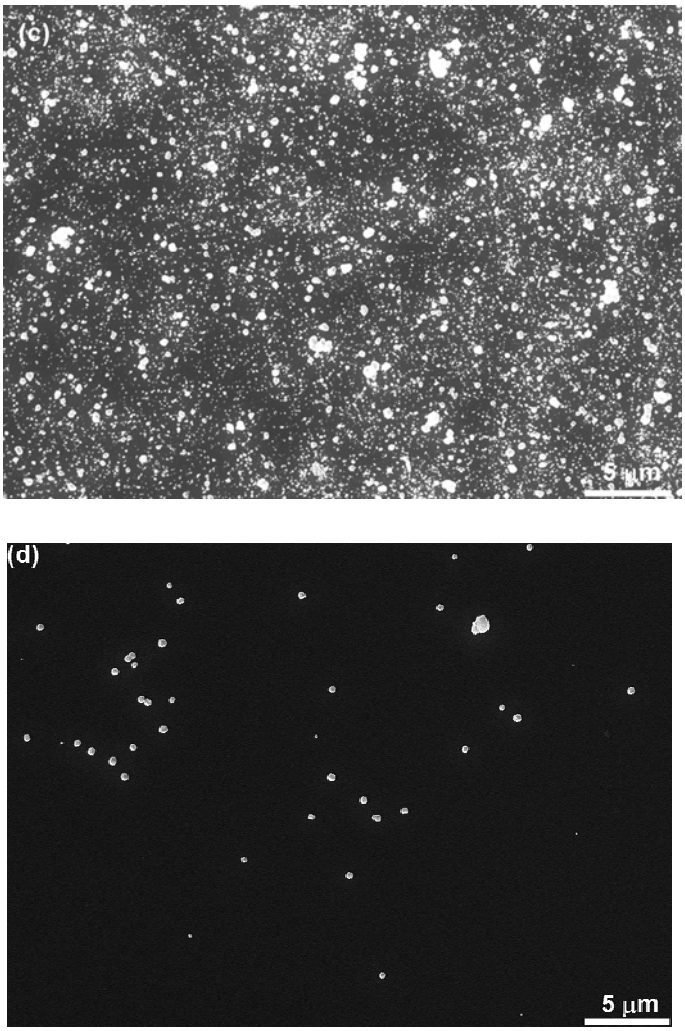

Figure 4.1 (Continued)

Raman spectra, taken from those fine particles after 20 min deposition, are shown in Figure 4.2 [175]. All the spectra reveal a clearly defined peak at around 1332 cm $^{-1}$, the characteristic peak of diamond, confirming that the particles initially formed are diamond in nature. Compared with the case of Si, the spectrum taken from the particles on Ti_3SiC_2 (Figure 4.2a) shows relative lower and broader diamond peak (full width at half maximum is around 16 cm^{-1}), indicating the smaller diamond grain size. The broad band at around 1550 cm^{-1}, attributed to the scattering from sp^2-bonded carbon, can also be found for all the samples. The relative intensity of 1550 cm^{-1} band taken from the particles on Ti_3SiC_2 is a little higher than on Si, this may be attributed to its smaller grain size. Considering the fact that Raman scattering in the

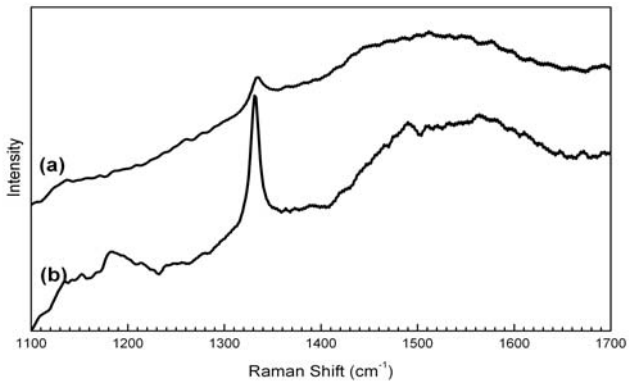

Figure 4.2 Typical Raman spectra of the newly formed particles on (a) Ti_3SiC_2 and (b) Si after 20 min deposition at 800 W [175].

visible range (514 nm) is about 200 times [21] more sensitive to sp^2-bonded carbon than to sp^3-bonded carbon and the grain boundaries consist of sp^2-bonded carbon, the diamond particles initially formed are likely of high purity. In addition, peaks centered at 1140 and 1180 cm^{-1} can also be found from the Raman spectrum shown in Figure 4-2b. The origin of these peaks is still controversial. Some researchers claimed them to be correlated with the nanocrystalline diamond [21, 176]. According to our previous results, they are related to unstable C-H bonds in the grain boundaries [177].

Present results show that diamond nucleation density on Ti_3SiC_2 (even without diamond scratching treatment) is much higher than on diamond scratched Si, supporting the previous finding [23, 55-72] that the formation of carbide interlayers assist diamond nucleation. Some researchers suggested that the carbide acts as diamond nuclei center due to their similarity in the lattice parameters [72,176]. Others proposed that the carbide layer acts as a diffusion barrier for carbon diffusion into the substrate, thus, the critical carbon concentration needed for diamond nucleation can be achieved faster [48]. Being a carbide material, Ti_3SiC_2 is expected to be a barrier for carbon diffusion. Diamond can nucleate directly on it with high rate and high density, and there is no need to form a carbide layer for diamond nucleation through the reaction between carbon and substrate.

4.2.2 Morphologies of Diamond Films

4.2.2.1 On Diamond Scratched Substrates Surface

With the high nucleation density, dense diamond thin films can be feasibly grown on Ti_3SiC_2 [175]. As shown in Figure 4.3, a dense continuous diamond film can be formed on Ti_3SiC_2 with 3 h deposition. On the other hand, the diamond grown on Si with the same deposition time is either separated particles (on unscratched Si, picture not shown here) or locally coalesced clusters (Figure 4.3b) due to the lower nucleation density. Furthermore, the diamond grown on Ti_3SiC_2 has much finer grain size and smoother surface than on Si. As shown in Figure 4.3a, diamond grains grown on Ti_3SiC_2 ranges approximately from 50 nm to 0.5 μm with smooth square facets. A preferred [001] orientation (vertical to the substrate surface) can be clearly seen. As shown in Figure 4.3b, the diamond grown on Si is triangle faceted and randomly oriented with an average grain size of approximately 1 μm.

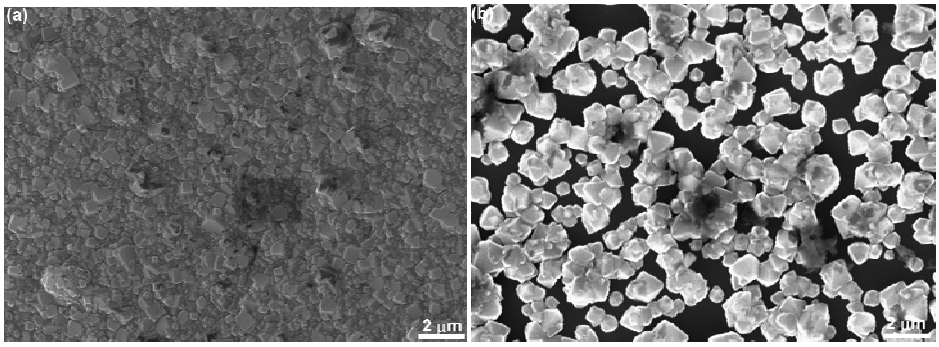

Figure 4.3 Typical SEM surface morphologies of samples after diamond deposition for 3 h on diamond scratched (a) Ti_3SiC_2, and (b) Si, at 800 W [175].

With further increase of the deposition time to 6 h, the diamond film grown on Ti_3SiC_2 keeps its dense smooth surface morphology with stronger [001] preferred orientation, as shown in Figure 4.4a, while the diamond grown on scratched Si is not dense enough to form a continuous film and the crystals exhibit randomly orientation (Figure 4.4b) [175]. Compared with the diamond deposition on Si, the diamond film

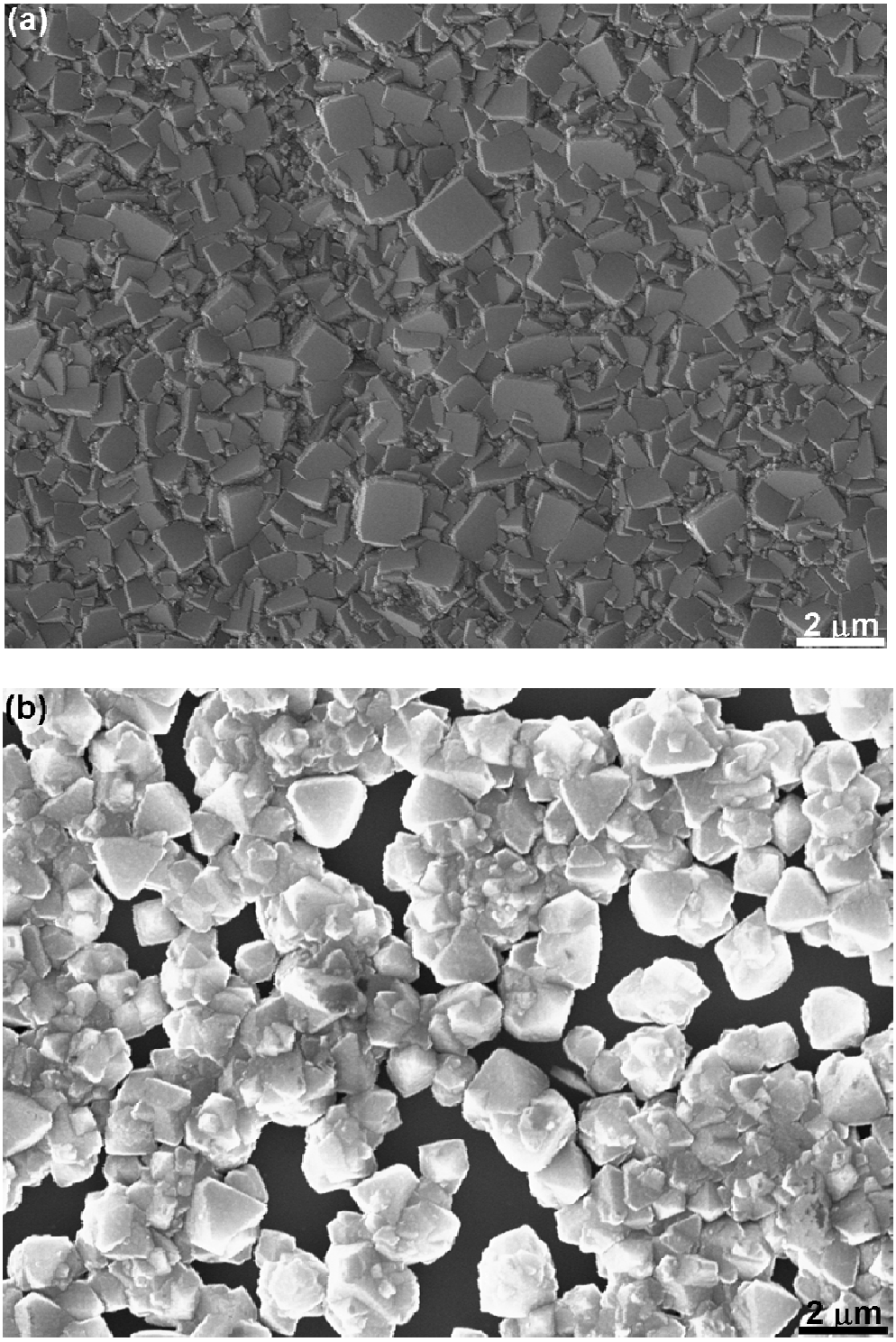

Figure 4.4 Typical SEM surface morphologies of samples after diamond deposition for 6 h on diamond scratched (a) Ti_3SiC_2, and (b) Si, at 800 W [175].

grown on Ti_3SiC_2 exhibits finer grain size, smoother surface, and much shorter film formation time.

4.2.2.2 On Unscratched Ti_3SiC_2 Surface

The high diamond nucleation density on unscratched Ti_3SiC_2 surface (as shown in Figure 4.1b) enables the possible formation of diamond thin films. As shown in Figure 4.5, after deposition at 700 W for 6 h, an almost continuous diamond thin film has been grown on the unscratched Ti_3SiC_2 surface. The size of diamond grains is less than 0.5 μm. The coverage of diamond is even much higher than that on the diamond scratched Si surface (Figure 4.4b). Compared with diamond thin films on scratched Ti_3SiC_2 substrate (Figure 4.4a), some bump-liked diamond clusters with clearly visible boundaries can be found. And the flat (100) facets of diamond grains are parallel to the slope of bumps. This result confirms the high diamond nucleation rate of diamond on Ti_3SiC_2. It also indicates that the distribution of diamond nuclei is more uniform on diamond scratched Ti_3SiC_2 than that on the one without diamond scratching.

4.2.3 Cross-Section of Diamond Films on Ti_3SiC_2

High nucleation density generally results in intimated contact between film and substrate. Figure 4.6 shows SEM cross-section images of diamond film on diamond scratched Ti_3SiC_2 for 6 h at 750 W [175]. As shown in Figure 4.6, the diamond film on Ti_3SiC_2 and film/substrate interface are dense without voids. Even though some pores present in the substrate (Figure 4.1) due to the nature of reactive sintering, there are no voids at the interface. On the contrary, diamond nucleates and grows inside the pores, and interlockers are formed at the film/substrate interface, resulting in an increased contact area between the film and the substrate. The thickness of the diamond film on Ti_3SiC_2 is approximately 18 μm, achieving an average film growth rate of 3.0 μm/h, while the diamond grown on Si under similar conditions does not form continuous film (Figure 4.4b). Even increasing deposition time to 20 h, the diamond film on Si is only approximately 6 μm, an average film

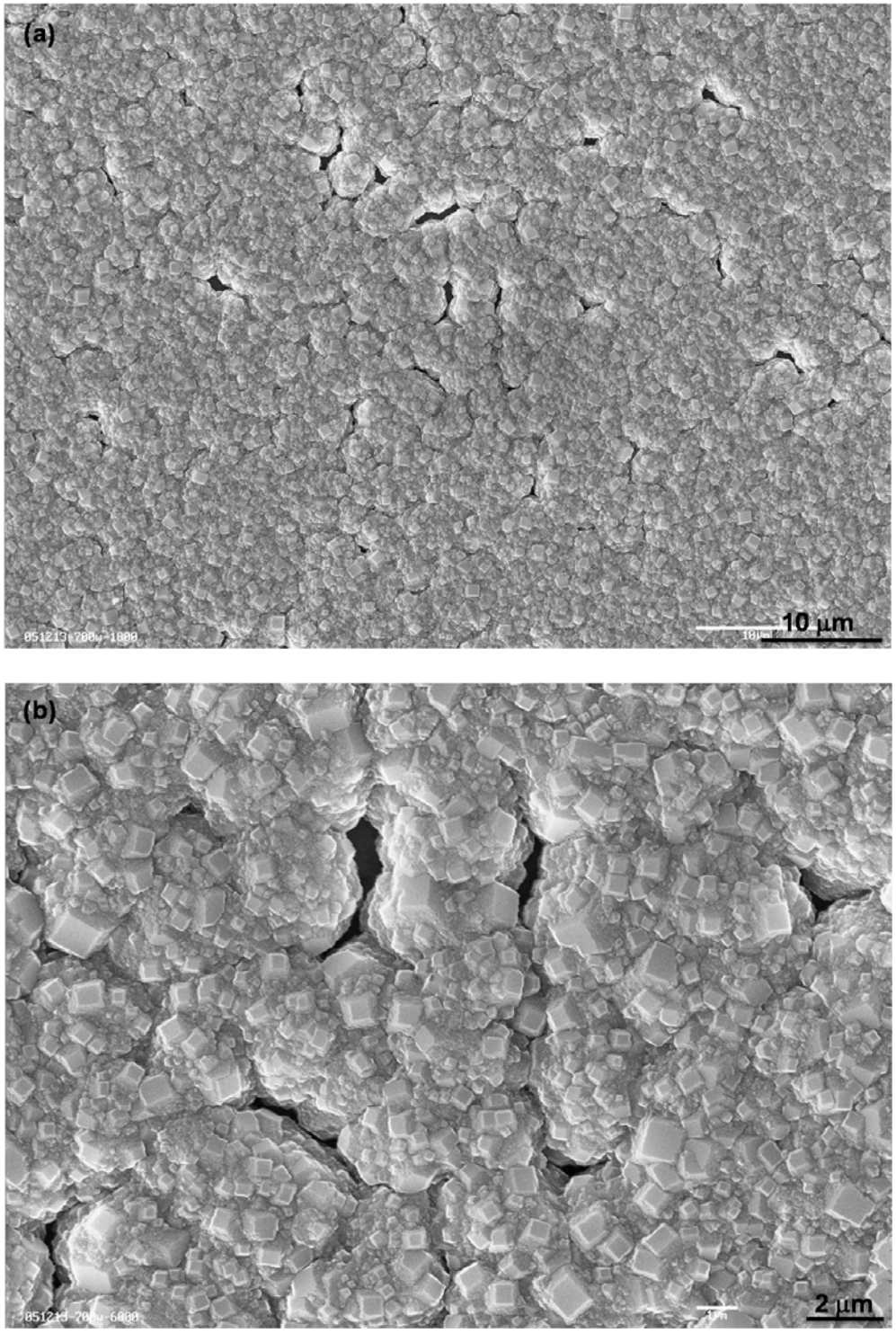

Figure 4.5 (a) Lower and (b) higher magnification SEM surface morphologies of diamond thin films formed on unscratched Ti_3SiC_2 substrate after 6 h deposition at 700 W.

growth rate of 0.3 μm/h, nine times lower than on Ti_3SiC_2. It should be noted that the surface temperature on Ti_3SiC_2 should be higher than that on Si, even though under

the same input microwave power, because the thermal conductivity of Ti_3SiC_2, 40 W/mK, is lower than that of Si, 124 W/mK, and the Ti_3SiC_2 substrate (2.0 mm) is thicker than Si substrate (0.66 mm). It has been found that the substrate surface temperature during the deposition is one of the important factors to determine the CVD diamond deposition rate. At temperature below 927 $^{\circ}$C, the diamond growth rate increases almost linearly with substrate temperature [178]. The higher surface temperature of Ti_3SiC_2 should make some contributions to the higher diamond growth rate on it. However, this contribution is relatively small. The optical pyrometer showed that the surface temperature of Ti_3SiC_2 under 750 W is lower than that of Si under 1000 W. But the diamond growth rate on Ti_3SiC_2 under 750 W is 6 times higher than that on Si under 1000 W (0.4 μm /h). These results suggest that the higher nucleation density and the higher nucleation rate on Ti_3SiC_2 may be the main factor contributing the higher diamond growth rate.

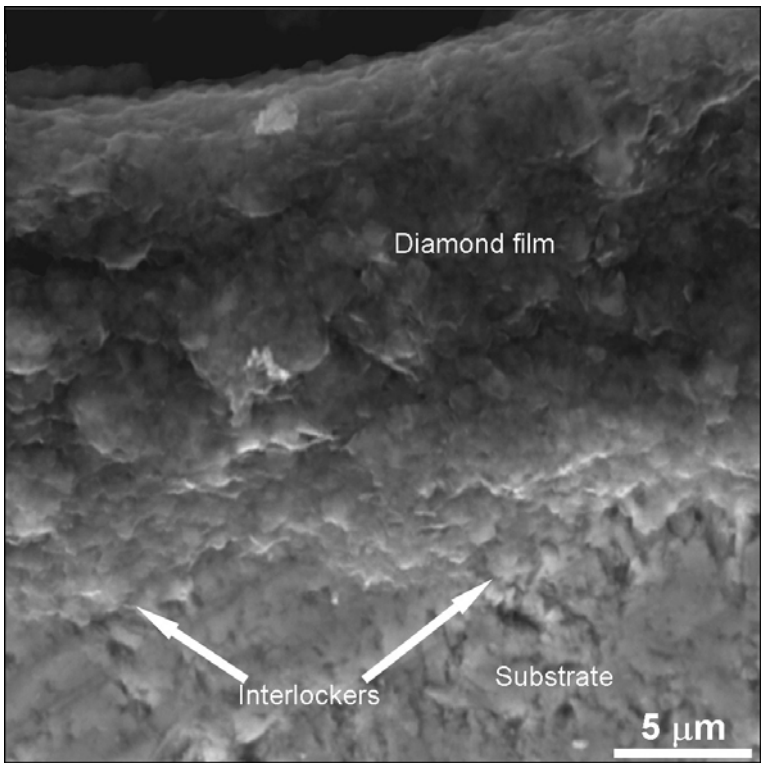

Figure 4.6 SEM cross-sectional image of the diamond film grown on Ti_3SiC_2 for 6 h at 750 W [175].

4.2.4 Adhesion of Diamond Films on Ti_3SiC_2

For most of the film applications, high film/substrate adhesion is a pre-requisite. A high nucleation density indicates a strong chemical interaction of the deposited atoms with the substrate surface and an intimated contact between the film and substrate, which are desirable for good adhesion. And the interlockers formed at the interface may further enhance the adhesion [7, 129, 179]. It is expected that the diamond films on Ti_3SiC_2 exhibit high film/substrate adhesion. There are various methods for assessing the adhesion of hard films to a substrate. Among them, scratching or indentation test is the most common method. Adhesion tests are generally very difficult to analyze analytically and are most often used as comparative tests. It has been well accepted that the diamond films grown on Si has good adhesion. In present study, a comparative test has been performed on diamond films on Ti_3SiC_2 and Si, respectively. Figure 4.7a and b show the SEM images of indentations under a load of 4.9 N on diamond films grown on Ti_3SiC_2 and Si, respectively [175]. There are radical cracks spreading from the four corners of indentation in the film on Si (Figure 4.7b, as indicated by arrows), while there are no such cracks in the film on Ti_3SiC_2 (Figure 4.7a), indicating that the film on Ti_3SiC_2 has higher fracture toughness [180], which is likely a result of its smaller grain size and non-columnar morphology (Figure 4.6) [181]. There is no flaking and film spallation occurred in the film on Ti_3SiC_2 (Figure 4.7a), while there is flaking and spallation occurred at the center of the indentation in the film on Si (Figure 4.7b). Film spallation is the result of deadhesion of film from the substrate. In the indentation test, the film and the underneath substrate are deformed under the point-loading, giving a complex stress to the film/substrate interface. Silicon is harder than Ti_3SiC_2, the interfacial stress between diamond and Si resulted from the deformation of film and substrate should be smaller than that between diamond and Ti_3SiC_2 under the same load, thus the film

on Si should be able to withstand higher load without spallation if the adhesion between the film and substrate is similar. The fact that the film on Ti_3SiC_2 withstands higher load without spallation indicates that the diamond on Ti_3SiC_2 has higher adhesion at the interface. Nevertheless, the higher fracture toughness of the diamond on Ti_3SiC_2 may prohibit the propagation of cracks to the interface, contributing to its higher critical indentation loads.

This successful synthesis of adhesive diamond films with high fracture toughness on machinable Ti_3SiC_2 substrate is of significant importance to many applications of both diamond and Ti_3SiC_2. Furthermore, the results suggest that Ti_3SiC_2 might be an ideal interlayer for diamond grown on metallic substrates. It is well known that diamond is an ideal material to be used as protective coatings to prolong the service lifetime of various machine components made of metals or their alloys. However, high quality adhesive diamond films are difficult to achieve on most metallic substrates. To apply a suitable interlayer is one of the most promising techniques to solve the problem. Present results have shown that adhesive diamond film with high quality and high fracture toughness can be obtained on Ti_3SiC_2 with high nucleation density and high growth rate. It is expected that adhesive Ti_3SiC_2 coatings can be obtained on metallic substrate due to its metallic properties. Technologies are already available to coat Ti_3SiC_2 on metallic substrate [181-184]. Ti_3SiC_2 as an interlayer for diamond growth on some important metallic substrates such as high speed steel and hard alloys will be investigated to expand diamond applications as protective coatings.

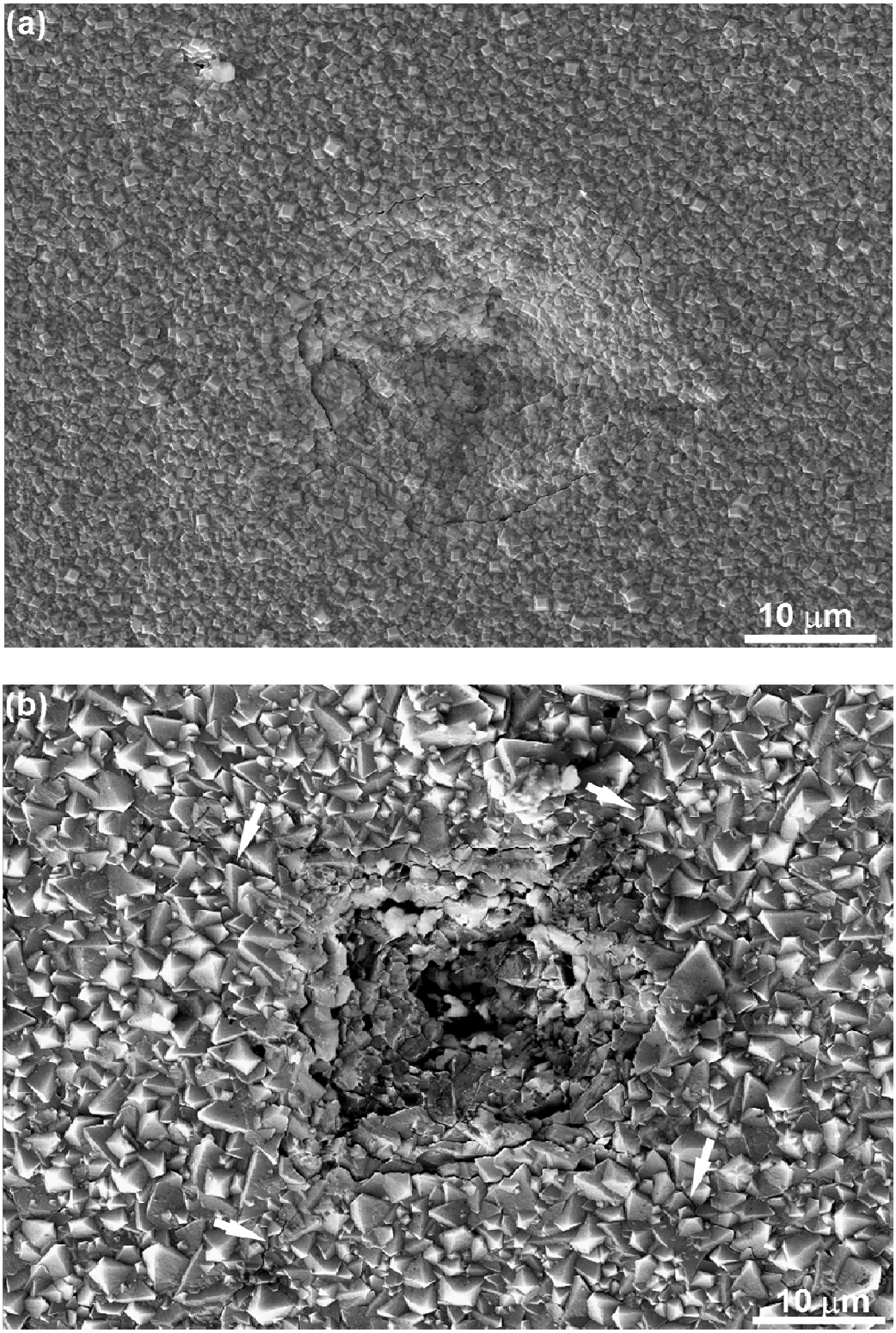

Figure 4.7 SEM images of Vicker's indentations under a load of 4.9 N on diamond films grown on (a) diamond scratched Ti_3SiC_2 for 6 h at 750 W, and (b) diamond scratched Si for 23 h at 800 W [175].

4.3 Summary and Conclusions

Nucleation and growth of diamond films on Ti_3SiC_2 has been investigated using MPECVD in a hydrogen and methane gas mixture. The diamond films grown on Ti_3SiC_2 have much higher nucleation density, much higher film formation rate, much higher growth rate, smaller grain size, smoother surface, higher interfacical adhesion, and higher fracture toughness than on Si. The results have demonstrated that Ti_3SiC_2 is a good substrate material for diamond nucleation and growth, and has the potentials to be applied as an interlayer on metallic substrates for diamond film deposition. Due to the unique combination of both metallic and ceramic properties of Ti_3SiC_2, this successful synthesis of adhesive diamond films on Ti_3SiC_2 may be greatly expand the applications of both diamond and Ti_3SiC_2.

* Part of this section has been published in the "Journal of Crystal Growth", according to the home page of this journal, author retains "the right to include the journal article, in full or in part, in a thesis or dissertation".

CHAPTER 5
SYNTHESIS AND CHARACTERIZATION OF NANOCRYSTALLINE DIAMOND THIN FILM ON TI_3SIC_2 BY MPECVD *

5.1 Introduction

Through Chapter 4, we have found that the adhesive sub-microcrystalline diamond (MCD) films can be synthesized on Ti_3SiC_2 with a high nucleation density and a high growth rate, and the results have demonstrated that Ti_3SiC_2 is a good substrate material for diamond nucleation and growth. It has been acknowledged that nanocrystalline diamond (NCD) films have many advantages over MCD films for such applications as protective coatings for machining tools and for biodevices, cold-cathode electron sources, surface acoustic wave devices, X-ray lithography masks, sensors, and structural materials for micro- and nano- electromechanical system (MEMS/NEMS) [117]. Nucleation is the first and the most important step for diamond film synthesis. The high diamond nucleation density on Ti_3SiC_2 is a great advantage to synthesize NCD films. This motivates me to investigate the feasibility of NCD film synthesis on Ti_3SiC_2. To further increase the diamond nucleation density, Ti_3SiC_2 substrates were ultrasonically scratched in a solution containing diamond powders with an average size of 25 nm. To avoid the coalescence of nanocrystalline diamond crystals into the large microscale crystallites, the deposition/growth rate of diamond thin films was decreased by adjusting the flow rate of H_2 and CH_4 from 99 and 1 sccm to 99.5 and 0.5 sccm, respectively. And for the first time, NCD films have been synthesized on Ti_3SiC_2 by MPECVD under the typical conditions for MCD synthesis.

5.2 Results and Discussion

Figure 5.1 shows a typical SEM surface image of the Ti_3SiC_2 substrate after 20 min deposition [185]. Nanoscale nuclei with an average density of $10^{11}/cm^2$, two orders higher than that reported in Chapter 4, have formed on the surface. Continuous thin film with a nucleation density as high as $10^{12}/cm^2$ has been locally formed preferably on the pores in the substrate. The average crystallite (nucleus) size is approximately 25 nm (Figure 5.1b).

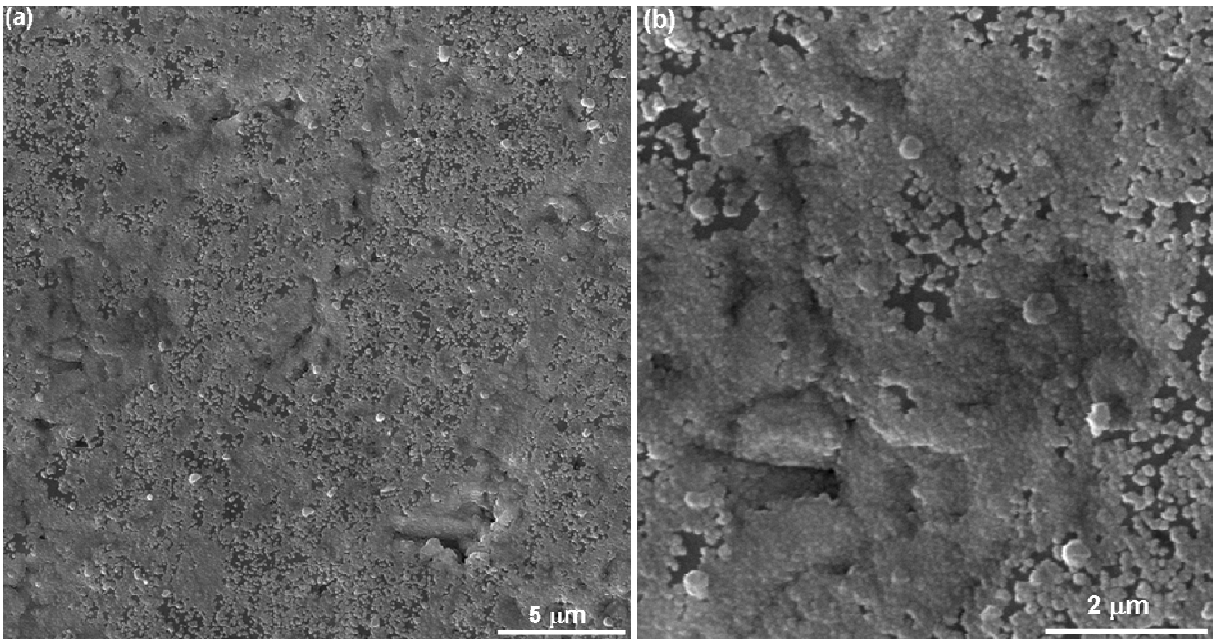

Figure 5.1 SEM surface morphologies of samples after 20 min deposition (a) low and (b) high magnification [185].

Due to the high nucleation density, a continuous dense thin film with an average grain size of 30 nm was formed within 2 h deposition, as shown in Figure 5.2a and b [185]. With further increase of deposition time up to 6 hours, the films exhibit the similar surface morphology (not shown here). The results indicate that nanocrystalline films can be synthesized on the nanodiamond treated Ti_3SiC_2 substrate.

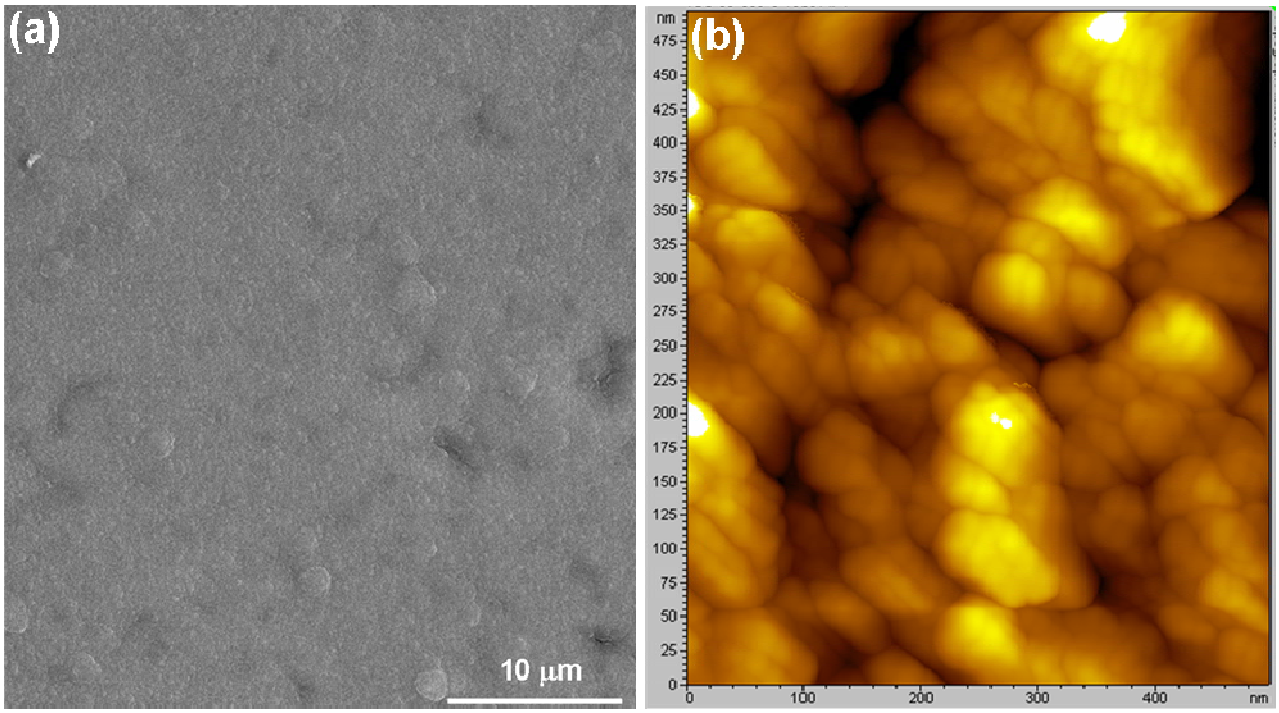

Figure 5.2 (a) SEM and (b) AFM surface morphologies of samples after 2 h deposition [185].

The microstructures of the nanocrystalline films and the film/substrate interfaces were further analyzed by SEM cross-sectional images. Figure 5.3 shows a cross-sectional image of the thin film on Ti_3SiC_2 after 6 h deposition [185]. Both the film and the film/substrate interface are very dense. Even though pores present in the substrate surface (Figure 5.1), resulted from the grinding and polishing, there are no voids at the interface. On the contrary, crystallites nucleate and grow inside the pores, forming interlockers at the film/substrate interface, resulting in an increased contact area between the film and the substrate. The thickness of the film on Ti_3SiC_2 is approximately 12 μm, achieving an average film growth rate of 2 μm/h, 6 times higher than that of the MCD films on silicon under the similar conditions.

Figure 5.3 SEM cross-sectional image of the samples after 6 h deposition [185].

It is very interesting that the deposited film exhibits an equiaxed grain structure rather than a typical columnar structure for the vapor deposited films. Similar results were observed for the synthesized films with different durations. Formation of equiaxed structure is a result of renucleation (continued nucleation) [186], indicating a high secondary nucleation rate during the growth. Figure 5.4 schematically illustrates the formation of equiaxed structure through high nucleation/renucleation rate. Firstly, randomly oriented primary nuclei with a high density of $10^{11}/cm^2$ are uniformly formed on the substrate surface. With the growth of nuclei, the nuclei contact with each other and a thin nanocrystalline layer is formed. The agglomeration of nuclei is difficult to occur because the deposition temperature is not high enough to allow the atomic diffusion (surface migration) and rearrangement to minimize the surface area, and the nanoscale crystalline size (parallel to the surface) is kept in the subsequent growth stage. If the nuclei continue to grow during the processing, a columnar structure would appear. However, due to the high

concentration of grain boundaries (GBs) and GB triple junctions in the thin nanocrystalline layer and the relative low deposition temperature, the renucleation on the GB and GB triple junctions prefers to occur. As a result, a nanocrystalline film with equiaxed grain structure is formed.

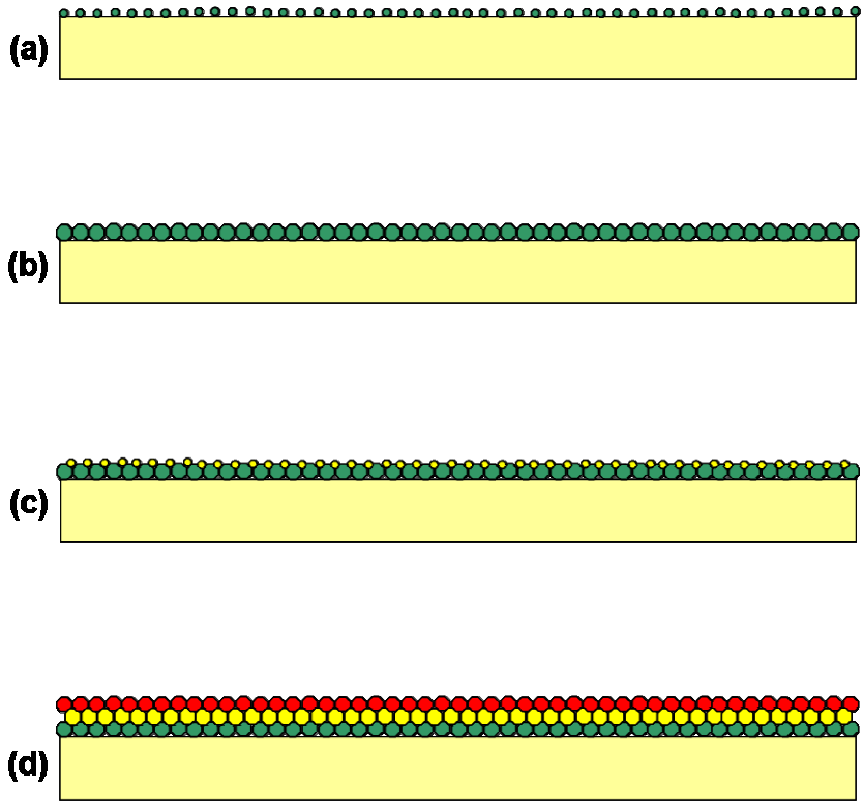

Figure 5.4 Schematic illustrations for (a) nucleation on Ti_3SiC_2; (b) formation of the first nanocrystalline layer on Ti_3SiC_2; (c) renucleation on the surface of nanocraystalline layer; and (d) growth of nanocrystaline films on Ti_3SiC_2.

Figure 5.5 shows the Raman spectra of samples after 20 min, 2h and 6h deposition. The spectra exhibit a clearly defined peak at ~1332 cm^{-1}, the signature of the crystalline diamond [187], confirming that the deposited nuclei or thin films are diamond in nature. Compared with the case of MCD thin films synthesized under the similar conditions, the diamond peaks of these samples are relatively lower in intensity and broader in width (full width at half maximum is approximately 19 cm^{-1}). This is attributed to their nanocrystalline structure. The broad peak centered at around

1550 cm^{-1}, corresponding to sp^2 carbon, is very strong. This is likely attributed to the large difference in the Raman cross sections for sp^2 graphitic features and sp^3 diamond hybridized carbon and the nanostructure of the crystallites [21]. Considering this and the fact that the grain boundaries consist of sp^2 carbon [188], the NCD formed are likely of high purity. In addition, two broad peaks centered at 1140 cm^{-1} and at about 1480 cm^{-1} can also be seen from the Raman spectra shown in Figure 5.5 and their relative intensity decreases with increasing deposition time. These two peaks originate from trans-polyacetylene in CVD NCD films [189-191]. It should be noted that the Raman spectra of NCD are dominated by non-diamond peaks and the diamond characteristic peak is overlapped by the D-band of graphitic carbon, indicating that Raman spectroscopy with a laser wavelength of 514.5 nm may be not appropriate to determine the sp^2 carbon concentration of NCD films. As described in Chapter 3, synchrotron-based NEXAFS has many advantages over Raman spectroscopy on characterization of NCD thin films. Figure 5.6 shows the C K-edge NEXAFS spectra of the 6 h deposited NCD film recorded in both surface sensitive total electron yield (TEY) and bulk sensitive fluorescence yield (FY). Similar to that of the CVD diamond [192], the spectra of our films exhibit a sharp spike at 289.3 eV (an excitonic transition) and a dip at 303 eV (both characteristics of the pure diamond [169]), and a weak peak at 285.5 eV (π bonding feature due to the unsaturated carbon in the films [193, 194]), indicating that the NCD film (both surface and bulk) predominately consists of crystalline diamond with a small amount of sp^2 carbon. A weak shoulder at ~288 eV, corresponding to C-H bond in the diamond film [194] can also be seen. The lower intensity of π peak and much lower intensity of the shoulder in FY spectrum (Figure 5.6b) than those in TEY spectrum (Figure 5.6a) indicates that the C-H bond is mainly near the surface of the film and that the bulk of the film is more diamond-like than the surface of the film.

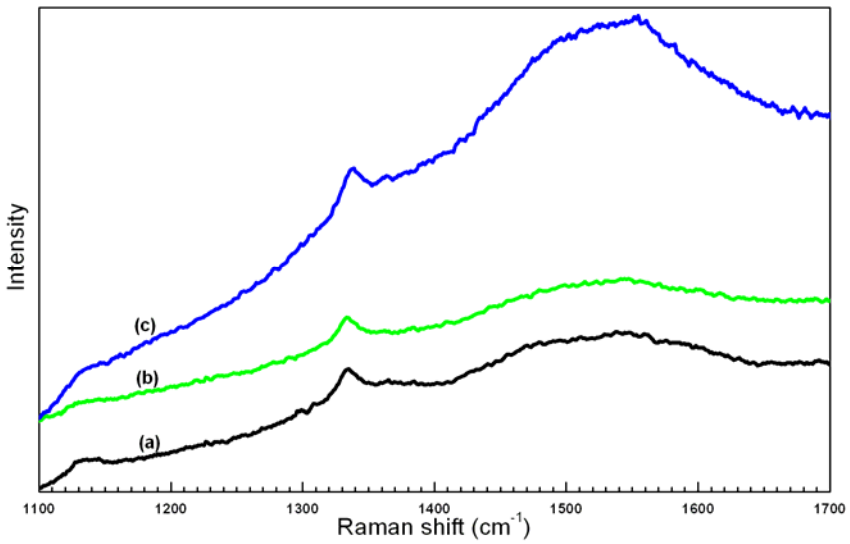

Figure 5.5 Raman spectra taken from the surface of samples after (a) 20 min, (b) 2h and (c) 6 h deposition [185].

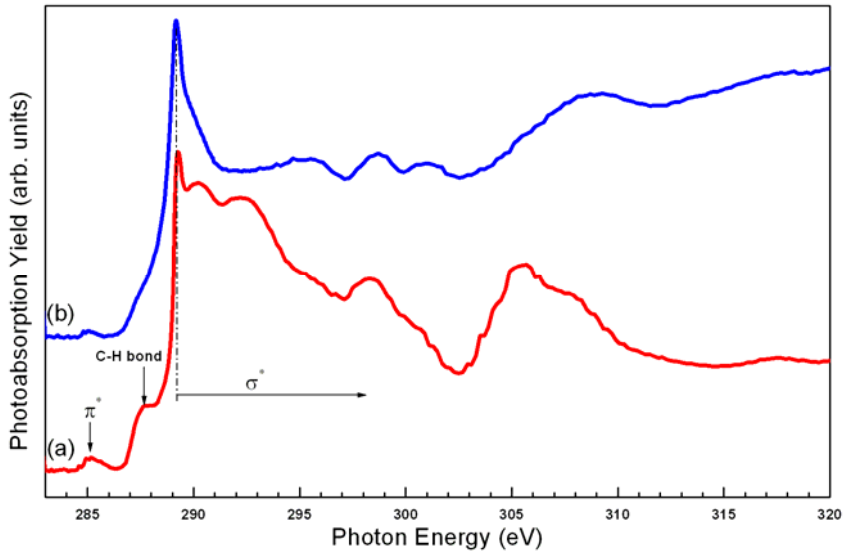

Figure 5.6 (a) TEY and (b) FY of C K-edge NEXAFS spectra of samples after 6 h deposition [185].

5.3 Conclusions

Dense NCD films with an equiaxed grain structure (an average grain size of 30 nm) have been synthesized on Ti_3SiC_2 using MPCVD in a 99.5 % H_2+0.5%CH_4 gas mixture regardless of growth durations. An average nucleation density of $10^{11}/cm^2$ and a film growth rate of 2 μm/h have been achieved. C K-edge NEXAFS results have shown that the synthesized NCD films predominately consist of crystalline diamond with a small amount of sp^2 carbon and C-H bond predominantly near the surface of the film.

* Part of this section has been published in "Nanotechnology", according to the Copyright Agreement of this journal, author retains the right "To include the Article (all or part) in a research thesis or dissertation".

CHAPTER 6

EFFECT OF POWER INPUTS ON FORMATION OF DIAMOND THIN FILMS ON TI_3SIC_2 BY CHEMICAL VAPOR DEPOSITION

6.1 Introduction

Both Chapter 4 and 5 demonstrated that Ti_3SiC_2 is a promising substrate and interlayer material for diamond nucleation and growth. As Ti_3SiC_2 combines properties of both ceramics and metals, the successful synthesis of adhesive diamond thin films on Ti_3SiC_2 may greatly expand the applications for both Ti_3SiC_2 and diamond thin films.

To fully understand the synthesis of diamond thin films on Ti_3SiC_2, it is desirable to further investigate the effect of deposition parameters. In this Chapter, different microwave input powers, ranging from 500 to 800 W, were applied for the deposition in order to investigate its effect on the nucleation and growth of diamond films. The Ti_3SiC_2 substrates were pre-treated through the sub-microcrystalline diamond powder scratching. The flow rate of H_2 and CH_4 were kept at 99 sccm and 1 sccm, respectively. The working gas pressure was maintained at 4 kPa.

6.2 Results and Discussion

Figure 6.1 shows a typical Raman spectrum taken from the carbon film on Ti_3SiC_2 after deposition for 6 h at 500 W [195]. The spectrum exhibits a clearly defined peak at around 1333 cm^{-1}, the signature of the sp^3-bonded diamond phase, confirming that the deposited thin film is diamond in nature. The diamond peak of this sample is relatively low in intensity and broad in width (the FWHM is approximately 19 cm^{-1}). A broad and strong peak centered at around 1550 cm^{-1},

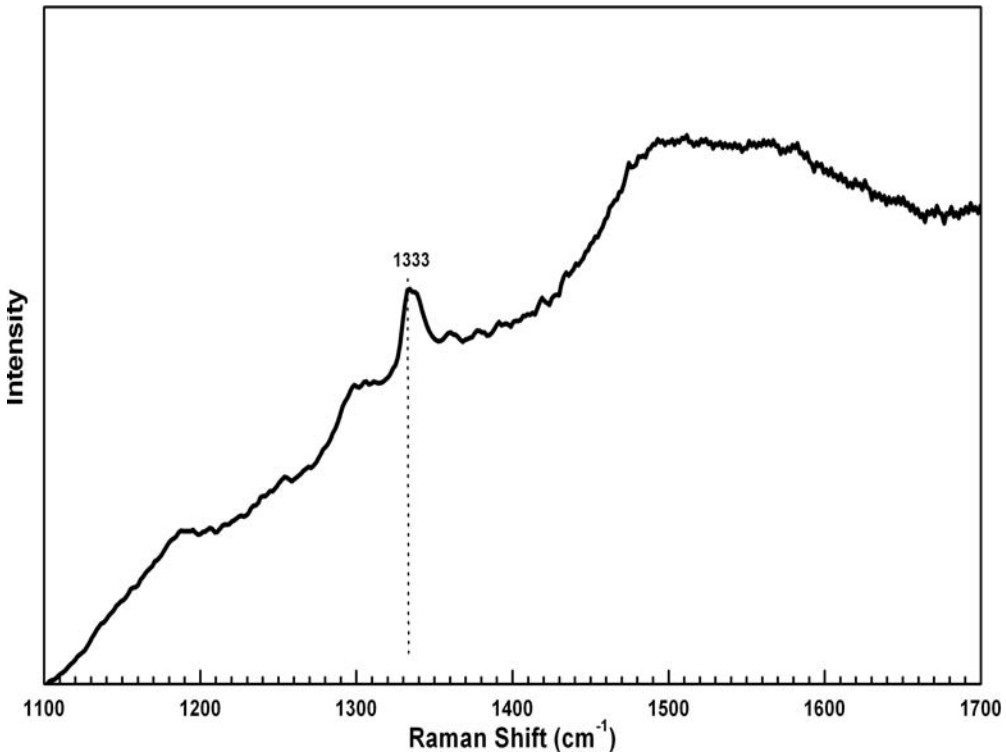

Figure 6.1 Typical Raman spectrum of diamond films on Ti_3SiC_2 after deposition for 6 h at 500 W [195].

corresponding to sp^2 carbon, can also be detected. These features are very similar to those reported for NCD thin films.

Figure 6.2 presents the typical SEM morphology of the thin film formed on Ti_3SiC_2 after deposition for 6 h at 500 W [195]. The pictures show that a very dense diamond film has been formed under the conditions. In consistence with the results from Raman spectrum, the film is composed of predominantly NCD grains with some triangle-shaped sub-micrometer-scaled diamond grains sparsely distributed. As discussed in previous chapters, the weak and broad diamond peak and the strong sp^2 graphite peak in the Raman spectrum (Figure 6.1) is likely attributed to the large difference in the Raman cross-sections for sp^2 graphitic and sp^3 diamond hybridized carbon and the nanostructure of the crystallites [21]. Compared with the results in Chapter 5, the NCD formed at 500W are likely of high purity.

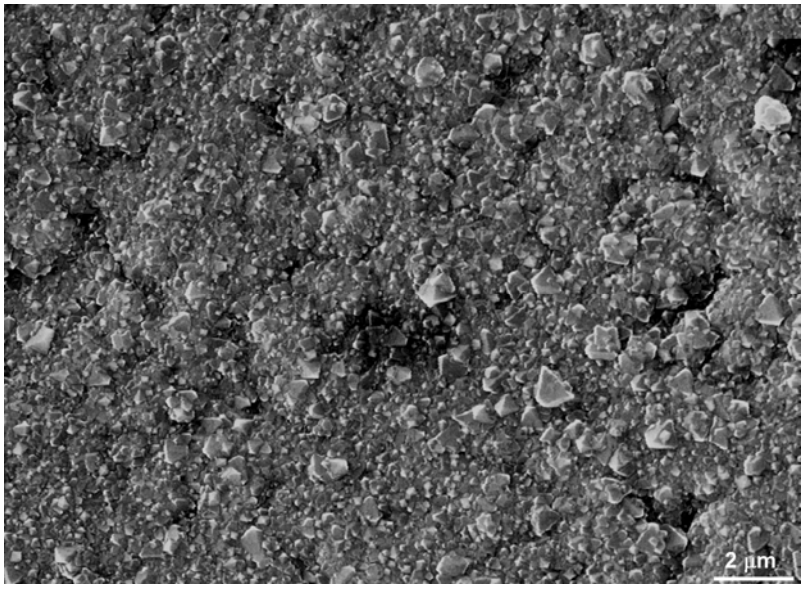

Figure 6.2 Typical SEM micrograph of diamond films on Ti_3SiC_2 after deposition for 6 h at 500 W [195].

With the increase of microwave power, the content of microcrystalline diamond grains increases obviously, as shown in Figure 6.3. The NCD grains distributed mainly among the microcrystalline grains when the microwave power is 650 W or above. It is very interesting that the (100) plane for the most of the microcrystalline grains is parallel to the substrate surface. It is reasonable to believe that the diamond films formed with microwave power 650 W or above are <001> oriented. It has been found that diamond thin films with a preferred <001> orientation have many advantages over randomly oriented films for such industry applications as protective coatings for machining tools. Thus heteroepitaxial growth of <001> highly oriented diamond films have been attracting great interests. Highly oriented or heteroepitaxial growth of diamond has been reported on several types of substrates, including cubic BN [196], Ni [197-198], SiC [199-203] and Si [204-208], via a BEN process. It has been found that, through BEN, the diamond nucleation density and nucleation rate can be significantly improved. And as we reported, the nucleation density and nucleation rate of diamond on Ti_3SiC_2 is significantly higher than that on Si under similar deposition conditions. Hence, relationships between the high

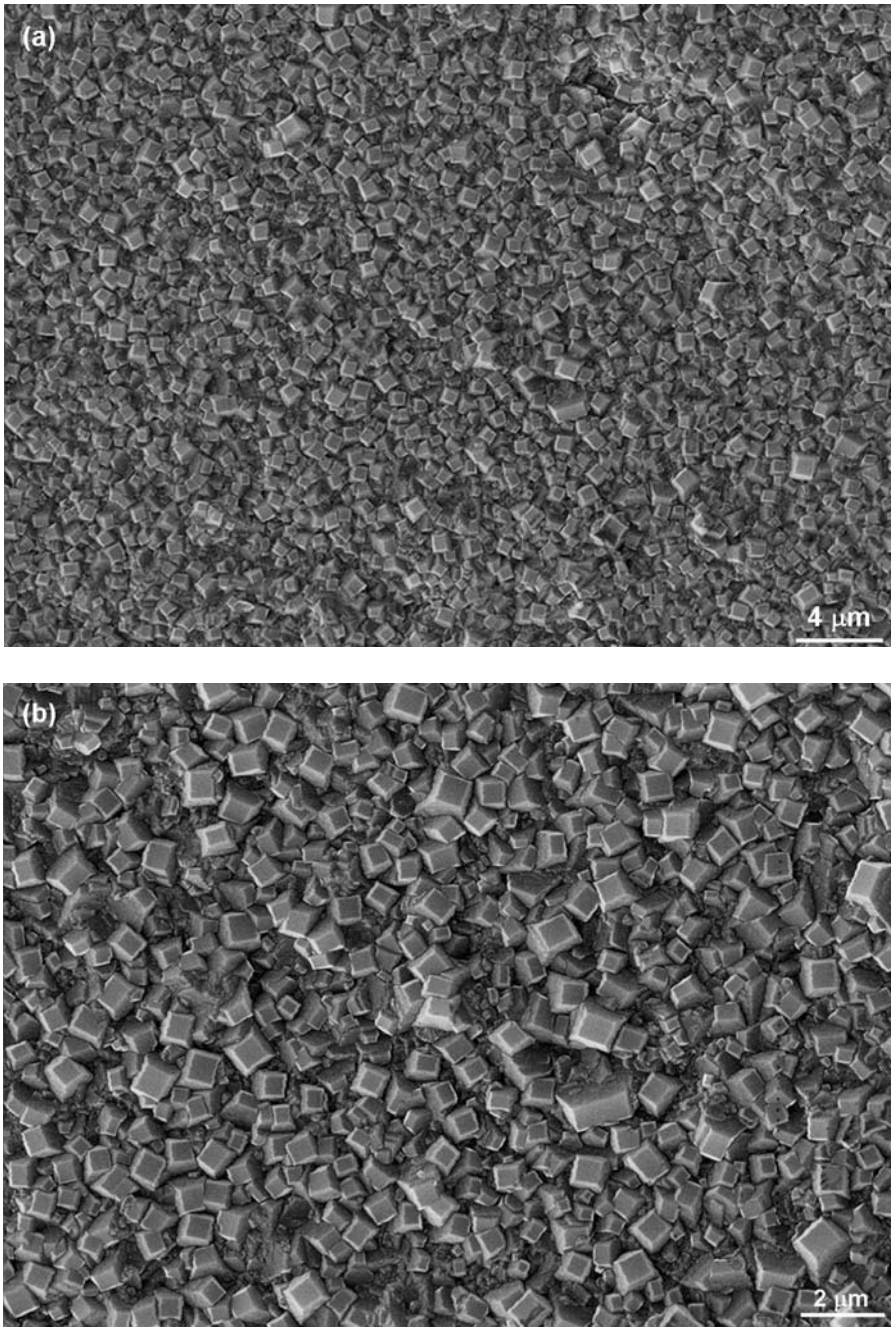

Figure 6.3 Typical SEM surface micrographs of the diamond films on Ti_3SiC_2 after deposition for 6 h at 650 W (a,b), 700 W (c,d), and 750W (e,f) at low (a, c, e) and high (b, d, f) magnification [195].

diamond nucleation density/rate with the <001> preferred orientation may exist. However, no report on this regard can be found on the literature up to now based on our knowledge, more detailed experiments need to be designed and performed in order to understand the phenomena.

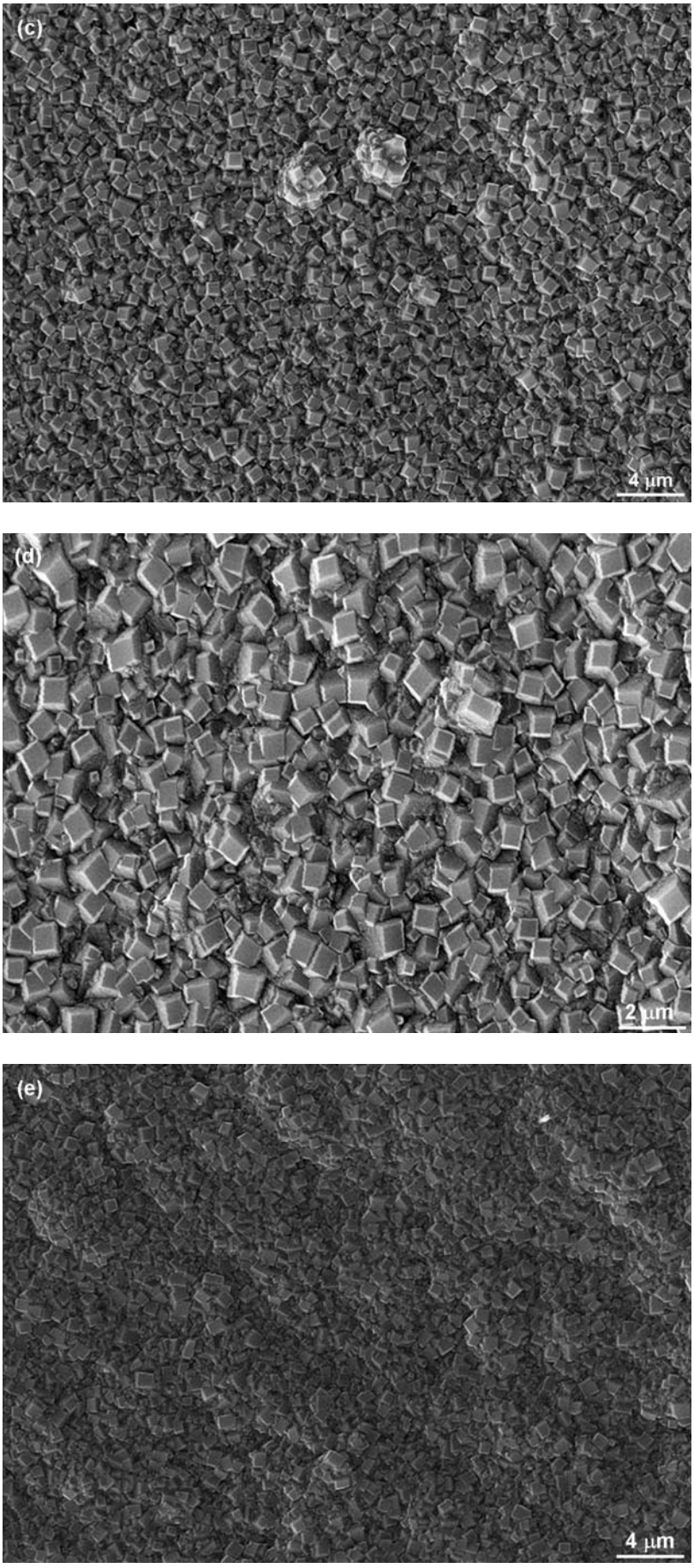

Figure 6.3 (Continued)

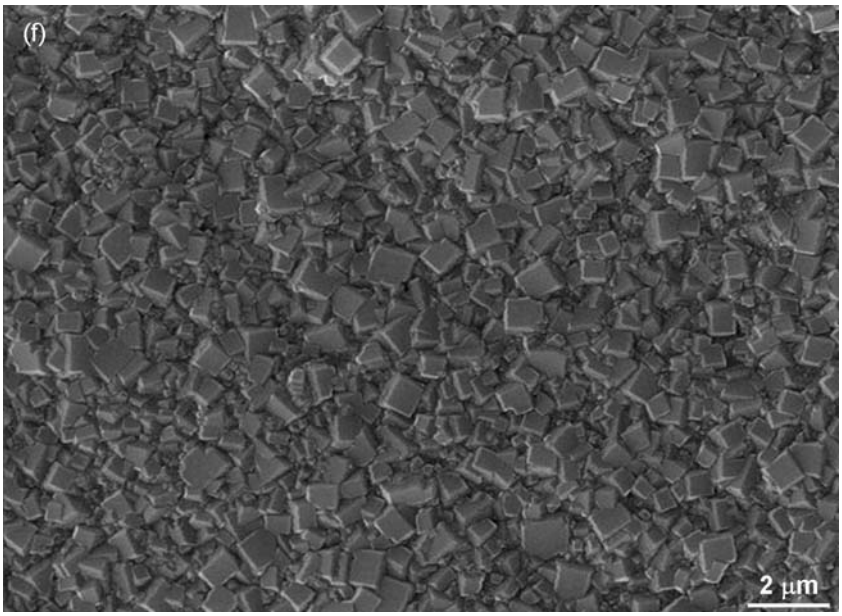

Figure 6-3. (Continued)

6.3 Conclusion

Diamond growth on Ti_3SiC_2 at different input powers has demonstrated that NCD thin film can be synthesized at low microwave power of 500 W and the increase of power inputs results in the formation of <001> highly oriented smooth diamond thin films.

CHAPTER 7
NUCLEATION AND EARLY STAGE GROWTH OF DIAMOND ON TI_3SIC_2 AND SI USING HOT FILAMENT CHEMICAL VAPOR DEPOSITION *

7.1 Introduction

The nucleation mechanisms of diamond on Ti_3SiC_2 have not been fully understood up to now. In this Chapter, we further investigate the nucleation and early stage growth of diamond thin films on Ti_3SiC_2 using HFCVD, the cheapest and most feasible technique for diamond thin film deposition, under typical MCD growth conditions in order to understand the nucleation mechanisms.

In this research, both diamond scratched Ti_3SiC_2 slices and Si wafers were used as the substrates. The diamond growth experiments were conducted in the HFCVD system. H_2 and CH_4 were introduced into the system through mass flow controllers at a flow rate of 50 sccm and 0.8 sccm, respectively. The total gas pressure was maintained at 500-700 Pa (typically 660 Pa). The filament was a coiled tungsten wire of 0.3 mm in diameter and was heated by an ac power supply at a voltage around 30 V and a current around 10 A. The substrate temperature was measured with a thermocouple mounted right behind the substrate holder. With a typical distance between filament and substrate of 8 mm, the measured temperature during deposition was 640 $^{\circ}$C. These conditions are typical for MCD thin films deposition. The deposition durations ranged from 5 min to 1 h.

7.2 Results and Discussion

After 5 min deposition, a dark layer is visible on the surface of Ti_3SiC_2. According to the typical SEM morphology (Figure 7.1a), this layer is composed of nanometer-scaled whisker-like structures, different from the typical morphology of

CVD diamond [209]. However, SEM cannot provide more detailed information for these nanostructured carbon whiskers due to its limited resolution. On the surface of Si (Figure 7.1b), fine particles with a size ranging from dozens of nanometers to submicrometer scale and a density of ~ $10^8/cm^2$ can be clearly seen. The fact that the particle density is obviously higher than that of the diamond powder remnant by diamond scratching (picture not shown here) indicates that diamond nucleation and growth start on the surface of Si within 5 min deposition and that diamond nucleate not only on the diamond remnants (seeds) but also directly on Si.

The structure of carbon whiskers on the surface of Ti_3SiC_2 were further analyzed by AFM, as shown in Figure 7.2 [209]. The average length of these whiskers is around 30 nm, and the average width of them is around 5 nm (Figure 7.2a). The higher magnification image further illustrates that two possible sub-microstructures are included in the carbon whiskers: small nano particles (brighter) embedded in whisker matrix, as marked in Figure 7.2b.

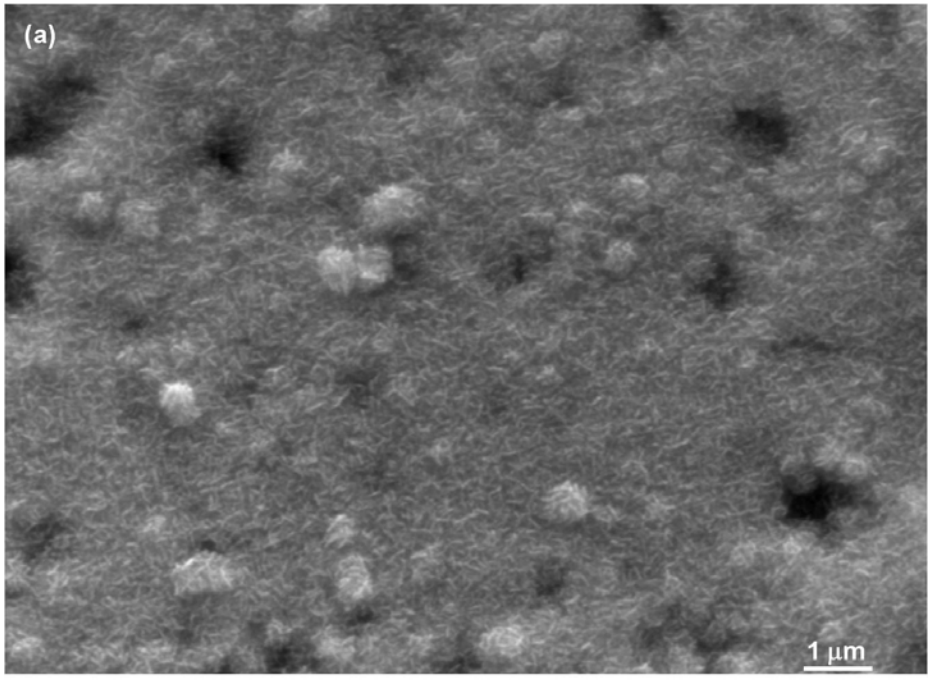

Figure 7.1 SEM surface morphologies for the surface of (a) Ti_3SiC_2 [209] and (b) Si after 5 min deposition.

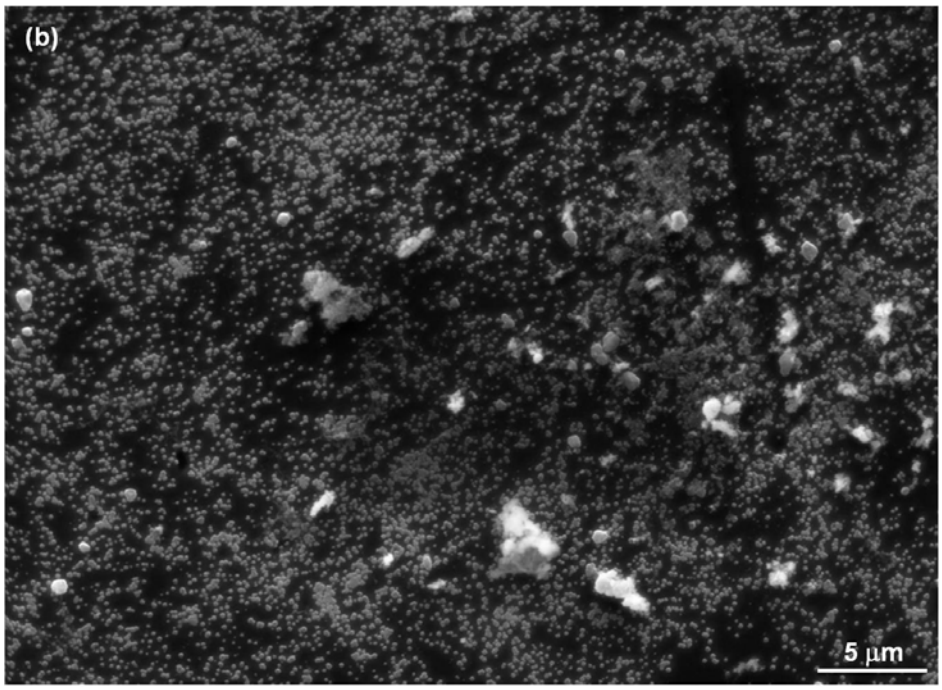

Figure 7.1 (Continued)

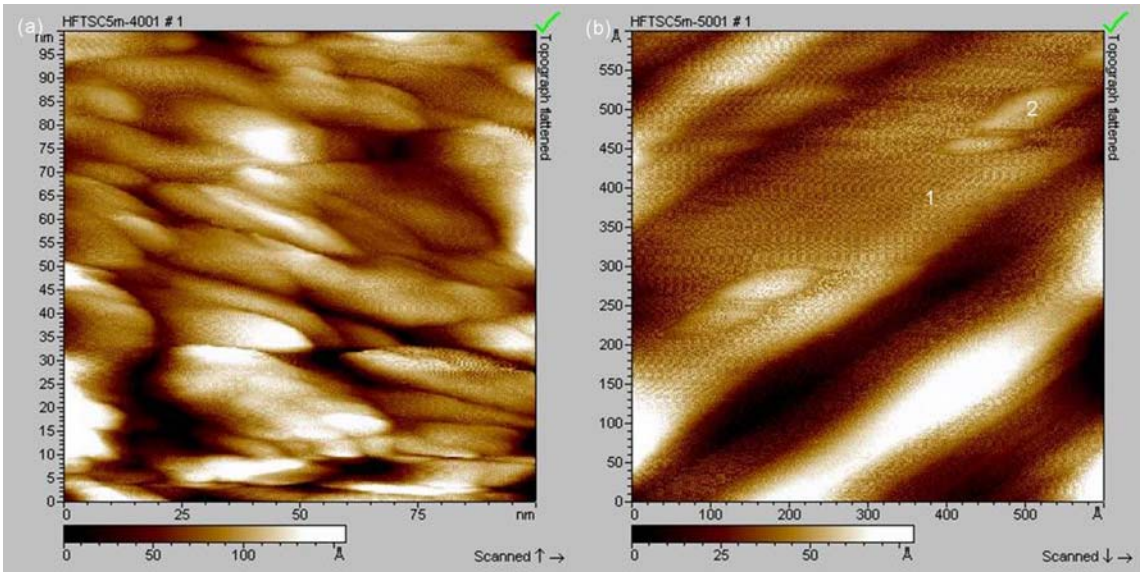

Figure 7.2 (a) lower, and (b) higher magnification AFM image of the nanostructured carbon whiskers presented in Figure 7.1a [209].

The typical Raman spectra taken from those particles (Figure 7.1b) on the surface of Si after 5 min deposition presents a clearly defined peak at around 1334 cm^{-1} (Figure 7.3a), the characteristic peak of diamond, confirming their diamond nature. The Raman spectrum in Figure 7.3a show a weak diamond band with a large FWHM (full width at half maximum), and a broad graphitic carbon band at around

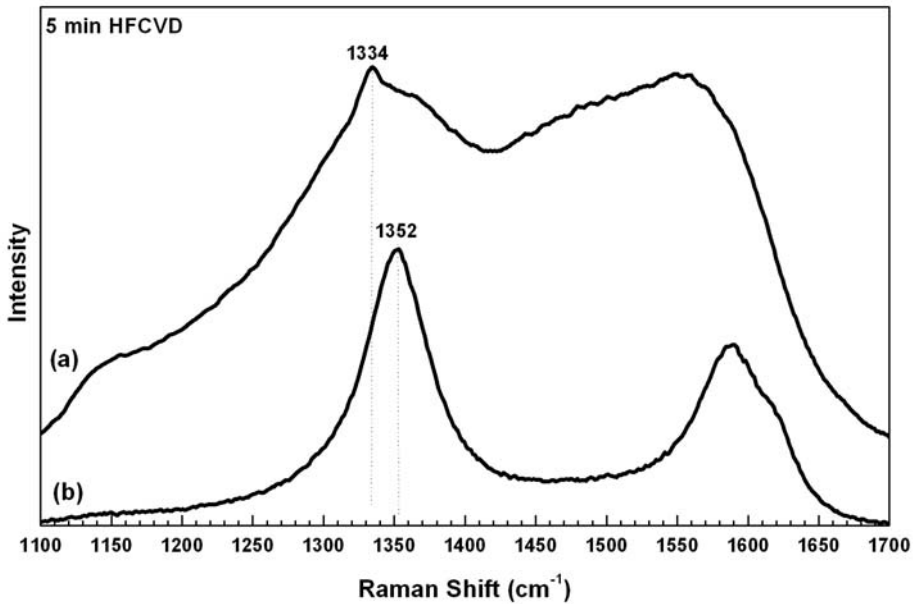

Figure 7.3 Typical Raman spectra taken from the surface of (a) Si and (b) Ti_3SiC_2 [210] after 5 min deposition.

1580 cm^{-1} from. On the contrary, no clear diamond peak can be detected by Raman spectroscopy on the surface of Ti_3SiC_2 after 5 min deposition (Figure 7.3b) [209], and the two peaks centered at around 1350 cm^{-1} and 1580 cm^{-1} are the signatures of sp^2-bonded graphite phase, indicating relatively high non-diamond carbon in the initial layer formed on Ti_3SiC_2 after short time deposition.

Figure 7.4 shows the C K-edge NEXAFS spectra taken from the surface of Si and Ti_3SiC_2 [209] after 5 min deposition recorded in surface sensitive TEY mode. The spectra taken from the surface of Si in Figure 7.4a exhibits a sharp spike at 288.7 eV and a dip at 302 eV, both characteristics of the pure diamond [169]as discussed before. The low intensity of the peak at 284.5 eV, from the π bonding feature of the unsaturated carbon in the films [193, 194] indicates that those newly deposited particles on Si predominately consist of the crystalline diamond. A weak shoulder at ~287 eV, corresponding to the C-H bond in the diamond film [194] can also be seen. In the case of the spectrum taken from the surface of Ti_3SiC_2 (Figure 7.4b), it is totally different from the NEXAFS spectra of the pure graphite [188]. It has a spike at

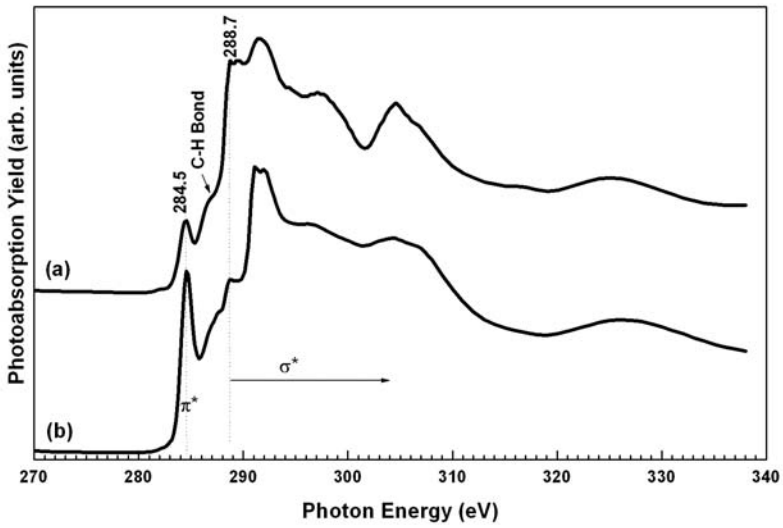

Figure 7.4 C K-edge NEXAFS spectra taken from the surface of (a) Si and (b) Ti_3SiC_2 [209] after 5 min deposition.

288.7 eV and a dip at 302 eV, characteristic diamond peaks. However, the intensity of peak for graphite π bonding is higher than that for diamond σ bonding, indicating that this nano structured carbon layer predominately consists of sp^2 graphitic structure with nano diamond crystals.

With the increase of deposition time, the intensity of peak for graphite π bonding decreases while that for diamond σ bonding increases gradually in both cases (Figure 7.5), especially on the surface of Ti_3SiC_2 (Figure 7.5b). The weak peaks of graphite π bonding at 284.5 eV after 1 h deposition indicate the high content of diamond structure on the surface of both samples. From the insert in Figure 7.5 a, the position of the peak for σ bonding, or C 1s absorption edge, on the surface of Si shifts to lower energy from at around 288.7 eV after 5 min deposition to 288.5 eV after 1 h deposition. And this C 1s absorption edge becomes sharper with time increasing. Both the shift and the sharpness of the C 1s absorption edge indicate the grain size increases with deposition time [210]. On the other hand, even after 1 h deposition, the position of the peak for σ bonding on the surface of Ti_3SiC_2 is still kept at around 288.7 eV (the insert in Figure 7.5b), the same as that after 5 min deposition, and the

width of this peak is obviously larger than that on Si. Therefore, the grain size of diamond on Ti_3SiC_2 after 1 h deposition should be in the same order of that after 5 min deposition, several nanometers.

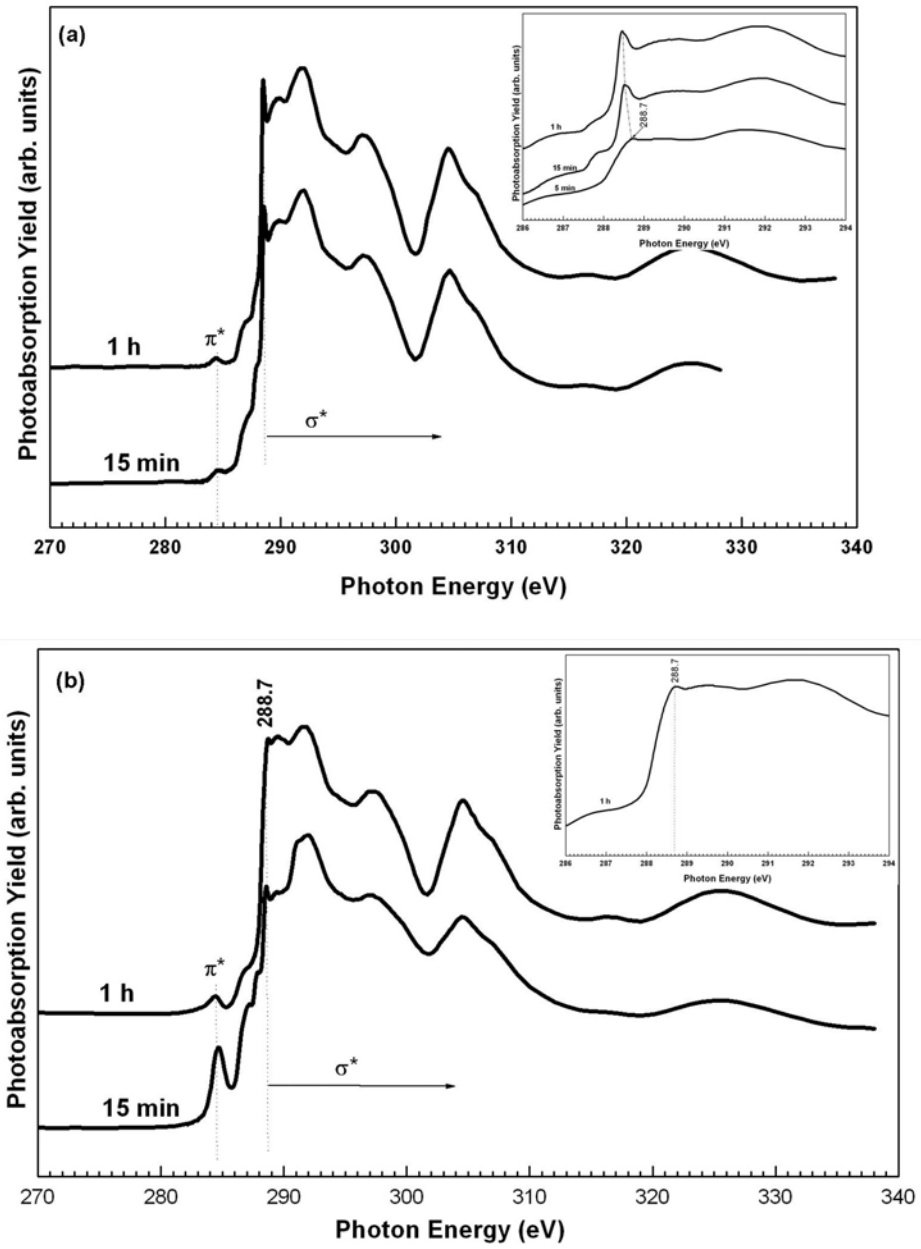

Figure 7.5 C K-edge NEXAFS spectra taken from the surface of (a) Si and (b) Ti_3SiC_2 after 15 min and 1 h deposition.

SEM observation as shown in Figure 7.6 revealed that the nano-whisker-like structure on the surface of Ti_3SiC_2 disappeared after 10 min and 15 min deposition, and fine particles with high density predominantly composed of diamond structure

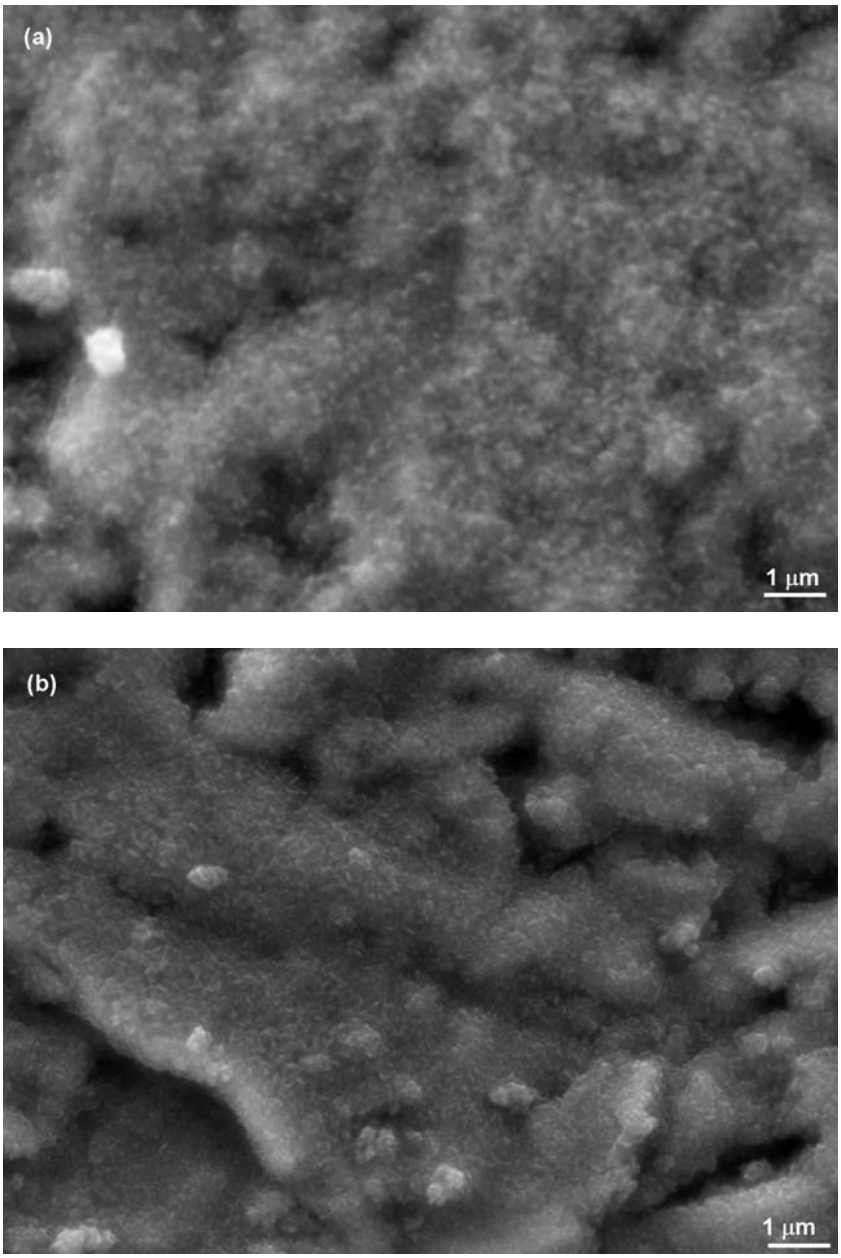

Figure 7.6 SEM surface morphologies for Ti_3SiC_2 after (a) 10 min and (b) 15 min deposition.

(based on the NEXAFS analysis shown in Figure 7.5) formed [209]. Therefore, it is reasonable to suppose that the initial nanostructured whisker-like carbon composite layer provides a rather high diamond nucleation density/rate on the surface of Ti_3SiC_2.

The high diamond nucleation density/rate on Ti_3SiC_2 induced a very high diamond thin film formation rate, as indicated in Figure 7.7 [209], after 1 h deposition, a very dense and flat NCD thin film has been formed on the surface of

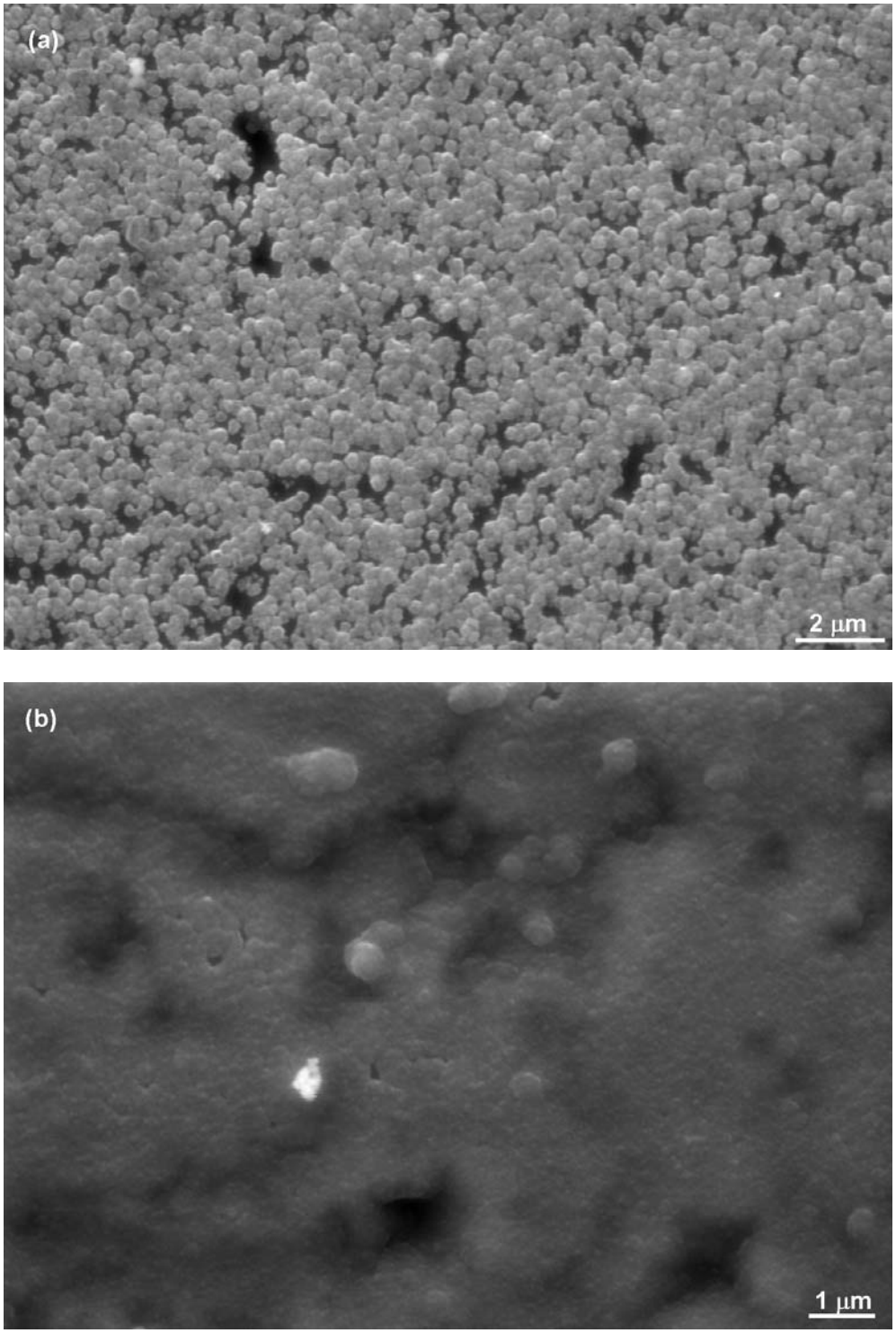

Figure 7.7 SEM surface morphologies for (a) Si and (b) Ti_3SiC_2 [209] after 1 h deposition.

Ti_3SiC_2 (Figure 7.7b). On the contrary, after 1 h deposition, diamonds formed on Si still exist as separated particles (Figure 7.7a), and the grain size of diamond on Si is in sub-microns scales.

7.3 Conclusions

(1) A nanowhisker-like diamond-graphite composite layer was initially formed on the surface of Ti_3SiC_2, which resulted in high diamond nucleation density, while, diamond nucleation on Si surface is predominantly based on those defect sites and diamond remnants on the surface created by the diamond scratching.

(2) The diamond thin films formation rate is obviously higher on Ti_3SiC_2 than that on Si. A dense and smooth NCD thin film has been feasibly synthesized on Ti_3SiC_2 after 1 time deposition.

* Part of this section has been published in "Canadian Metallurgical Quarterly (CMQ)", which has been cited as reference [209]. According to the journal office, reproduction of CMQ copyrighted material is allowed "as long as credit is given to the CMQ". (The email communication between the author and the officer has been attached in Appendix.)

CHAPTER 8
NEXAFS CHARACTERIZATION OF NCD THIN FILMS SYNTHESIZED WITH HIGH METHANE CONCENTRATIONS *

8.1 Introduction

Increasing the relative proportion of CH_4 in a CH_4-H_2 mixture during deposition is the simplest and the most common process to synthesize NCD films [211]. However, the investigations have limited the CH_4 concentration up to 15 % [211-214]. As mentioned, Raman has been the predominant technique for characterization of the deposited diamond thin films. But when the CH_4 content arrived at 15 %, it is difficult to detect the characteristic peaks from diamond phase [214], which is the main shortage of Raman spectroscopy. Based on our results in Chapter 6 and 7, NEXAFS is a powerful tool to characterize the chemical bonding of nanostructured carbon materials.

In the present study, we investigated the growth of diamond thin films with CH_4 concentrations ranging from 1% to 100% to obtain NCD films with a wide range of sp^2 carbon concentrations and applied NEXAFS to characterize the structure and the sp^2 carbon concentrations of the synthesized films in order to investigate the potential correlations between the sp^2 carbon concentration and the properties (mechanical, optical, electronic and biomedical) of the films.

In this research, diamond scratched Si wafers were used as substrates. The diamond growth experiments were conducted in the MPECVD reactor. During the deposition, CH_4 concentrations were ranged from 1% to 100% (1%, 2%, 3.5%, 5%, 10%, 15%, 20%, 30%, 50%, 100%) in the H_2-CH_4 mixture. The total gas pressure and

microwave power were maintained at 4 kPa and 1000 W, respectively. The deposition duration varied from 1.5 and 20 hours depending on the methane concentration.

8.2 Results and Discussions

Figure 8.1 shows the typical SEM micrographs (plane-view) of the films deposited on Si substrates with different CH_4 concentrations [215]. With the increase of CH_4 concentration, the grain size gradually decreases from microscale to nanoscale. At relatively low CH_4 concentrations (1% and 2%), well-faceted diamond thin films with an average grain size of approximately 0.3 μm were deposited (Figure 8.1a and b). At CH_4 concentration of 5%, the films consist of a mixture of nano-sized and micro-sized crystals (Figure 8.1c). Further increase in the CH_4 concentration (Figure 8-1d-h) resulted in the formation of films with a nanocrystalline structure with smooth surface. The facets and the exact size of the crystallites can not be clearly identified in the SEM images due to its limited resolution. The cross-section SEM images of films (not shown) were used to estimate the film thickness. The average growth rate of diamond films increases from 0.3 μm/h to 3.2 and 3.5 μm/h when the CH_4 concentration increased from 1% to 50% and 100%, respectively. The film growth rate at high CH_4 concentrations (50% or above) is more than 10 times the growth rate at typically used 1% CH_4.

Figure 8.2 shows AFM images of a nanocrystalline film deposited from 50% methane concentration [215]. Low magnification AFM images over a 20 μm ×20 μm area (see Figure 8.2a) were used to estimate the overall surface roughness of the films. It decreases from 224 nm to 29 and 26 nm as the CH_4 concentration increases from 1% to 50% and 100% respectively, consistent with the SEM observation (see Figure 8.1). The high resolution AFM image (Figure 8.2b) shows the details of the individual grains. The average grain size of the films, obtained through detailed computer

analysis of five images, decreases from 0.3 μm to 4 and 3 nm when CH_4 concentration increased from 1% to 50% and 100%, respectively.

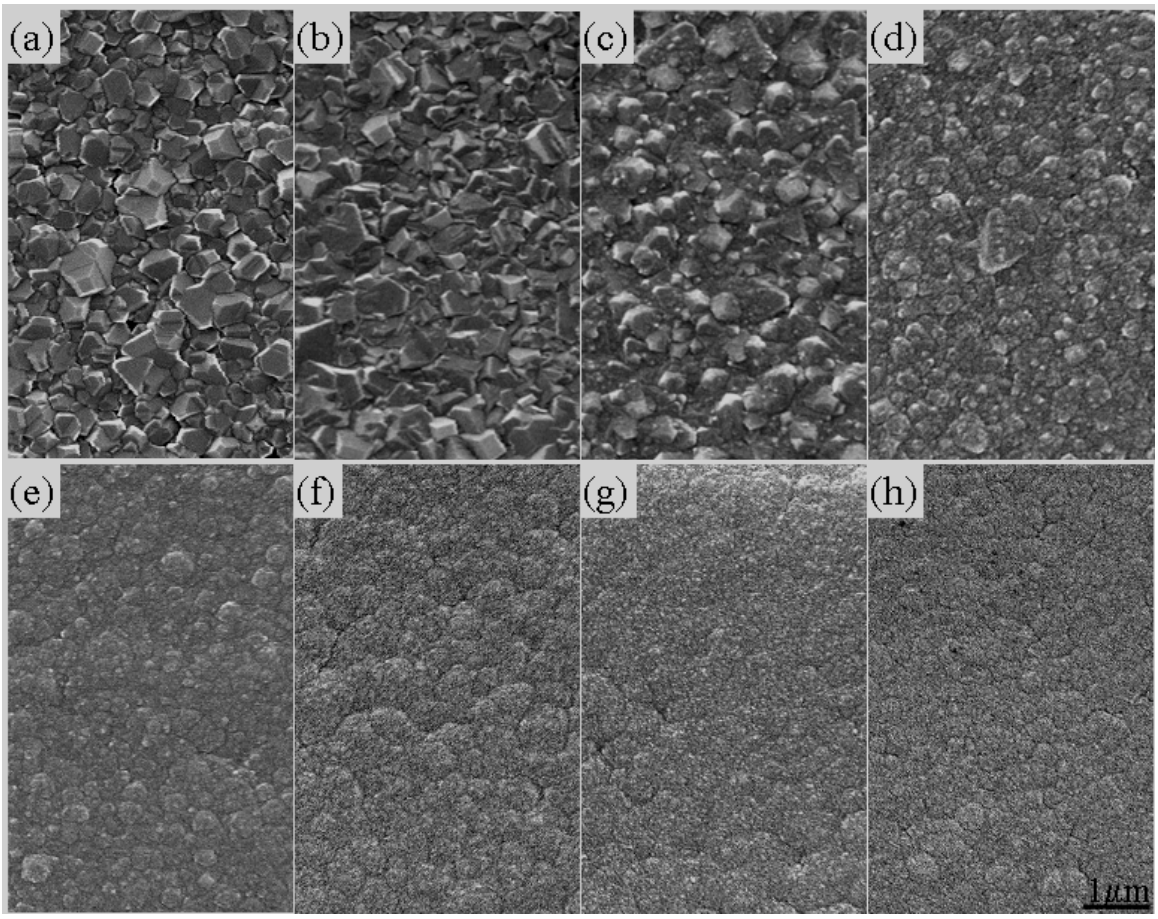

Figure 8.1 SEM micrographs (top-view) of the films synthesized with different CH_4 concentrations: (a) 1%, (b) 2%, (c) 5%, (d) 10%, (e) 15%, (f) 20%, (g) 50%, and (f) 100% [215].

Figure 8.3 shows the C K-edge NEXAFS spectra of the diamond films recorded in both TEY (a) and FY (b) [215]. We can see that the spectra exhibit a sharp 1s absorption edge at 289 eV and a large dip at 303 eV, characteristic features of pure diamond spectrum, confirming that all the films, even grown from pure CH_4, are diamond in nature. Close observation reveals that the films (10 % CH_4 or above) exhibit a slightly broadened exciton transition with a 0.25 eV blue shift. The broadened exciton transition is associated with the small size of the diamond nanocrystallites [216, 217], consistent with the SEM and AFM observations. The blue

shift may be caused by the quantum confinement effect due to the decrease of crystallite size [210, 216], or by the poor crystallinity of the nanocrystals and the high graphite content in CVD films [216]. There is also a weak peak at 285.5 eV in the spectra, which is the signature of π bonding from the non-diamond carbon. This peak is very weak at 1% CH_4 concentration and becomes more intense, indicating an increase of sp^2 concentration, with increasing CH_4 concentration. By comparing the surface sensitive TEY spectra with the bulk sensitive FY spectra shown in Figure 8.3, we can see that the bulk of the films is more diamond-like (relatively lower π bonding) than the surface of the films and the variation trend of sp^2 carbon concentration with the CH_4 concentration in the bulk of the films is similar to that of the surface of the film, indicating that our diamond films (both bulk and surface), even the NCD films grown from pure CH_4, consists of predominately diamond crystallites with a small amount of sp^2 carbon. Based on the analytical method developed by T. Hamilton [218], we calculated the sp^2 carbon concentration of the samples. It increases steadily from 2% to 25 % in the surface (based on TEY) and from 1% to 23 % in the bulk (based on FY) when the CH_4 concentration increases from 1% to 100%. It should be noted that the FY spectra look different from the corresponding TEY spectra. This is probably due to the distortions resulted from the self-absorption of the relative thick diamond films. In the present study, the thickness of the diamond thin film samples ranges from a few micrometers to ten micrometers, which is too thick to avoid the self-absorption effect.

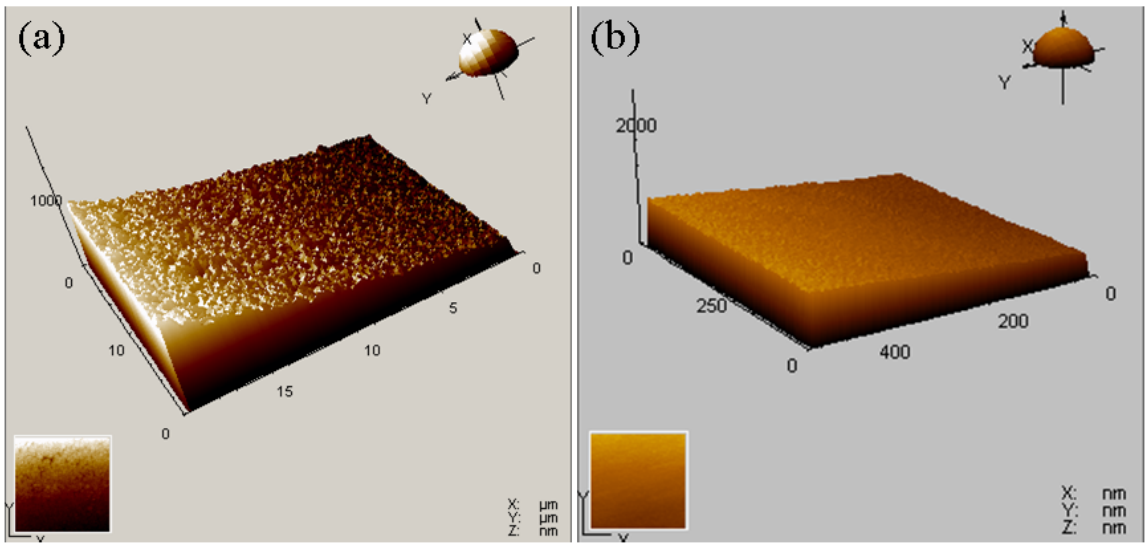

Figure 8.2 AFM images of the film synthesized with a CH_4 concentration of 50%: (a) low magnification, (b) high magnification [215].

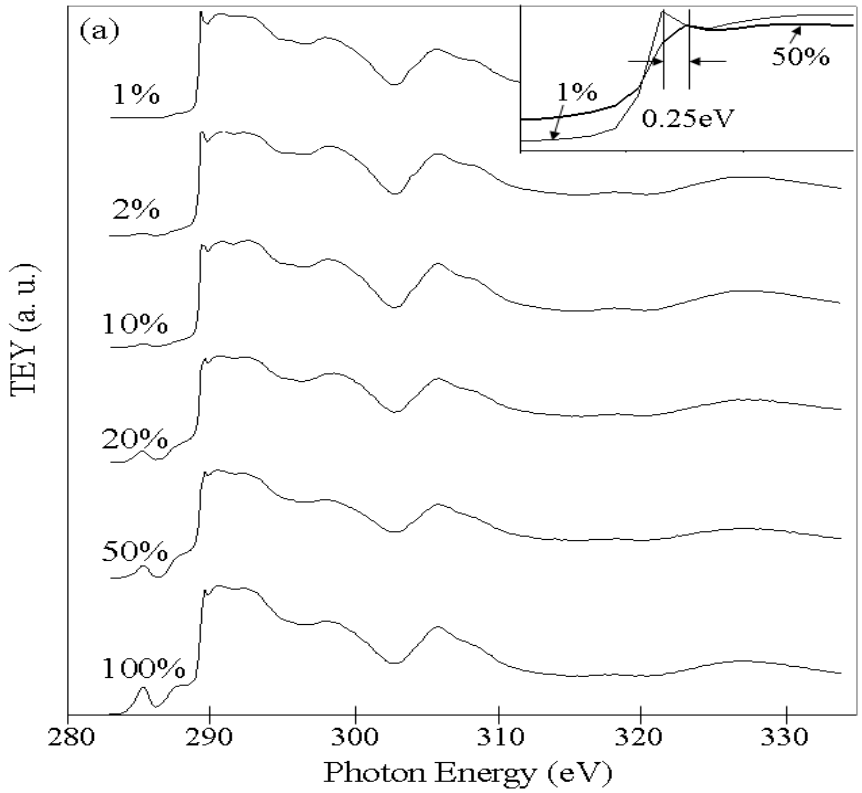

Figure 8.3 C K-edge NEXAFS of the films synthesized with different CH_4 concentrations: (a) TEY of C K-edge; (b) FY of C K-edge [215].

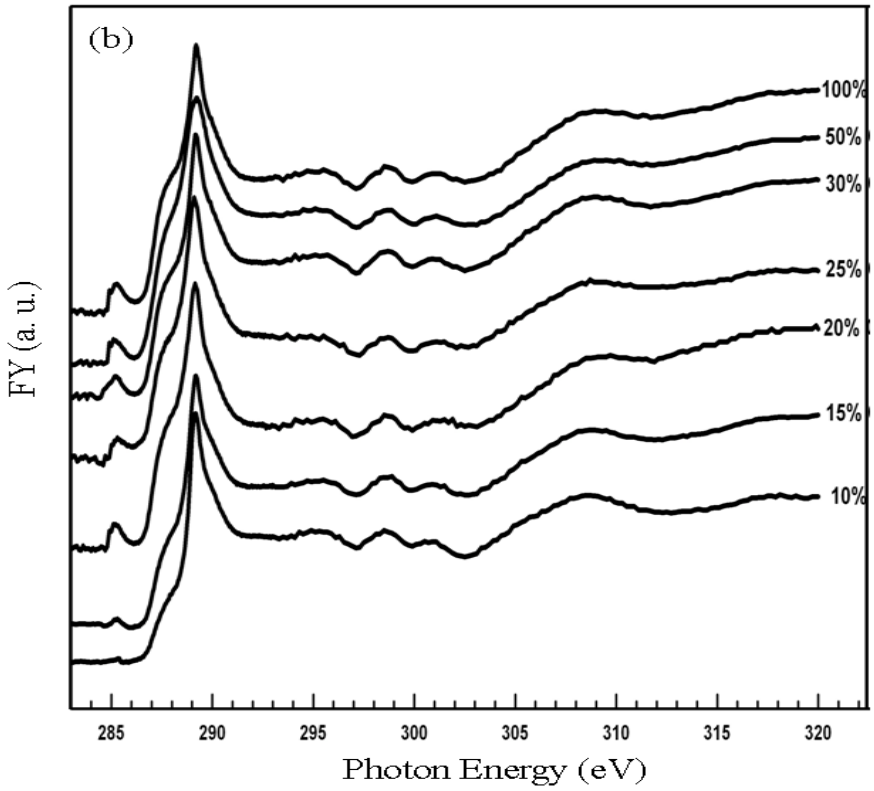

Figure 8.3 (Continued).

The films were also analyzed by Raman spectroscopy. Figure 8.4 shows the Raman spectra of the films grown with different CH_4 concentrations. As the CH_4 concentration increases, the spectrum gradually changes from the typical spectrum of microcrystalline diamond thin films to those of NCD thin films. A sharp peak around 1333 cm^{-1}, characteristic of the sp^3 diamond phase, is clearly seen in the spectra of the samples grown at low CH_4 concentrations. The full width at half maximum (FWHM) of this peak for the samples deposited at CH_4 concentrations of 1% and 2 % is around 6.1 cm^{-1}. This peak becomes broadened as the CH_4 concentration increases. The FWHM of the peak increases to 6.8 and 10.3 cm^{-1} for the samples grown at 5 % and 10 %, respectively. At a CH_4 concentration of 20%, the FWHM of this peak increases further to 20.5 cm^{-1}. The broadening of the diamond peak at 1333 cm^{-1} is mainly attributed to the decrease of grain size in the films [219]. A broad peak centered at around 1580 cm^{-1}, corresponding to sp^2 carbon, also appears in all the spectra and increases steadily, indicating a steady increase of sp^2 carbon concentration with the

increase of CH_4 concentration, consistent with the trend seen in NEXAFS spectra. In addition, peaks centered at around 1140 and 1480 cm^{-1} emerge when the CH_4 concentration increased to 10% and above. These two peaks originate from trans-polyacetylene in NCD films [191]. It should be noted that the spectra are dominated by non-diamond peaks and the diamond characteristic peak is ambiguous when the methane concentration increases to 10% or above, indicating that Raman spectroscopy with a laser wavelength of 514 nm is not appropriate to examine the structure of NCD films.

The experimental results show that very smooth (with a roughness below 30 nm) fine grained (with an average grain size below 5 nm) NCD thin films with reasonably low sp^2 carbon concentrations (below 25 %) have been synthesized at high CH_4 concentrations (50% or above) with a much higher growth rate. These films are expected to exhibit superior mechanical, electronic, optical and biomedical properties. The promising properties of the films such as friction and wear, bio- and haemo-compatibility, field electron emission, and their correlations with the sp^2 carbon concentration in the films are being investigated and will be presented in future papers.

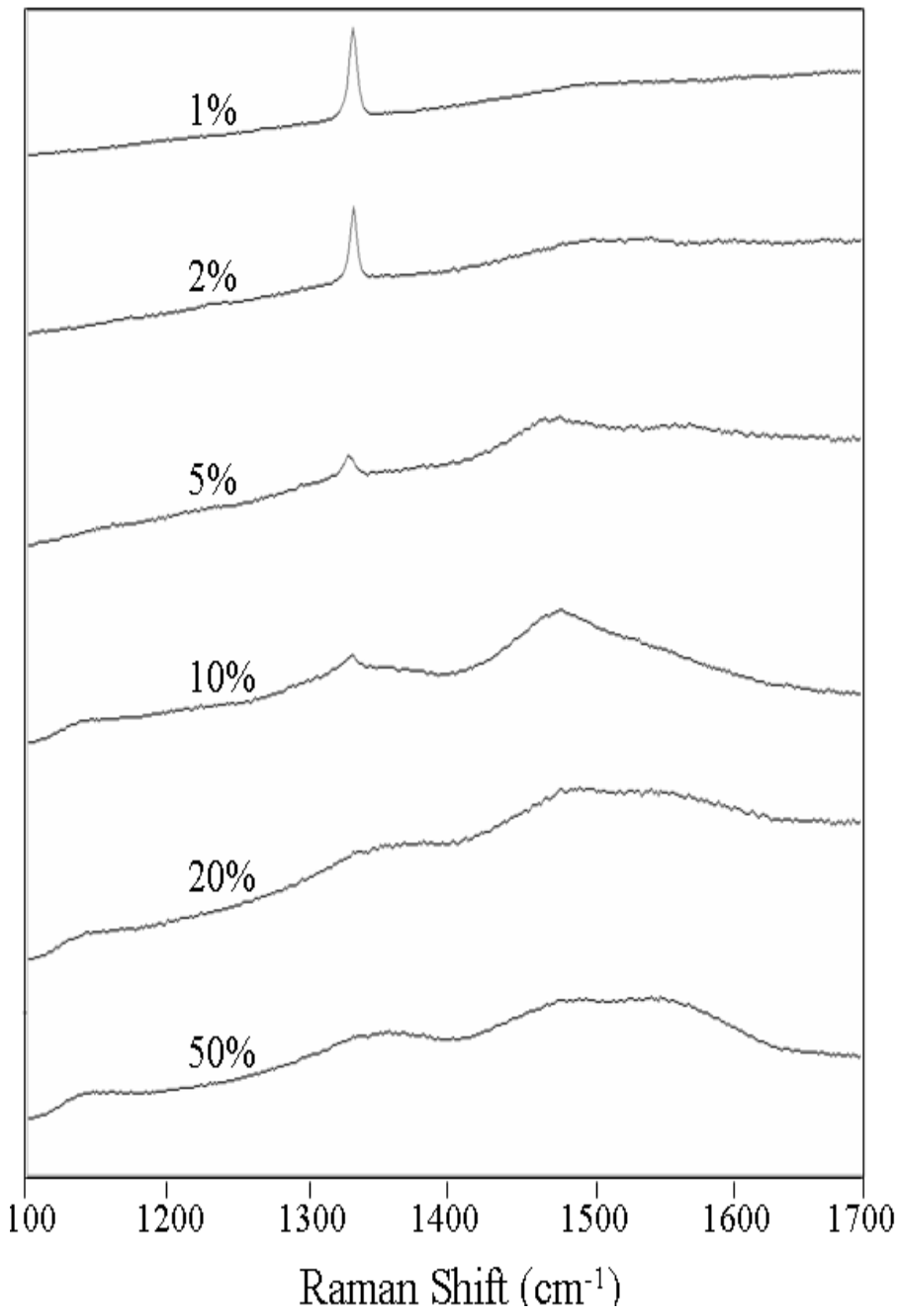

Figure 8.4 Raman spectra taken from the films synthesized with different CH_4 concentrations [215].

8.3 Conclusions

Diamond thin films, synthesized under a wide range of CH_4 concentrations from 1% to 100% using microwave plasma assisted CVD with a CH_4–H_2 mixture, were investigated using SEM, Raman spectroscopy, NEXAFS and AFM. The results show that variation of CH_4 concentration has significant influence on the grain size, surface roughness, growth rate and sp^2 carbon concentration in the synthesized films. With the increase of the CH_4 concentration, the growth rate, the surface smoothness, and the sp^2 carbon concentration of the films increase while the grain size decreases. The NEXAFS spectra of the NCD films exhibit clear spectral characteristics of diamond and the nanostructure of the films can be clearly identified. The results have demonstrated that NEXAFS is reliable to identify NCD films, and that smooth fine NCD thin films with reasonably low sp^2 carbon concentration can be synthesized in pure CH_4 atmosphere with high growth rate. It has been well accepted that diamond can be only synthesized with CH_4 highly diluted by hydrogen. The finding that NCD thin films can be synthesized from high CH_4 concentrations is encouraging and expected to accelerate industrial applications of CVD diamond.

* Part of this section has been published in “Diamond and Related Materials”, according to the Copyright Agreement of this journal, author retains the right “To include the Article, in full or in part, in a thesis or dissertation”.

CHAPTER 9
CONCLUSIONS AND FUTURE WORK

9.1 Conclusions

The main findings in this thesis are as follows:

(1) Nucleation and growth of diamond films on Ti_3SiC_2 has been investigated using MPECVD in a H_2 and CH_4 gas mixture. The diamond films grown on Ti_3SiC_2 have much higher nucleation density, much higher film formation rate, much higher growth rate, smaller grain size, smoother surface, higher interfacical adhesion, and higher fracture toughness than on Si.

(2) Dense NCD films with an equiaxed grain structure (an average grain size of 30 nm) have been synthesized on Ti_3SiC_2 using MPECVD in a 99.5% H_2+0.5% CH_4 gas mixture regardless of growth durations. An average nucleation density of $10^{11}/cm^2$ and a film growth rate of 2 μm/h have been achieved. C K-edge NEXAFS results have shown that the synthesized NCD films predominately consist of crystalline diamond with a small amount of sp^2 carbon and C-H bond predominantly near the surface of the film.

(3) Diamond growth on Ti_3SiC_2 at different input powers by MPECVD has demonstrated that NCD thin film can be synthesized at low microwave power of 500 W and the increase of power inputs results in the formation of <001> highly oriented smooth diamond thin films.

(4) The results on diamond nucleation and early stage growth through HFCVD show that a nanowhisker-like diamond-graphite composite layer was initially formed on the surface of Ti_3SiC_2, which resulted in high diamond nucleation density, whereas diamond nucleation on Si surface is predominantly based on defect sites and diamond remnants on the surface created by the diamond scratching. The diamond thin films formation rate is obviously higher on Ti_3SiC_2 than that on Si. A dense and smooth NCD thin film has been synthesized on Ti_3SiC_2 after 1 hour deposition.

(5) Diamond thin films on Si, synthesized under a wide range of CH_4 concentrations from 1% to 100% using microwave plasma assisted CVD with a CH_4–H_2 mixture were investigated using SEM, Raman spectroscopy, NEXAFS and AFM. The results show that variation of CH_4 concentration has significant influence on the grain size, surface roughness, growth rate and sp^2 carbon concentration in the synthesized films. With the increase of the CH_4 concentration, the growth rate, the surface smoothness, and the sp^2 carbon concentration of the films increase while the grain size decreases.

(6) The results have demonstrated that Ti_3SiC_2 is a good substrate material for diamond nucleation and growth, and has the potentials to be applied as an interlayer on metallic substrates for diamond film deposition. Due to the unique combination of both metallic and ceramic properties of Ti_3SiC_2, this successful synthesis of adhesive diamond films on Ti_3SiC_2 may be greatly expand the applications of both diamond and Ti_3SiC_2.

(7) The results demonstrated that synchrotron-based NEXAFS is a reliable and powerful technique to characterize the structure of NCD thin films.

9.2 Suggestions for Future Work

(1) The experimental results in this thesis demonstrated that the nucleation density of diamond on Ti_3SiC_2 is much higher than that on Si. The low carbon solubility in Ti_3SiC_2 should be one of factors responsible for this. Nucleation of new phase increases energy, thus nucleation prefers to start at high-energetic sites, such as grain boundary and pores, to decrease the nucleation energy. The higher nucleation density along the pores of Ti_3SiC_2 verified this. As the Ti_3SiC_2 samples used in this thesis are polycrystalline, grain boundary density is high. In addition, Ti_3SiC_2 has nanolayered microstructure. The interfaces of those nanolayers are also high-energetic. It is desirable to study the effect of grain boundaries and interfaces of nanolayers on nucleation of diamond. For this study, Ti_3SiC_2 samples with different grain size will be synthesized, and TEM is employed to provide high resolution to observe the nucleation of diamond along grain boundaries/nanolayer interfaces.

(2) Due to the unique combination of both metallic and ceramic properties of Ti_3SiC_2, Ti_3SiC_2 thin films is promising to be used as an interlayer for diamond deposition on steels and other metallic materials to enhance diamond nucleation and adhesion. Therefore, synthesis of Ti_3SiC_2 thin films on steels and other metallic materials as an interlayer for diamond formation is an interesting offshoot of my previous research. Ti_3SiC_2 thin films can be synthesized by high-temperature reactive magnetron or ionic sputtering by using solid targets of Ti, Si and C. Nanacystalline Ti_3SiC_2 thin films can be easily obtained. The high grain boundary density in nanocrystaline Ti_3SiC_2 thin films will probably further enhance the

nucleation rate/density of diamond, facilitating the formation of NCD thin films.

(3) Adhesion of diamond thin films on Ti_3SiC_2 has been tested using indentation method. However, only qualitative results can be obtained using this method. Although scratching tests have been widely used to obtain quantitative information on adhesion of thin film materials, the costly diamond tips or blades used for scratching are very easy to be damaged due to the high hardness of diamond. Thus, new methods are needed to be developed for quantitative measurement of diamond thin film adhesion on Ti_3SiC_2.

(4) Thin films usually have high residual stress due to their non-equilibrium deposition conditions and the difference in thermal expansion coefficient between thin films and substrate materials. The residual stress may combine with in-service mechanical stress to cause film failure. The understanding of residual stress is thus very important for applications. X-ray diffraction (XRD) is one of the effective methods for stress measurements. Residual stress measurement and investigation using XRD will be another aspect of future work.

REFERENCES

1. J. Stohr, NEXAFS Spectroscopy, Springer Series in Surface Sciences, (Springer Verlag, Berlin, 1992).
2. http://www.mhhe.com/physsci/chemistry/essentialchemistry/flash/hybrv18.swf, accessed on 20th December, 2008.
3. http://newton.ex.ac.uk/research/qsystems/people/sque/diamond/structure/, accessed on 20th December, 2008.
4. R. F. Davis, Diamond Films and Coatings, William Andrew Publishing/Noyes, 1993.
5. M. N. R. Ashfold, P. W. May, C. A. Rego and N. M. Everitt, Thin-Film Diamond by Chemical Vapor Deposition Methods, Chemical Society Reviews, 23(1994) 21-30.
6. F. P. Bundy, The P, T Phase and Reaction Diagram for Elemental Carbon, 1979; Journal of Geophysical Research, 85 (B12) (1980) 6930-6936.
7. H. O. Pierson, Handbook of Carbon, Graphite, Diamond and Fullerenes - Properties, Processing and Applications, William Andrew Publishing/Noyes, 1993.
8. F. P. Bundy, Direct Conversion of Graphite to Diamond in Static Pressure Apparatus, Science, 137 (1962) 1057.
9. F. P. Bundy, Direct Conversion of Graphite to Diamond in Static Pressure Apparatus, Journal of Chemical Physics, 38 (1963) 631.
10. F. P. Bundy, H. M. Strong, Behavior of Metals at High Temperatures and Pressures, Solid State Physics-Advances in Research and Applications, 13

(1962) 81-146.

11. G. T. Austin, Diamond, American Ceramic Society Bulletin, 70 (1991) 859.
12. P. W. May, Diamond Thin Films: A 21-Century Material, Philosophical Transactions of the Royal Society of London Series A-Mathematical Physical and Engineering Sciences, 358 (2000) 473-495.
13. S. Matsumoto, Y. Sato, M. Tsutsumi, and N. Setaka, Growth of Diamond Particles From Methane-Hydrogen Gas , Journal of Materials Science, 17 (1982) 3106-3112.
14. F. G. Celii and J. E. Bultler, Diamond Chemical Vapor-Deposition, Annual Review of Physical Chemistry, 42 (1991) 643-684.
15. Norton CVD Diamond, Technical Bulletin from Norton Co., Northboro, MA (1992).
16. Diamond Coating, A world of Opportunity, Technical Brochure, Genasystems Inc., Worthington, OH (1991).
17. D. J. Pickrell, K. A. Kline, R.E. Taylor, Thermal-Expansion of Polycrystalline Diamond Produced by Chemical-Vapor-Deposition, Applied Physics Letters, 64 (1994) 2353-2355.
18. L. Schafer, M. Sattler, and C. P. Klages, Application of Diamond Films and Related Materials, (Y. Tzeng, et al., eds.), 453-460, Elsevier Science Publishers (1991).
19. J. E. Graebner, S. Jin, G. W. Kammlott, J. A. Herb, C. F. Gardinier, Unusually High Thermal-Conductivity in Diamond Films, Applied Physics Letters, 60 (1992) 1576-1578.
20. K. L. Choy, Chemical Vapor Deposition of Coatings, Progress in Materials Science, 48 (2003), 57-170.
21. W. A. Yarbrough, and R. Messier, Current Issues and Problems In The

Chemical Vapor-Deposition Of Diamond, Science, 247 (1990) 688-696.

22. P. O. Joffreau, R. Haubner,and B. Lux, in Diamond and Diamond-like Materials Synthesis, (G. Johnson, A. Badzian and M. Geis, eds.) Materials Research Society Proceeding, Vol. EA-15, P. 15, Pittsburgh, PA (1988).
23. M. Kamo, Y. Sato, S. Matsumoto, and N. J. Setaka, Diamond Synthesis from Gas-Phase in Microwave Plasma , Journal of Crystal Growth, 62 (1983) 642-644.
24. P. K. Bachmann, and R. Messier, Emerging Technology of Diamond Thin-Films, Chemical & Engineering News, 67 (1989) 24.
25. N. Ohtake and M. Yoshikawa, Diamond Film Preparation by Arc-Discharge Plasma-Jet Chemical Vapor-Deposition in the Methane Atmosphere, Journal of the Electrochemical Society, 137 (1990) 717-722.
26. L. M. Hanssen, W. A. Carrington, J. E. Butler and K. A. Snail, Diamond Synthesis Using An Oxygen-Acetylene Torch, Materials Letter, 7 (1988) 289-292.
27. P. W. Morrison and J. T. Glass, In Properties and Growth of Diamond (ed. G. Davies), p. 380. London: INSPEC, 1994.
28. B. Dischler and C. Wild, Low-Pressure Synthetic Diamond, Springer, 1998.
29. K. E. Spear, Diamond Ceramic Coating of the Future, Journal of the American Ceramic Society, 72 (1989) 171-191.
30. O. Matsumoto, H. Toshima, and Y. Kanzaki, Effect of Dilution Gases in Methane on the Deposition of Diamond-Like Carbon in A Microwave-Discharge, Thin Solid Films, 128 (1985) 341-351.
31. Y. Saito, S. Matsuda, and S. Nogita, Synthesis of Diamond by Deposition of Methane in Microwave Plasma, Journal of Materials Science Letter, 5 (1986) 565-568.

32. O. Matsumoto, and T. Katagiri, Effect of Dilution Gases in Methane on the Deposition of Diamond-Like Carbon in a Microwave-Discharge II: Effect of Hydrogen, Thin Solid Films, 146 (1987) 283-289.
33. Y. Mitsuda, Y. Kojima, T. Yoshida, and K. Akashi, The Growth of Diamond in Microwave Plasma under Low-Pressure, Journal of Materials Science, 22 (1987) 1557-1562.
34. K. Suzuki, A. Sawabe, and T. Inuzuka, Characterization of the DC Discharge Plasma during Chemical Vapor Deposition for Diamond Growth, Applied Physics Letters, 53 (1988) 1818-1819.
35. F. G. Celili, P. E. Pehrsson, H. T. Wang, and J. E. Butler, Infrared Detection of Gaseous Species During the Filament-Assisted Growth of Diamond, Applied Physics Letter, 52 (1988) 2043-2045.
36. F. G. Celili, J. E. Butler, Hydrogen-Atom Detection in the Filament-Assisted Diamond Deposition Environment, Applied Physics Letter, 54 (1989) 1031-1033.
37. J. E. Butler, F. G. Celili, D. B. Oakes, et al., Study of Diamond Chemical Vapor Deposition, High Temperature Science, 27 (1989) 183-197.
38. W. A. Yarbrough, K. Tankala, T. DebRoy, Diamond Growth with Local Supplied Methane and Acetylene, Journal of Materials Research, 7 (1992) 379-383.
39. W. A. Yarbrough, Vapor-Phase-Deposited Diamond - Problems and Potential, Journal of the American Ceramic Society, 75 (1992) 3179-3200.
40. N. Ohtake and M. Yoshikawa, Diamond Film Preparation by Arc-Discharge Plasma-Jet Chemical Vapor-Deposition in the Methane Atmosphere, Journal of the Electrochemical Society, 137 (1990) 717-722.
41. S. T. Lee, Z. D. Lin, X. Jiang, CVD Diamond Films: Nucleation and Growth,

Materials Science and Engineering R-Report, 25 (1999) 123-154.

42. P. E. Pehrsson, J. Glesener and A. Morrish, Chemical Vapor-Deposition Diamond Nucleation Induced by sp^2 Carbon on Unscratched Silicon, Thin Solid Films, 212 (1992) 81-90.
43. H. M. Liu, D. S. Dandy, Studies on Nucleation Process in Diamond CVD: An Overview of Recent Development, Diamond and Related Materials, 4 (1995) 1173-1188.
44. E. A. Brandes, Smithells Metals Reference Book, Butterworth, London, 6th edn., 1983.
45. J. Shackelford and W. Alexander, The CRC Materials Science and Engineering Handbook, CRC Press, Boca Raton, FL, 1992.
46. T. P. Ong, F. L. Xiong, R. P. H. Chang and C. W. White, Nucleation and Growth of Diamond on Carbon-Implanted Single-Crystal Copper Surfaces, Journal of Materials Research, 7 (9) (1992) 2429-2439.
47. L. Z. Mezey and J. Giber, The Surface Free-Energies of Solid Chemical-Elements-Calculation from Internal Free Enthalpies of Atomization, Japan Journal of Applied Physics Part I-Regular Papers Short Notes & Review Papers, 21 (1982)1569-1571.
48. B. Lux and R. Haubner, in R. E. Clausing, L. L. Horton, J. C. Angus and P. Koidl (eds.), Diamond and Diamond-like Films and Coatings, Ploenum Press, New York, 1991, p.579.
49. P. T. B. Shaffer, Plenum Press Handbooks of High-Temperature Materials, No.1-Materials Index, Plenum Press, New York, 1964; G.V. Samsonov, Plenum Press Handbooks of High-Temperature Materials, No.2-Properties Index, Plenum Press, New York, 1964.
50. M. S. Wong, R. Meilunas, T. P. Ong and R. P. H. Chang, Tribological

Properties of Diamond Films Grown by Plasma-Enhanced Chemical Vapor Deposition, Applied Physics Letters, 54 (1989) 2006-2008.

51. J. Singh, Nucleation and Growth Mechanism of Diamond during Hot-Filament Chemical Vapor Deposition, Journal of Materials Science, 29 (1994) 2761-2766.
52. R. Csencsits, J. Rankin, R. E. Boekenhauer, M. K. Kundmann and B. W. Sheldon, in H. A. Atwater, E. Chason, M. H. Grabow and M. G. Lagally (eds.), Evolution of Surface and Thin Film Microstructure Symposium, Materials Research Society, Pittsburgh, PA, 1993, p. 695.
53. K. Tamaki, Y. Watanabe, Y. Nakamura and S. Hirayama, Nucleation of Diamond Particles by Hot-Filament Chemical-Vapor-Deposition, Thin Solid Films, 236 (1993) 115-119.
54. J. J. Dubray, C. G. Pantano, M. Meloncell and E. Bertran, Nucleation of Diamond on Silicon, Sialon, and Graphite Substrates Coated With an A-C-H Layer, Journal of Vacuum Science & Technology A-Vacuum Surfaces and Films, 9 (1991) 3012-3018.
55. D. J. Kim, H. C. Lee and J. Y. Lee, Effect of Reaction Pressure on the Nucleation Behaviour of Diamond Synthesized by Hot-Filament Chemical Vapour Deposition, Journal of Materials Science, 28 (1993) 6704-6708.
56. G. A. Hirata, L. Cota-Araiza, M. Avalos-Borja, M. H. Farias, O. Contreras and Y. Matsumoto, Nucleation and Growth of Diamond Films on Mu-C-SiC X-Si By Hot-Filament CVD, Journal of Physics-Condensed Matter, 5 (1993) A305-A306.
57. P. Bou, L. Vandenbulcke, R. Herbin and F. Hillion, Diamond Film Nucleation and Interface Characterization, Journal of Materials Research, 7 (1992) 2152-2159.

58. P. E. Pehrsson, F. G. Gelii and J. E. Butler, in R. F. Davis (ed.), Diamond Films and Coatings: Development, Properties, and Applications, Noyes, Park Ridge, NJ, 1993, p. 68.

59. D. N. Belton, S. J. Harris, S. J. Schmieg, A. M. Weiner and T. A. Perry, In-situ Characterization of Diamond Nucleation and Growth, Applied Physics Letters, 54 (1989) 416-418.

60. M. A. George, A. Burger, W. E. Collins, J. L. Davidson, A. V. Barnes and N. H. Tolk, Investigation of Nucleation and Growth-Processes of Diamond Films by Atomic-Force Microscopy, Journal of Applied Physics, 76 (1994) 4099-4106.

61. B. R. Stoner, S. R. Sahaida, J. P. Bade, P. Southworth and P. J. Ellis, Highly Oriented, Textured Diamond Films on Silicon via Bias-Enhanced Nucleation and Textured Growth, Journal of Materials Research, 8 (1993) 1334-1340.

62. S. D. Wolter, B. R. Stoner, J. T. Glass, P. J. Ellis, D. S. Buhaenko, C. E. Jenkins and P. Southworth, Textured Growth of Diamond on Silicon via In-situ Carburization and Bias-Enhanced Nucleation, Applied Physics Letter, 62 (1993) 1215-1217.

63. B. R. Stoner, G. H. M. Ma, S. D. Wolter and J. T. Glass, Characterization of Bias-Enhanced Nucleation of Diamond on Silicon by Invacuo Surface-Analysis And Transmission Electron-Microscopy, Physical Review B, 45 (1992) 11067-11084.

64. S. D. Wolter, B. R. Stoner, G. H. M. Ma and J. T. Glass, in C. L. Renschler, J. J. Pouch and D. M. Cox (eds.), Novel Forms of Carbon Symp., Pittsburgh, PA, Materials Research Society, Pittsburgh, PA, 1992, p. 347.

65. A. A. Smolin, S. M. Pimenov, V. G. Ralchenko, T. V. Kononenko and E. N. Loubnin, Optical Monitoring of Nucleation and Growth of Diamond Films,

Applied Physics Letters, 62 (1993) 3449-3451.

66. A. R. Badzian and T. Badzian, Nucleation and Growth Phenomena in Chemically Vapor-Deposited Diamond Coatings, Surface & Coatings Technology, 36 (1988) 283-293.
67. B. E. Williams and J. T. Glass, Characterization of Diamond Thin-Films-Diamond Phase Identification, Surface-Morphology, and Defect Structures, Journal of Materials Research, 4 (1989) 373-384.
68. S. Yugo, T. Kimura and T. Muto, Effects of Electric-Field on the Growth of Diamond by Microwave Plasma CVD, Vacuum, 41 (1990) 1364-1367.
69. B. E. Williams, J. T. Glass, R. F. Davis and K. Kobashi, The Analysis of Defect Structures and Substrate Film Interfaces of Diamond Thin-Films, Journal of Crystal Growth, 99 (1990) 1168-1176.
70. P. O. Joffreau, R. Haubner and B. Lux, Low-Pressure Diamond Growth on Refractory Metals, International Journal of Refractory Metals and Hard Materials, 7 (1988) 186-194.
71. R. Meilunas, M. S. Wong, K. C. Sheng, R. P. H. Chang and R. P. Vanduyne, Early Stages of Plasma Synthesis of Diamond Films , Applied Physics Letter, 54 (1989) 2204-2206.
72. D. Michau, B. Tanguy, G. Demazeau, M. Couzi and R. Cavagnat, Influence on Diamond Nucleation of the Carbon Concentration Near the Substrate Surface, Diamond Related Materials, 2 (1993) 19-23.
73. D. N. Belton and S. J. Schmieg, Nucleation of Chemically Vapor-Deposited Diamond on Platinum and Nickel Substrates, Thin Solid Film, 212 (1992) 68-80.
74. M. M. Waite and S. I. Shah, X-Ray Photoelectron-Spectroscopy of Initial-Stages of Nucleation and Growth of Diamond Thin-Films during Plasma

Assisted Chemical Vapor-Deposition, Applied Physics Letter, 60 (1992) 2344-2346.

75. T. P. Ong, F. Xiong, R. P. H. Chang and C. W. White, Nucleation and Growth of Diamond on Carbon-Implanted Single-Crystal Copper Surfaces, Journal Materials Research, 7 (1992) 2429-2439.
76. T. P. Ong, F. Xiong, R. P. H. Chang and C. W. White, Mechanism for Diamond Nucleation and Growth on Single-Crystal Copper Surfaces Implanted with Carbon, Applied Physics Letter, 60 (1992) 2083-2085.
77. S. D. Wolter, B. R. Stoner, G. H. M. Ma and J. T. Glass, in C. L. Renschler, J. J. Pouch and D. M. Cox (eds.), Novel Forms of Carbon Symp., Pittsburgh, PA, Materials Research Society, Pittsburgh, PA, 1992, p. 347.
78. J. C. Angus, A. Argoitia, R. Gat, Z. Li, M. Sunkara, L. Wang and Y. Wang, Chemical Vapor-Deposition of Diamond, Philosophical Transactions of The Royal Society of London Series A-Mathematical Physical and Engineering Sciences, 342 (1993) 195-208.
79. W. R. L. Lambrecht, C. H. Lee, B. Segall, J. C. Angus, Z. Li and M. Sunkara, Diamond Nucleation by Hydrogenation of The Edges of Graphitic Precursors, Nature, 364 (1993) 607-610.
80. R. Haubner, A. Lindlbauer and B. Lux, On the Formation of Diamond Coatings on WC/Co Hard Metal Tools, International Journal of Refractory Metals and Hard Materials, 14 (1996) 111-118.
81. Y. Mitsuda, Y. Kojima, T. Yoshida, K. Akashi, The Growth of Diamond in Microwave Plasma under Low-Pressure, Journal of Materials Science, 22 (1987) 1557-1562.
82. A. Sawabe, T. Inuzuka, Growth of Diamond Thin-Films by Electron-Assisted Chemical Vapor-Deposition and Their Characterization, Thin Solid Films, 137

(1986) 89-99.

83. K. Suzuki, A. Swabe, H. Yasuda, T. Inuzuka, Growth of Diamond Thin-Films by DC Plasma Chemical Vapor-Deposition, Applied Physics Letters, 50 (1987) 728-729.
84. S. Iijima, Y. Aikawa, K. Baba, Growth of Diamond Particles in Chemical Vapor-Deposition, Journal of Materials Research, 6 (1991) 1491-1497.
85. S. P. Murarka, M. C. Peckerar, Electronic Materials Science and Technology, Academic Press Inc. San Diego, CA, 1989.
86. S. Yugo, A. Izumi, T. Kanai, T. Muto, T. Kimura, Proc. of the 2nd Int. Conf. on New Diamond Science and Technology, Pittsburg, PA, MRS, 1991, pp. 385-390.
87. S. Yugo, T. Kanai, T. Kimura, T. Muto, Generation of Diamond Nuclei by Electric-Field in Plasma Chemical Vapor-Deposition, Applied Physics Letters, 58 (1991) 1036-1038.
88. S. Yugo, T. Kimura, T. Kanai, Nucleation Mechanisms of Diamond in Plasma Chemical-Vapor-Deposition, Diamond and Related Materials, 2 (1993) 328-332.
89. J. Gerber, S. Sattel, K. Jung, H. Ehrhard, J. Robertson, Experimental Characterization of Bias-Enhanced Nucleation of Diamond on Si, Diamond and Related Materials, 4 (1995) 559-562.
90. B. R. Stoner, G. H. Ma, S. D. Wolter, W. Zhou, Y. C. Wang, R. F. Davis, J. T. Glass, Epitaxial Nucleation of Diamond on Beta-Sic via Bias-Enhanced Microwave Plasma Chemical-Vapor-Deposition, Diamond and Related Materials, 2 (1993) 142-146.
91. X. Jiang, K. Schiffmann, C. P. Klages, Nucleation and Initial Growth-Phase of Diamond Thin-Films on (100)-Silicon, Physical Review B, 50 (1994) 8402-

8410.

92. X. Jiang, C. P. Klages, Recent Developments in Heteroepitaxial Nucleation and Growth of Diamond on Silicon, Physica Status Solidi A-Applications and Materials Science, 154 (1996) 175-183.

93. S. T. Lee, Y. W. Lam, Z. D. Lin, Y. Chen, Q. J. Chen, Pressure Effect on Diamond Nucleation in a Hot-Filament CVD System, Physics Review B, 5524 (1997) 15937-15941.

94. J. Yang, X. W. Su, Q. J. Chen, Z. D. Lin, Si^+ Implantation - A Pretreatment Method for Diamond Nucleation on a Si Wafer, Applied Physics Letters, 66 (1995) 3284-3286.

95. V. I. Konov, A. A. Smolin, V. G. Ralchenko, E. D. Obratzva, E. N. Loubnin, S. M. Metev and G. Sepold, D.C. Arc Plasma Deposition of Smooth Nanocrystalline Diamond Films, Diamond and Related Materials, 4 (1995) 1073-1078.

96. J. M. Ting, Diamond Formation on Carbon-Carbon Composite, Journal of Materials Science, 30 (1995) 4095-4100.

97. E. J. Bienk and S. S. Eskildsen, The Effect of Surface Preparation on the Nucleation of Diamond on Silicon, Diamond and Related Materials, 2 (1993) 432-437.

98. R. Erz, W. Dötter, K. Jung and H. Ehrhardt, Preparation of Smooth and Nanocrystalline Diamond Films, Diamond and Related Materials, 2 (1993) 449-453.

99. L. C. Nistor, J. Van Landuyt, V. G. Ralchenko, E. D. Obratzva, K. G. Korotushenko, A. A. Smolin, Structural Studies of Nanocrystalline Diamond Thin Films, Materials Science Forum, 239-241 (1997) 115-118.

100. L. C. Nistor, J. Van Landuyt, V. G. Ralchenko, E. D. Obratzva, K. G.

Korotushenko, A. A. Smolin, Nanocrystalline Diamond Films: Transmission Electron Microscopy and Raman Spectroscopy Characterization, Diamond Related Materials, 6 (1997) 159-168.

101. T. Lin, G. Y. Yu, T. S. Wee and Z. X. Shen, Compositional Mapping of the Argon-Methane-Hydrogen System for Polycrystalline to Nanocrystalline Diamond Film Growth in a Hot-Filament Chemical Vapor Deposition System, Applied Physics Letters, 77 (2000) 2692-2694.

102. S. R. P. Silva, K. M. Knoeles, G. A. J. Amartunga, A. Putnis, The Microstructure of Inclusions in Nanocrystalline Carbon-Films Deposited at Low-Temperature, Diamond and Related Materials, 3 (1994) 1048-1055.

103. J. H. Lee, B. Y. Hong, R. Messier, R. W. Collins, Nucleation and Bulk Film Growth Kinetics of Nanocrystalline Diamond Prepared by Microwave Plasma-Enhanced Chemical Vapor Deposition on Silicon Substrates, Applied Physics Letters, 69 (1996) 1716-1718.

104. D. M. Bhusari, J. R. Yang, T. Y. Wang, K. H. Chen, S. T. Lin, L. C. Chen, Effects of Substrate Pretreatment and Methane Fraction on the Optical Transparency of Nanocrystalline Diamond Thin Films, Journal of Materials Research, 7 (1998) 1769-1773.

105. S. N. Kundu, M. Basu, A. B. Maity, S. Chaudhuri, A. K. Pal, Nanocrystalline Diamond Films Deposited by High Pressure Sputtering of Vitreous Carbon, Materials Letters, 31 (1997) 303-309.

106. M. Zarrabian, N. Fourches-Coulon, G. Turban, C. Marhic, M. Lancin, Observation of Nanocrystalline Diamond in Diamondlike Carbon Films Deposited at Room Temperature in Electron Cyclotron Resonance Plasma, Applied Physics Letters, 70 (1997) 2535-2537.

107. S. M. Huang, Z. Sun, Y. F. Lu, M. H. Hong, Ultraviolet and Visible Raman

Spectroscopy Characterization of Chemical Vapor Deposition Diamond Films, Surface and Coating Technology, 151 (2002) 263-267.

108. S. H. Seo, T. H. Lee, J. S. Park, Roughness Control of Polycrystalline Diamond Films Grown by Bias-Enhanced Microwave Plasma-Assisted CVD, Diamond and Related Materials, 12 (2003) 1670-1674.

109. K. Subramanian, W. P. Kang, J. L. Davidson, W. H. Hofmeister, Growth Aspects of Nanocrystalline Diamond Films and Their Effects on Electron Field Emissions, Journal of Vacuum Science & Technology B, 23 (2005) 786-792.

110. K. Subramanian, W. P. Davidson and W. H. Hofmeister, The Effect of Growth Rate Control on the Morphology of Nanocrystalline Diamond, Diamond and Related Materials, 14 (2005) 404-410.

111. R. B. Corvin, J. G. Harrison, S. A. Catledge, and Y. K. Vohra, Gas-Phase Thermodynamic Models of Nitrogen-Induced Nanocrystallinity in Chemical Vapor-Deposited Diamond, Applied Physics Letter, 80 (2002) 2550-2552.

112. S. T. Kshirsagar, R. B. Kshirsagar, P. S. Patil, A. Kulkarni, A. B. Mandate, A. B. Gaikwad, S. P. Gokhale, Gradual Transitions in Morphology of Diamond Films Grown by Using N_2 Admixtures of CH_4+H_2 Gas in a Hot Filament Assisted Chemical Vapour Deposition System, Diamond and Related Materials, 14 (2005) 232-242.

113. S. Chowdhury, D. A. Hillman, S. A. Catledge, W. Konovalov and Y. K. Vohra, Synthesis of Ultrasmooth Nanostructured Diamond Films by Microwave Plasma Chemical Vapor Deposition Using a He/H_2/CH_4/N_2 Gas Mixture, Journal of Materials Research, Journal of Materials Research, 21 (2006) 2675-2682.

114. C. J. Tang, A. J. Neves, A. J. S. Fernandes, J. Gracio and M. C. Carmo, The

Effect of Oxygen and Nitrogen Additives on the Growth of Nanocrystalline Diamond Films, Journal of Physics-Condensed Matter, 19 (2007) Article No. 386236.

115. D. M. Gruen, S. Liu, A. R. Krauss, J. Luo and X. Pan, Fullerenes as Precursors for Diamond Film Growth without Hydrogen or Oxygen Additions, Applied Physics Letters, 64 (1994) 1502-1504.

116. D. Zhou, T. G. McCauley, L. C. Qin, A. R. Kraus and D. M. Gruen, Synthesis of Nanocrystalline Diamond Thin Films from an Ar-CH_4 Microwave Plasma, Journal of Applied Physics, 83 (1998) 540-543.

117. D. M. Gruen, Nanocrystalline Diamond Films, Annual Review of Materials Science, 29 (1999) 211-259.

118. S. Jiao, A. Sumant, M. A. Kirk, D. M. Gruen, A. R. Kraus and O. Auciello, Microstructure of Ultrananocrystalline Diamond Films Grown by Microwave Ar-CH_4 Plasma Chemical Vapor Deposition with or without Added H_2, Journal of Applied Physics, 90 (2001) 118-122.

119. J. Birrel, J. A. Carlisle, O. Auciello, D. M. Gruen and J. M. Gibson, Morphology and Electronic Structure in Nitrogen-Doped Ultrananocrystalline Diamond, Applied Physics Letters, 81 (2002) 2235-2237.

120. X. Xiao, J. Birrell, J. E. Gerbi, O. Auciello and J. A. Carlisle, Low temperature growth of ultrananocrystalline diamond, Journal of Applied Physics, 96 (2004) 2232-2239.

121. X. Xiao, J. W. Elam, S. Trasobares, O. Auciello and J. A. Carlisle, Synthesis of a Self-Assembled Hybrid of Ultrananocrystalline Diamond and Carbon Nanotubes, Advanced Materials, 17 (2005) 1496-1500.

122. E. M. Mattox, in K. L. Mittal (ed.), Adhesion Measurement of Thin Films, Thick Films, and Bulk Coatings, ASTM International, 1978, P54.

123. A. K. Mehlmann, A. Fayer, S. F. Dimfield, Y. Avigal, R. Porath and A. Kochman, Nucleation and Growth of Diamond on Cemented Carbides by Hot-Filament Chemical-Vapor-Deposition, Diamond and Related Materials, 2 (1993) 317-322.

124. M. Murakawa and S. Takeuchi, H. Miyazawa and Y. Hirose, Chemical Vapor-Deposition of a Diamond Coating onto a Tungsten Carbide Tool Using Ethanol, Surface and Coatings Technology, 36 (1988) 303-310.

125. B. S. Park, Y. J. Baik, K. R. Lee, K. Y. Eun and D. H. Kim, Behavior of Co Binder Phase during Diamond Deposition on Wc-Co Substrate, Diamond and Related Materials, 2 (1993) 910-917.

126. T. H. Huang, C. T. Kuo, C. S. Chang, C. T. Kao and H. Y. Wen, Tribological behaviours of the diamond-coated cemented carbide tools with various cobalt contents, Diamond and Related Materials, 1 (1992) 594-599.

127. F. M. Pan, J. L. Chen, T. Chou, T. S. Lin and L. Chang, Interface Studies of the Diamond Film Grown on the Cobalt Cemented Tungsten Carbide, Journal of Vacuum Science Technology A -Vacuum Surfaces And Films, 12 (1994) 1519-1522.

128. A. Inspektor, C. E. Bauer and E. J. Oles, Superhard Coatings for Metal Cutting Applications, Surface and Coatings Technology, 68/69 (1994) 359-368.

129. M. A. Taher, W. F. Schmidt, A. P. Malshe, E. J. Oles and A. Inspector, in K.L. Mittal (ed.), Adhesion Aspects of Thin Films, Vol. 1, VSP 2001, P79.

130. S. J. Bull, D. S. Rickerby, in: D. S. Rickerby, A. Matthews (Eds.), Advanced Surface Coatings: A Handbook of Surface Engineering, Chapman and Hall Inc, New York, 1991, p. 315.

131. K. Saijo, M. Yagi, K. Shibuki and S. Takatsu, The Improvement of the Adhesion Strength of Diamond Films, Surface and Coating Technology, 43/44

(1990) 30-40.

132. J. Oakes, X.X. Pan, R. Haubner and B. Lux, Chemical Vapor-Deposition Diamond Coatings on Cemented Carbide Tools, Surface and Coatings Technology, 47 (1991) 600-607.

133. S. A. Catledge, Y. K. Vohra, D. D. Jackson, S. T. Weir, Adhesion of Nanostructured Diamond Film on a Copper-Beryllium Alloy, Journal of Materials Research, 23 (2008) 2373-2381.

134. Y. Saito, T. Isozaki, A. Masuda, K. Fukumoto, M. Chosa, T. Ito, C. E. Bauer, A. Inspektor and E. J. Oles. Adhesion Strength of Diamond Film on Cemented Carbide Insert, Diamond and Related Materials, 2 (1993) 1391-1395.

135. T. Isozaki, Y. Saito, A. Masuda, K. Fukumoto, M. Chosa, T. Ito, E. J. Oles, A. Inspektor and C.E. Bauer, Improvement on Adhesion Strength of Diamond Film on Cemented Carbide by Heated Intermediate Layer, Diamond and Related Materials, 2 (1993) 1156-1159.

136. M. Nesladek, J. Spinnewyn, C. Asinari, R. Lebout and R. Lorent, Improved Adhesion of CVD Diamond Films to Steel and Wc-Co Substrates, Diamond and Related Materials, 3 (1994) 98-104.

137. W. D. Fan, X. Chen, K. Jagannadham and J. Narayan, Diamond Ceramic Composite Tool Coatings, Journal of Materials Research, 9 (1994) 2850-2867.

138. P. X. Ling and G. Z. Ping, Morphologies and adhesion strength of diamond films deposited on WC-6%Co cemented carbides with different surface characteristics, Thin Solid Films, 239 (1994) 47-50.

139. M. A. Taher, W. F. Schmidt, W. D. Brawn, S. Nasrazadani, H. A. Naseem and A. P. Malshe, Effect of Methane Concentration on Mechanical Properties of HFCVD Diamond-Coated Cemented Carbide Tool Inserts, Surface and Coatings Technology, 86-87 (1996) 678-685.

140. M. B. Guseva, V. G. Babaev, V. V. Khvostov, G. M. Lopes Lundena, A. Y. Bregadze, I. Y. Konyashin and A. E. Alexenko, High Quality Diamond Films on WC-Co Surfaces, Diamond and Related Materials, 6 (1997) 89-94.

141. I. Y. Konyashin, M. B. Guseva, V. G. Babaev, V. V. Khvostov, G. M. Lopez and A. E. Alexenko, Diamond Films Deposited on WC-Co Substrates by Use of Barrier Interlayers and Nano-Grained Diamond Seeds, Thin Solid Films, 300 (1997) 18-24.

142. B. Zhang and L. Zhou, Effect of Sandblasting on Adhesion Strength of Diamond Coatings, Thin Solid Films, 307 (1997) 21-28.

143. W. Jeitschko and H. Nowotny, Monatasch fur Chemie, 98 (1967) 329.

144. M. W. Barsoum and T. EI-Raghy, The MAX Phases: Unique New Carbide and Nitride Materials - Ternary Ceramics Turn out to Be Surprisingly Soft and Machinable, Yet also Heat-Tolerant, Strong and Lightweight, American Scientist, 89 (2001) 334-343.

145. Z. M. Sun, S. L. Yang, H. Hashimoto, S. Tada, T. Abe, Synthesis and Consolidation of Ternary Compound Ti_3SiC_2 From Green Compact of Mixed Powders, Materials Transections, 45 (2004) 373-375.

146. M. W. Barsoum, The $M_{N+1}AX_N$ Phases: A New Class Of Solids : Thermodynamically Stable Nanolaminates, Progress in Solid State Chemistry, 28 (2000) 201-208.

147. T. Goto, T. Hirai, Chemically Vapor-Deposited Ti_3SiC_2, Materials Research Bulletin, 22 (1987) 1195-1201.

148. M. W. Barsoum, T. EIRaghy, Synthesis and Characterization of a Remarkable Ceramic: Ti_3SiC_2, Journal of American Ceramic Society, 79 (1996):1953-1956.

149. N. F. Gao, Y. Miyamoto and K. Tanihata, Dense Ti_3SiC_2 Prepared by Reactive HIP, Journal of Materials Science, 34 (1999) 4385-4392.

150. J. F. Li, F. Sato, and R. Watanabe, Synthesis of Ti_3SiC_2 Polycrystals by Hot-Isostatic Pressing of the Elemental Powders, Journal of Materials Science Letters, 18 (1999)1595-1597.

151. T. El-Raghy, and M. W. Barsoum, Processing and Mechanical Properties of Ti_3SiC_2: I, Reaction Path and Microstructure Evolution, Journal of American Ceramic Society, 82 (1999) 2849-2854.

152. C. Racault, F. Langlais and R. Naslain, Solid-State Synthesis and Characterization of the Ternary Phase Ti_3SiC_2, Journal of Materials Science, 29 (1994) 3384-3392.

153. R. Radhakrishnan, C. H. Jr. Henager, J. L. Brimhall and S. B. Bhaduri, Synthesis of Ti_3SiC_2/SiC and $TiSi_2$/SiC Composites Using Displacement Reactions in the Ti-Si-C System, Scripta Materialia, 34 (1996) 1809-1814.

154. R. Radhakrishnan, J. J. Williams and M. Akinc, Synthesis and High-Temperature Stability of Ti_3SiC_2, Journal of Alloys and Compounds, 285 (1999) 85-88.

155. F. Sato, J. F. Li and R. Watanabe, Reaction Synthesis of Ti_3SiC_2 from Mixture of Elemental Powders, Materials Transactions JIM, 41 (2000) 605-608.

156. Y. C. Zhou, Z. M. Sun, S. Q. Chen and Y. Zhang, In-Situ Hot Pressing Solid-Liquid Reaction Synthesis of Dense Titanium Silicon Carbide Bulk Ceramics, Materials Research Innovations, 2 (1998) 142-146.

157. Z. M. Sun, Y. C. Zhou, Synthesis of Ti_3SiC_2 Powders by a Solid-Liquid Reaction Process, Scripta Materialia, 41 (1999) 61-66.

158. J. T. Li and Y. Miyamoto, Fabrication of Monolithic Ti_3SiC_2 Ceramic through Reactive Sintering of Ti/Si/2TiC, Journal of Materials Synthesis and Processing, 7 (1999) 91-96.

159. Z. F. Zhang, Z. M. Sun, H. Hashimoto, Fabrication and Microstructure

Characterization of Ti_3SiC_2 Synthesized from Ti/Si/2TiC Powders Using the Pulse Discharge Sintering (PDS) Technique, Journal of American Ceramic Society, 86 (2003) 431-436.

160. Z. M. Sun, S. L. Yang, H. Hashimoto, Effect of Al on the Synthesis of Ti_3SiC_2 by Reactively Sintering Ti-SiC-C Powder Mixtures, Journal of Alloys and Compounds, 439 (2007) 321-325.

161. S. L. Yang, Z. M. Sun, Q. Q. Yang, Effect of Al Addition on the Synthesis of Ti_3SiC_2 Bulk Material by Pulse Discharge Sintering Process, Journal of European Ceramic Society, 27 (2007) 4807-4812.

162. T. El-Raghy, P. Blau and M. W. Barsoum, Effect of Grain Size on Friction and Wear Behavior of Ti_3SiC_2, Wear, 238 (2000) 125-130.

163. http://www.purdue.edu/REM/rs/sem.htm, accessed on 4th January, 2009.

164. http://www.nanotech-now.com/images/Art_Gallery/AS-AFM.jpg, accessed on 4th January, 2009.

165. http://en.wikipedia.org/wiki/Raman_spectroscopy, accessed on 21th, March, 2009.

166. B. Schrader, Infrared and Raman Spectroscopy, Method and Application, VCH Verlagsgesellschaft mbH, Weinheim, New York (1995).

167. J. C. Rivière, Surface Analytical Techniques, Clarendon Press, Oxford (1990) P13.

168. G. Irmer and A. Dorner-Reisel, Advanced Engineering Materials, 7 (2005) 703.

169. J. F. Morar, F. J. Himpsel, G. Hollinger, G. Hughes and J. L. Jordan, Observation of a C-1s Core Exciton in Diamond, Physics Review Letters, 54 (1985) 1960-1963.

170. www.lightsouce.ca/education, accessed on 7th March, 2009.

171. B. Watts, L. Thomsen, P. C. Dastoor, Methods in Carbon K-edge NEXAFS: Experiment and Analysis, Journal of Electron Spectroscopy and Related Phenomena, 151 (2006) 105-120.

172. D. Briggs, M. P. Seah (Eds.), Practical Surface Analysis, 2nd ed., vol. 1, Wiley, 1990.

173. L. Jaworska, Diamond Composites with TiC, SiC and Ti_3SiC_2 Bonding Phase, High Pressure Research, 22 (2002) 531-533.

174. T. Abe, T. Takagi , Z. M. Sun , T. Uchimoto , J. Makino, H. Hashimoto, Machinable Ceramic Substrate for CVD Diamond Coating, Diamond Related Materials, 13 (2004) 819-822.

175. S. L. Yang, Q. Yang, Z. M. Sun, Nucleation and Growth of Diamond on Titanium Silicon Carbide By Microwave Plasma Enhanced Chemical Vapor Deposition, Journal of Crystal Growth, 294 (2006) 452-458.

176. R. J. Nemanich, J. T. Glass, G. Lucovsky, R. E. Shroder, Raman-Scattering Characterization of Carbon Bonding in Diamond and Diamondlike Thin-Films, Journal of Vacuum Science & Technology A-Vacuum Surfaces and Films, 6 (1988) 1783-1787.

177. Q. Yang, W. Chen, C. Xiao, A. Hirose, M. Bradly, Low Temperature Synthesis of Diamond Thin Films through Graphite Etching in a Microwave Hydrogen Plasma, Carbon, 43 (2005) 2635-2638.

178. M. R. Sheng, H. Wang, Z. Y. Ning, C. Ye and Z. X. Xin, Modelling the Substrate-Temperature-Dependence of Diamond Film Growth, Journal of Physics: Condensed Matter, 8 (1996) 8953-8958.

179. S. Kubelka, R. Hauber, B. Lux, R. Steiner, G. Stingeder, M. Grasserbauer, Chemical Interactions of WC/Co Hard Metal Substrates with Low-Pressure Diamond Coatings, Diamond Films and Technology, 5 (1995) 105-120.

180. G. R. Anstis, P. Chantikul, B. R. Lawn and D. B. Marshall, A Critical-Evaluation of Indentation Techniques for Measuring Fracture-Toughness I: Direct Crack Measurements, Journal of the American Ceramic Society, 64 (1981) 533-538.

181. N. Dubrovinskaia, S. Dub, and L. Dubrovinsky, Superior Wear Resistance of Aggregated Diamond Nanorods, Nano Letters, 6 (2006) 824-826.

182. S. Jacques, H. Di-Murro, M. P. Berthet and H. Vicent, Pulsed Reactive Chemical Vapor Deposition in the C-Ti-Si System from $H_2/TiCl_4/SiCl_4$, Thin Solid Films, 478 (2005) 13-20.

183. E. Pickering, W. J. Lackey, S. Crain, CVD of Ti_3SiC_2, Chemical Vapor Deposition, 6 (2000) 289-295.

184. C. Racault, F. Langlais, C. Bernara, On the Chemical-Vapor-Deposition of Ti_3SiC_2 from $TiCl_4SiCl_4$-CH_4-H_2 Gas-Mixtures I: A Thermodynamic Approach, Journal of Materials Science, 29 (1994) 5023-5040.

185. S. L. Yang, Q. Yang, Z. M. Sun, Synthesis and Characterization of Nanocrystalline Diamond Thin Film on Ti_3SiC_2, Nanotechnology, 18 (2007), Article No. 065703.

186. D. Zhou, D. M. Gruen, L. C. Qin, T. G. McCauley and A. R. Krauss, Control of Diamond Film Microstructure by Ar Additions to CH_4/H_2 Microwave Plasmas, Journal of Applied Physics, 84 (1998) 1981-1989.

187. D. S. Knight and W. B. White, Characterization of Diamond Films by Raman-Spectroscopy, Journal of Materials Research, 4 (1989) 385-393.

188. P. E. Batson, Carbon 1s Near-Edge-Absorption Fine Structure in Graphite, Physical Review B, 48 (1993) 2608-2610.

189. P. Keblinski, S. R. Phillpot, D. Wolf and H. Gleiter, On the Nature of Grain Boundaries in Nanocrystalline Diamond, Nanostructured Materials, 12 (1999) 339-344.

190. C. Ferrari and J. Robertson, Origin of the 1150 cm^{-1} Raman Mode in Nanocrystalline Diamond, Physical Review B, 63 (2001) 1214051-1214054.

191. H. Kuzmany, R. Pfeiffer, N. Salk and B. Gunther, The Mystery of the 1140 cm^{-1} Raman Line in Nanocrystalline Diamond Films, Carbon, 42 (2004) 911-917.

192. A. Laikhtman, I. Gouzman, A. Hoffman, G. Comtet, L. Hellner and G. Dujardin, Sensitivity of Near-Edge X-ray Absorption Fine Structure Spectroscopy to Ion Beam Damage in Diamond Films, Journal of Applied Physics, 86 (1999) 4192-4198.

193. J. Nithianandam, J. C. Rife, H. Windischmann, Carbon-K Edge Spectroscopy of Internal Interface and Defect States of Chemical Vapor-Deposited Diamond Films, Applied Physics Letters, 60 (1992) 135-137.

194. M. M. Garcia, I. Jimenez, L. Vazquez, C. Gomez-Aleixandre, J. M. Albella, O. Sanchez, L. J. Terminello and F. J. Himpsel, X-ray Absorption Spectroscopy and Atomic Force Microscopy Study of Bias-Enhanced Nucleation of Diamond Films, Applied Physics Letters, 72 (1998) 2105-2107.

195. S. L. Yang, Q. Yang, Z. M. Sun, Y. J. Tang, W. W. Yi, Effect of Power Inputs on Formation of Diamond Thin Films on Ti_3SiC_2 by Chemical Vapor Deposition, The 2007 Joint International Conference of the 3rd International Conference on Surface and Interface Science and Engineering (SISE 2007) and The Symposium on Surface Engineering for Industrial Applications (SEIA 2007), Sinapore, December 10-12, 2007.

196. S. Koizumi, T. Murakami, T. Inuzuka and K. Suzuki, Epitaxial-Growth of Diamond Thin-Films on Cubic Boron Nitride (111) Surfaces by DC Plasma Chemical Vapor-Deposition, Applied Physics Letters, 57 (1990) 563-565.

197. Y. Sato, H. Fujita, T. Ando, T. Tanaka and M. Kamo, Local Epitaxial-Growth Of Diamond On Nickel From The Vapor-Phase, Philosophical Transactions of the Royal Society of London Series A-Mathematical Physical and Engineering Sciences, 342 (1993) 225-231.

198. W. Zhu, P. C. Yang and J. T. Glass, Oriented Diamond Films Grown on Nickel Substrates, Applied Physics Letters, 63 (1993)1640-1642.

199. B. R. Stoner and J. T. Glass, Textured Diamond Growth on (100) Beta-SiC via Microwave Plasma Chemical Vapor-Deposition, Applied Physics Letters, 60 (1992) 698-700.

200. T. Suzuki, M. Yagi and K. Shibuki, Growth of Oriented Diamond on Single-Crystal of Silicon-Carbide (0001), Applied Physics Letters, 64 (1994) 557-559.

201. R. Kohl, C. Wild, N. Herres, P. Koidl, B. R. Stoner and J. T. Glass, Oriented Nucleation and Growth of Diamond Films on Beta-SiC and Si, Applied Physics Letters, 63 (1993) 1792-1794.

202. H. Kawarada, T. Suesada and H. Nagasawa, Heteroepitaxial Growth of Smooth and Continuous Diamond Thin Films on Silicon Substrates via High-Quality Silicon-Carbide Buffer Layers, Applied Physics Letters, 66 (1995) 583-585.

203. H. Kawarada, C. Wild, N. Herres, R. Locher, P. Koidl and N. Nagasawa, Heteroepitaxial Growth of Highly Oriented Diamond on Cubic Silicon Carbide, Journal of Applied Physics, 81 (1997) 3490-3493.

204. X. Jiang, C. P. Klages, R. Zachai, M. Hartweg and H. J. Fusser, Epitaxial Diamond Thin-Films on (001) Silicon Substrates, Applied Physics Letters, 62 (1993) 3438-3440.

205. X. Jiang and C. L. Jia, Diamond Epitaxy on (001) Silicon - An Interface Investigation, Applied Physics Letters, 67 (1995) 1197-1199.

206. S. D. Wolter, B. R. Stoner, J. T. Glass, P. J. Ellis, D. S. Buhaenko, E. E. Jenkins and P. Southworth, Textured Growth of Diamond on Silicon via Insitu Carburization and Bias-Enhanced Nucleation, Applied Physics Letters, 62 (1993) 1215-1217.

207. H. Maeda, M. Irie, T. Hino, K. Kusakabe and S. Morooka, Formation of Highly Oriented Diamond Film on Carburized (100) Si Substrate, Journal of Materials Research, 10 (1995) 158-164.

208. T. Tachibana, K. Hayashi and K. Kobashi, Azimuthal Rotation of Diamond Crystals Epitaxially Nucleated on Silicon {001}, Applied Physics Letter, 68 (1996) 1491-1492.

209. S. L. Yang, Q. Yang, Growth of Nanocrystalline Diamond Thin Films on Titanium Silicon Carbide Using Different Chemical Vapor Deposition Process, Canadian Metallurgical Quarterly, 48 (2009) 27-32.

210. Y. K. Chang, H. H. Hsieh, W. F. Pong, M. H. Tsai, F. Z. Chien, P. K. Tseng, L. C. Chen, T. Y. Wang, K. H. Chen, D. M. Bhusari, J. R. Yang, S. T. Lin, Quantum Confinement Effect in Diamond Nanocrystals Studied by X-Ray-Absorption Spectroscopy, Physical Review Letters, 82 (1999) 5377-5380.

211. S. M. Huang, Z. Sun, Y. F. Lu and M. H. Hong, Ultraviolet and Visible Raman Spectroscopy Characterization of Chemical Vapor Deposition Diamond Films, Surface and Coating Technology, 151 (2002) 263-267.

212. K. H. Wu, E. G. Wang, Z. X. Cao, Z. L. Wang, X. Jiang, Microstructure and its Effect on Field Electron Emission of Grain-Size-Controlled Nanocrystalline Diamond Films, Journal of Applied Physics, 88 (2000) 2967-2974.

213. S. A. Catledge, Y. K. Vohra, P. B. Mirkarimi, Low Temperature Growth of Nanostructured Diamond on Quartz Spheres, Journal Of Physics D-Applied Physics, 38 (2005) 1410-1414.

214. S. H. Seo, T. H. Lee, J. S. Park, Roughness Control of Polycrystalline Diamond Films Grown by Bias-Enhanced Microwave Plasma-Assisted CVD, Diamond and Related Materials, 12 (2003) 1670-1674.

215. Q. Yang, S. Yang, Y. S. Li, X. Lu, A. Hirose, NEXAFS Characterization of Nanocrystalline Diamond Thin Films Synthesized with High Methane Concentrations, Diamond and Related Materials, 16 (2007) 730-734.

216. Y. H. Tang, X. T. Zhou, Y. F. Hu, C. S. Lee, S. T. Lee, T. K. Sham, A Soft X-Ray Absorption Study of Nanodiamond Films Prepared by Hot-Filament Chemical Vapor Deposition, Chemical Physics Letters, 372 (2003) 320-324.

217. J. Y. Raty, G. Galli, C. Bostedt, T. W. van Buuren, and L. J. Terminello, Quantum Confinement and Fullerenelike Surface Reconstructions in Nanodiamonds, Physical Review Letters, 90 (2003) Article No.037401.

218. T. Hamilton, Determining the sp^2/sp^3 bonding concentrations of carbon films using X-ray absorption spectroscopy, M.Sc. Thesis, University of Saskatchewan, 2005.

219. L. H. Robins, E. N. Farabaugh, A. Feldman, Line Shape Analysis of the Raman Spectrum of Diamond Films Grown by Hot-Filament and Microwave-Plasma Chemical Vapor Deposition, Journal of Materials Research, 5 (1990) 2456-2468.

Appendix A: Email communication with Canadian Metallurgical Quarterly, regarding the use of the published paper in my thesis

On 5/27/09 6:35 PM, Office wrote:

> Good evening, thank you for your email. Our policy is to allow reproduction
> of CMQ copyrighted material as long as credit is given to the CMQ. I hope
> that this information is helpful. Please let us know if you need anything
> futher.
>
> Sincerely
>
> Debbie Fisher
>
> ----- Original Message -----
> From: "Songlan Yang" <Soy545@mail.usask.ca>
> To: <office@cmq-online.ca>
> Sent: Monday, May 25, 2009 2:44 PM
> Subject: Re: Use my paper in CMQ in my thesis
> > Dear Sir/Madam,
> > This is Songlan Yang from University of Saskatchewan.
> > Previously I published a paper in your Journal: Growth of
> > Nanocrystalline Diamond Thin Films on Titanium Silicon Carbide Using

> > Different Chemical Vapor Deposition Process, Canadian Metallurgical

> > Quarterly, 48 (2009) 27-32.

> > This is part work for my PH.D. thesis, now I need your permission to

> > use this paper in my thesis.

> > Your kindly permission will be appreciated.

> > Best,

> > Songlan

>